To the Graduate Council:

I am submitting herewith a dissertation written by Jing Jiang Wen entitled "Gaussian Beam Representation of Beam-Like Ultrasonic Fields." I have examined the final copy of this dissertation for form and content and recommend that it be accepted in partial fulfillment of the requirements for the degree of Doctor of Philosophy, with a major in Physics.

M. A. Breazeale, Major Professor

We have read this dissertation
and recommend its acceptance:

Accepted for the Council:

Vice Provost
and Dean of the Graduate School

GAUSSIAN BEAM REPRESENTATION OF BEAM-LIKE ULTRASONIC FIELDS

A Dissertation

Presented for the

Doctor of Philosophy

Degree

The University of Tennessee, Knoxville

Jing Jiang Wen

June 1988

ACKNOWLEDGEMENTS

The author wishes to express his special appreciation to Dr. M. A. Breazeale for his valuable guidance, encouragement and patience during the preparation and writing of this dissertation.

The author also would like to acknowledge the following individuals: Mr. Wenhua Jiang and Prof. Gonghuan Du, Nanjing University, for many helpful discussions during their stay at The University of Tennessee; Mr. Lida Lin, Polytechnic University of New York, for providing the program for calculating Bertoni-Tamir's solution and help in computer programming; Mr. Jeong Kwan Na for help in experimental work; and Mrs. Maxine Martin for typing the manuscript.

Finally, the author would like to express his gratefulness to his parents for their continuing support and encouragement. Special thanks go to his wife Shiqi Liu whose eternal love and assistance is a contributing factor of this work.

ABSTRACT

A systematic method of analysis of beam-like wave fields—the Gaussian beam representation—is established in this dissertation. Through a computer determination of the coefficient and beam parameter sets based on optimization theory, any wave field satisfying the condition $(ka)^2 >> 1$ can be expressed as a superposition of a number of Gaussian beams with different beam waists, about the same (axisymmetric case) or different beam axes, and propagating in the same direction. Two typical beam fields—the diffraction fields of axisymmetric piston radiators and the non-axisymmetric reflected field of a bounded beam incident at or near the Rayleigh angle—are used as a demonstration of the new method. Experimental results obtained with a new Gaussian transducer are presented as a verification of the physical existence of a single ultrasonic Gaussian beam—the basic unit of the Gaussian beam representation.

TABLE OF CONTENTS

CHAPTER		PAGE
I.	INTRODUCTION	1
	1.1. The Plane Wave Representation of a Beam Field	1
	1.2. The Diffraction Pattern of a Circular Radiator	2
	1.3. Reflection Problems at the Rayleigh Angle	5
II.	GAUSSIAN BEAM FUNCTION	8
	2.1. Parabolic Approximation	8
	2.2. The Fresnel Paraxial Approximation	11
	2.3. Physical Significance	13
III.	THE GAUSSIAN BEAM FUNCTION AS A BASE FUNCTION SET	14
	3.1. General Considerations	15
	3.2. Method I: The Conventional Procedure	17
	3.3. Method II: The Optimization Procedure	21
	3.4. Discussion of Uniqueness and Completeness	22
IV.	GAUSSIAN BEAM REPRESENTATION IN DIFFRACTION PROBLEMS	24
	4.1. The Reference Solution from the Rayleigh Integral	25
	4.2. Boundary Condition Matching and Its Effect on the Solution	28
	4.3. On-Axis Behavior Matching as a Constraint	32
	4.4. Effect of Changing Number of Gaussian Beams	35
	4.5. Use of Conventional Procedure	48
	4.6. The Radiating Dipole Model as a Reference	55
	4.7. Piston Transducer Supported at the Edge	58
	4.8. Gaussian Beam and Gaussian Transducer	61
V.	EXPERIMENTAL VERIFICATION—GAUSSIAN ULTRASONIC BEAM	65
	5.1. The Gaussian Transducer	65
	5.2. Experimental Technique and Field Distribution Study	68
VI.	NON-AXISYMMETRIC CASES—REFLECTION PROBLEMS	82
	6.1. The Axis Parameter of a Gaussian Beam	83
	6.2. A Plane Wave Representation	86
	6.3. A Short Review on Previous Works	89

CHAPTER PAGE

6.4. The Spectrum Function and Its Effect to the Reflectance 91
6.5. A New Approximation to the Reflectance Function 94
6.6. The Gaussian Beam Representation of a Reflected Field 95

VII. SUMMARY 106

BIBLIOGRAPHY 109

VITA 112

LIST OF TABLES

TABLE		PAGE
4.1.	The Coefficient and Beam Parameter Sets of a 15-Term Gaussian Beam Solution of the Field of a Rigid Piston Transducer (Without On-Axis Matching)	29
4.2.	The Coefficient and Beam Parameter Sets of a 15-Term Gaussian Beam Solution (Calculated with On-Axis Matching) of the Field of a Rigid Piston Transducer . . .	34
4.3.	The Coefficient and Beam Parameter Sets of a 10-Term Gaussian Beam Solution (Calculated with On-Axis Matching) of the Field of a Rigid Piston Transducer . . .	41
4.4.	The Coefficient and Beam Parameter Sets of a 6-Term Gaussian Beam Solution (Calculated with On-Axis Matching) of the Field of a Rigid Piston Transducer . . .	41
4.5.	The Coefficient and Beam Parameter Sets of a 15-Term Gaussian Beam Solution of the Field of a Rigid Piston Transducer Calculated by the Conventional Procedure Using the B_n Set in Table 4.2 (p. 34)	49
4.6.	The Coefficient and Beam Parameter Sets of a 10-Term Gaussian Beam Solution of the Field of a Rigid Piston Transducer Calculated by the Conventional Procedure Using the B_n Set in Table 4.3 (p. 41)	50
4.7.	The Coefficient and Beam Parameter Sets of a 6-Term Gaussian Beam Solution of the Field of a Rigid Piston Transducer Calculated by the Conventional Procedure Using the B_n Set in Table 4.4 (p. 41)	50
4.8.	The Coefficient and Beam Parameter Sets of a 15-Term Gaussian Beam Solution of the Field of a Rigid Piston Transducer Using Radiating Dipole Model as the On-Axis Constraint	57
4.9.	The Coefficient and Beam Parameter Sets of a 6-Term Gaussian Beam Solution (Calculated with On-Axis Matching) of the Field of a Piston Transducer Supported at r = a	61

TABLE PAGE

6.1. The Coefficient and Beam Parameter Sets of Gaussian Beam Representations of Reflected Fields of Gaussian Beams with Different Beam Waists Incident Onto a Water-Aluminum Interface at Angles Near the Rayleigh Angle $\theta_R = 30.5°$ 97

LIST OF FIGURES

FIGURE		PAGE
4.1.	The Surface Velocity Distribution of a 15-Term Gaussian Beam Solution (Table 4.1) (Without On-Axis Matching) of a Rigid Piston Radiator	30
4.2.	The On-Axis Behavior of a 15-Term Gaussian Beam Solution (Table 4.1) (Without On-Axis Matching) of the Field of a Rigid Piston Radiator Compared with the On-Axis Expression of the Rayleigh Integral (Eq. 4.4)	31
4.3.	The Surface Velocity Distribution of a 15-Term Gaussian Beam Solution (Table 4.2) (Calculated with On-Axis Matching) of a Rigid Piston Radiator	36
4.4.	The On-Axis Behavior of a 15-Term Gaussian Beam Solution (Table 4.2) (Calculated with On-Axis Matching) of the Field of a Rigid Piston Radiator Compared with the On-Axis Expression of the Rayleigh Integral (Eq. 4.4)	37
4.5.	The Profile at $z = 0.10\ z_0$ of a 15-Term Gaussian Beam Solution (Table 4.2) (Calculated with On-Axis Matching) of the Field of a Rigid Piston Radiator Compared with the Numerical Evaluation of the Rayleigh Integral	38
4.6.	The Profile at $z = 0.13\ z_0$ of a 15-Term Gaussian Beam Solution (Table 4.2) (Calculated with On-Axis Matching) of the Field of a Rigid Piston Radiator Compared with the Numerical Evaluation of the Rayleigh Integral	39
4.7.	The On-Axis Behavior of a 10-Term Gaussian Beam Solution (Table 4.3) (Calculated with On-Axis Matching) of the Field of a Rigid Piston Radiator Compared with the On-Axis Expression of the Rayleigh Integral (Eq. 4.4)	42
4.8.	The On-Axis Behavior of a 6-Term Gaussian Beam Solution (Table 4.4) (Calculated with On-Axis Matching) of the Field of a Rigid Piston Radiator Compared with the On-Axis Expression of the Rayleigh Integral (Eq. 4.4)	43

FIGURE PAGE

4.9. The Profile at $z = 0.13\ z_0$ of a 10-Term Gaussian Beam Solution (Table 4.3) (Calculated with On-Axis Matching) of the Field of a Rigid Piston Radiator 44

4.10. The Profile at $z = 0.25\ z_0$ of a 10-Term Gaussian Beam Solution (Table 4.3) (Calculated with On-Axis Matching) of the Field of a Rigid Piston Radiator 45

4.11. The Profile at $z = 0.45\ z_0$ of a 10-Term Gaussian Beam Solution (Table 4.3) (Calculated with On-Axis Matching) of the Field of a Rigid Piston Radiator 46

4.12. The Profile at $z = z_0$ of a 10-Term Gaussian Beam Solution (Table 4.3) (Calculated with On-Axis Matching) of the Field of a Rigid Piston Radiator 47

4.13. The Surface Velocity Distributions of 15-Term Gaussian Beam Solutions with Same Beam Waist Parameter Set but Different Coefficient Sets Obtained by (a) the Conventional Procedure (Table 4.5); (b) the Optimization Procedure (Table 4.2) Compared with That of a Rigid Piston Radiator 51

4.14. The Surface Velocity Distributions of 10-Term Gaussian Beam Solutions with Same Beam Waist Parameter Set but Different Coefficient Sets Obtained by (a) the Conventional Procedure (Table 4.6); (b) the Optimization Procedure (Table 4.3) Compared with That of a Rigid Piston Radiator 52

4.15. The On-Axis Behavior of a 15-Term Gaussian Beam Solution (Table 4.5) Obtained by the Conventional Procedure Using a Beam Waist Parameter Set Provided by the Optimization Procedure Compared with the On-Axis Expression of the Rayleigh Integral (Eq. 4.4) 53

4.16. The On-Axis Behavior of a 10-Term Gaussian Beam (Table 4.6) Obtained by the Conventional Procedure Using a Beam Waist Parameter Set Provided by the Optimization Procedure Compared with the On-Axis Expression of the Rayleigh Integral (Eq. 4.4) 54

FIGURE PAGE

4.17. The Surface Velocity Distribution of a 15-Term Gaussian Beam Solution Calculated Using Radiating Dipole as On-Axis Constraint (Table 4.8) Compared with the One of a Rigid Piston Radiator 59

4.18. The On-Axis Behavior of a 15-Term Gaussian Beam Solution Calculated Using Radiating Dipole Model as On-Axis Constraint (Table 4.8) Compared with the Exact On-Axis Expression Given by Eq. 4.11 60

4.19. The Surface Velocity Distribution of a 6-Term Gaussian Beam Solution (Table 4.9) (Calculated with On-Axis Matching) of a Piston Radiator Supported at r = a 62

4.20. The On-Axis Behavior of a 6-Term Gaussian Beam Solution (Table 4.9) (Calculated with On-Axis Matching) of the Field of a Piston Radiator Supported at r = a Compared with the Exact On-Axis Expression . . . 63

5.1. Schlieren System 69

5.2. Schlieren Photographs of the Ultrasonic Field Produced by a 4 MHz, 0.36 Inch Diameter Gaussian Transducer 71

5.3. Schlieren Photograph of the Field of a Piston Transducer 72

5.4. The Measured On-Axis Behavior of the Beam Field Produced by a 4 MHz, 0.36 Inch Diameter Gaussian Transducer Compared with Theory 73

5.5. The Measured Transverse Profile of the Beam Field Produced by a 4 MHz, 0.36 Inch Diameter Gaussian Transducer at z - 20 mm Compared with Theory 74

5.6. The Measured Transverse Profile of the Beam Field Produced by a 4 MHz, 0.36 Inch Diameter Gaussian Transducer at z = 30 mm Compared with Theory 75

5.7. The Measured Transverse Profile of the Beam Field Produced by a 4 MHz, 0.36 Inch Diameter Gaussian Transducer at z = 40 mm Compared with Theory 76

5.8. The Measured Transverse Profile of the Beam Field Produced by a 4 MHz, 0.36 Inch Diameter Gaussian Transducer at z = 50 mm Compared with Theory 77

FIGURE PAGE

5.9. The Measured Transverse Profile of the Beam Field Produced by a 4 MHz, 0.36 Inch Diameter Gaussian Transducer at z = 100 mm Compared with Theory 78

5.10. The Measured Transverse Profile of the Beam Field Produced by a 4 MHz, 0.36 Inch Diameter Gaussian Transducer at z = 150 mm Compared with Theory 79

5.11. The Measured Transverse Profile of the Beam Field Produced by a 4 MHz, 0.36 Inch Diameter Gaussian Transducer at z = 200 mm Compared with Theory 80

5.12. The Measured Transverse Profile of the Beam Field Produced by a 4 MHz, 0.36 Inch Diameter Gaussian Transducer at z = 300 mm Compared with Theory 81

6.1. A Schlieren Photograph of an Ultrasonic Beam Incident at the Rayleigh Angle Onto a Water-Aluminum Interface 84

6.2. The Coordinate System Used for Beam Field Reflection Problem 87

6.3. Reflected Beam Profiles on a Water-Aluminum Interface Calculated by Numerical Integration, Bertoni-Tamir's Solution, and Gaussian Beam Representation for a Gaussian Beam of Half Width w = 1.5 cm Incident at the Rayleigh Angle θ_i = 30.5° 98

6.4. Reflected Beam Profiles on a Water-Aluminum Interface Calculated by Numerical Integration, Bertoni-Tamir's Solution, and Gaussian Beam Representation for a Gaussian Beam of Half Width w = 1.0 cm Incident at the Rayleigh Angle θ_i = 30.5° 99

6.5. Reflected Beam Profiles on a Water-Aluminum Interface Calculated by Numerical Integration, Bertoni-Tamir's Solution, and Gaussian Beam Representation for a Gaussian Beam of Half Width w = 0.5 cm Incident at the Rayleigh Angle θ_i = 30.5° 100

FIGURE PAGE

6.6. Reflected Beam Profiles on a Water-Aluminum Interface Calculated by Numerical Integration, Bertoni-Tamir's Solution, and Gaussian Beam Representation for a Gaussian Beam of Half Width w = 1.0 cm Incident at θ_i = 29.5° 101

6.7. Reflected Beam Profiles on a Water-Aluminum Interface Calculated by Numerical Integration, Bertoni-Tamir's Solution, and Gaussian Beam Representation for a Gaussian Beam of Half Width w = 1.0 cm Incident at θ_i = 28.5° 102

6.8. Phase Distributions in the Reflected Beam on a Water-Aluminum Interface Calculated by Numerical Integration, Bertoni and Tamir's Solution, and Gaussian Beam Representation for a Gaussian Beam of Half Width w = 1.0 cm Incident at the Rayleigh Angle θ_i = 30.5° 104

CHAPTER I

INTRODUCTION

1.1. The Plane Wave Representation of a Beam Field

Waves propagating as a beam of finite width can be described by use of spatial Fourier analysis in which the beam field is represented by the superposition of infinite plane waves. When a beam field is subjected to a physical process, such as propagation, diffraction, reflection, focusing, scattering, etc., the resultant field can be described by two consecutive mathematical steps. First, the initial beam is decomposed into a continuous spectrum of plane waves propagating in different directions with respect to the beam axis. This is done by the use of the spatial Fourier transform:

$$G(k_x, k_y) = \frac{1}{(2\pi)^2} \int_{-\infty}^{\infty} \int_{-\infty}^{\infty} \phi_0(x, y, 0)\, e^{-ik_x x - ik_y y}\, dx\, dy, \tag{1.1}$$

where $G(k_x,k_y)$ is the angular spectrum function and $\phi_0(x,y,0)$ is the profile of the initial beam field in the plane $z = 0$ on which the physical process takes place. After application of knowledge about plane wave (geometric acoustics or optics) to each planar wavelet produces a modified spectrum function, an inverse Fourier transform is employed to rewrite the field solution in terms of the spatial cordinates, i.e.,

$$\phi(x,y,z) = \int_{-\infty}^{\infty}\int_{-\infty}^{\infty} G(k_x,k_y)\cdot F(k_x,k_y)\, e^{i(k_x x+k_y y+k_z z)}\, dk_x\, dk_y. \qquad (1.2)$$

In Eq. (1.2), $F(k_x,k_y)$ stands for the physical process imposed on the initial beam field, and $\phi(x,y,z)$ is the resultant field. In the sense that the field solution is expressed as a superposition of plane waves, Eq. (1.2) may be called the plane wave representation of a beam field.

The plane wave representation is limited in two ways. First, a plane wave representation is possible only when the boundary conditions are so simple that the corresponding Green's function is available. Secondly, even though a plane wave representation is obtained in terms of the Fourier integrals in Eqs. (1.1) and (1.2), it can seldom be solved analytically in practical physical situations. The lack of an analytical solution complicates theoretical studies and many applications.

1.2. The Diffraction Pattern of a Circular Radiator

The radiated field (diffraction pattern) of a planar circular (piston) vibration source in an infinite rigid baffle is a most important beam field. An analogue in optics is the diffraction field of a circular aperture illuminated by a parallel coherent light source. Both the two beam fields are characterized by a complicated nearfield (the Fresnel zone) crowded with interference maxima and minima and a series of sidelobes about the main beam. As the

mathematical representation of an often used ultrasonic source, the diffraction pattern of a piston radiator (transducer) has been studied as a most fundamental problem in acoustics. The Rayleigh surface integral [Rayleigh, 1945] based on Huygens' Theorem is considered the first exact expression of the problem. A later alternative, King's integral [King, 1934], is essentially an application of spatial Fourier analysis to planar sound sources. It is found that the Rayleigh integral and King's integral are equivalent and can be derived from each other [Oberhettinger, 1961; Greenspan, 1979]. Thus, either of them is actually a plane wave representation of the diffraction problem. However, neither expression can be solved analytically even for boundary conditions describing a piston transducer. Although the on-axis behavior and an approximation to the farfield can be expressed in a closed form, to describe the near-field (the Fresnel zone) and the transition zone, a numerical integration has to be carried out point by point. A general review of the integral expressions describing the piston radiator is presented by Harris [1981].

Infinite series solutions for describing beam field problems appear more attractive than spatial Fourier analysis because of their better performance in mathematical analyses. Many series solutions using different base function sets have been developed to represent the diffraction field of a piston transducer. Gaussian-Laguerre functions [Cavanagh and Cook, 1980], Bessel functions [Tjøtta and Tjøtta, 1980] and products of spherical Bessel functions, Hankel

functions and Legendre polynomials [Hawegawa et al., 1983] are some base function sets employed in series solutions. However, because of the discontinuity at the edge, the number of terms needed to represent the field of a piston is large. The mathematical analysis is difficult with a large number of functions having different analytical form.

Besides the rigid piston transducer, planar ultrasonic sources with other surface distributions have been investigated. Greenspan [1979] and Novikov et al. [1981] studied source distributions with different degrees of discontinuity. Tjøtta and Tjøtta [1982] reported studies of the Gaussian radiator, parabolic radiator, elliptical piston radiator and step function with a smooth edge. The descriptions of these diffraction fields are still either integrals or infinite series. Because of the increasing demands in acoustics as well as optic applications, even though the diffraction theory has been established since Huygens' time, the search for a better description to the diffraction problem has never ceased.

In this dissertation, a new approach for beam field description—the Gaussian beam representation—is developed to represent the diffraction fields. In the Gaussian beam representation, instead of plane waves propagating in different directions, a set of Gaussian beams with different beam parameters is employed as the basic unit. Through the computer determination of the coefficient and beam parameter sets by the imposed physical constraints, an axisymmetric field is expressed in a unified, analytical form—a

superposition of a number of Gaussian beams with different beam waists located at different positions along the bxis. As a logical conclusion, a single Gaussian beam produced by a vibration source with Gaussian distribution makes an extreme simplification of the diffraction pattern [Wen and Breazeale, 1987, 1988]. This conclusion is supported by the experimental verification of a single Gaussian beam produced by a recently developed Gaussian ultrasonic transducer.

1.3. Reflection Problems at the Rayleigh Angle

To emphasize the generality of the Gaussian beam representation, we consider a non-axisymmetric problem. An ultrasonic beam incident onto a liquid-solid interface is found to exhibit some unusual beam effects at or near the Rayleigh angle at which surface waves propagate along the interface. A lateral displacement of the reflected beam was first reported by Goos and Hänchen [1947], who stimulated a wave of intensive studies on the intriguing nonspecular phenomena associated with reflection at and near the Rayleigh angle. Schoch [1950] provided the first experimental demonstration and a qualitative theoretical explanation. Brekhovskikh developed a more detailed theory based on spatial Fourier analysis [1960]. A comprehensive review of the studies until 1970 is given by Lotsch [1970, 1971]. An angular deviation of the reflected beam from the direction predicted by Snell's law is reported by Ra et al. [1973], Antar and Boerner [1974], White et al. [1977], Chan and Tamir [1985]. McGuirk and Carniglia [1977] predicted that the reflected beam may also undergo a

longitudinal (rather than lateral) shift along its axis. Tamir [1986] pointed out the possible reduction or expansion in the magnitude of the beam waist in the reflected beam. However, the use of a truncated Taylor expansion limits the validity of these theories. Many observed experimental phenomena, such as a null or minimum of intensity within the reflected beam (the splitting of the reflected beam), a weak trailing field on only one side of the reflected beam [Neubauer, 1973], cannot be explained by these theories.

Significant progress was made by Tamir and Bertoni [1971] in optics and Bertoni and Tamir [1973] in acoustics. By using a Laurent expansion to approximate the reflectance and assuming the incident beam to have a Gaussian profile distribution at the reflection plane, Bertoni and Tamir gave the first analytical solution to the problem. This solution agrees with the integral solution very well [Ngoc and Mayer, 1980] when the incidence occurs at or close to the Rayleigh angle and the half beam waist (denoted by w) of the incident beam is large. Experimental verifications are made by Breazeale et al. [1974], Breazeale and Torbett [1976], and Breazeale et al. [1977] with a 2-dimensional Gaussian beam [Martin and Breazeale, 1971]. However, for non-Gaussian beams, Gaussian beams with small waists, or for incidence at angles different from the Rayleigh angle, Bertoni and Tamir's solution is not adequate. At this point, the Gaussian beam representation proves to be capable of describing such a challenging beam field. Through the introduction of the beam axis parameter, the solution is successfully represented as a superposition of a few

Gaussian beams with different beam waists, about different axes, but propagating in the same direction [Wen and Breazeale, 1987].

The discussion starts with the physical background and mathematical derivation of the symmetric Gaussian beam functions in Chapter II. The complex beam waist parameter is also defined and discussed. In Chapter III, two approaches are outlined for determining the coefficients and the beam waist parameters by the given boundary conditions. The first is the conventional procedure based on the use of the orthogonality relations of the base function set; the second is a new procedure based on optimization theory. These two procedures are then used to describe the diffraction field of a piston transducer in Chapter IV, and the validity of the approach is tested by comparing with other solutions whenever possible. The experimental verification of a single Gaussian beam composes the material of Chapter V. In Chapter VI a new beam parameter, the axis parameter, is introduced to describe the non-axisymmetric Rayleigh angle reflection problem. Through these two typical beam fields: the diffraction field of a piston radiator and the reflected field at Rayleigh angle incidence, a systematic method of analysis—the Gaussian beam representation—is established. The results are summarized in Chapter VII.

CHAPTER II

GAUSSIAN BEAM FUNCTION

The Gaussian beam function is a three-dimensional field configuration that differs from the Gaussian function extensively used in statistics and probability as a linear or planar distribution function. In this chapter, the Gaussian beam function is derived from the parabolic equation—an approximation to the Helmholtz equation, the space dependence part of the wave equation. The restriction on the use of the parabolic equation and the definition of beam field are given in the process of derivation. In order to show the physical correspondence between the parabolic approximation and the frequently used Fresnel paraxial approximation, a separate derivation of the Gaussian beam function using the Fresnel approximation in the spatial Fourier analysis is also carried out. The physical significance of the Gaussian beam function and the role it can play in the description of beams fields is considered.

2.1. Parabolic Approximation

For a sound (or light) beam with its axis parallel to the propagation direction defined by the z-axis, the velocity potential can be written in the form of

$$\phi(x,y,z) = u(x,y,z)\, e^{ikz}. \tag{2.1}$$

In Eq. (2.1) the factor $e^{i\omega t}$ has been suppressed since only the space dependence described by the Helmholtz equation

$$\nabla^2\phi + k^2\phi = 0 \tag{2.2}$$

is considered. Substituting Eq. (2.1) into Eq. (2.2) yields

$$\frac{\partial^2 u}{\partial z^2} + \frac{\partial^2 u}{\partial x^2} + \frac{\partial^2 u}{\partial y^2} + 2ik\frac{\partial u}{\partial z} = 0. \tag{2.3}$$

The parabolic equation (it is extensively used in underwater acoustics) can be obtained by omitting the first term from Eq. (2.3); i.e.,

$$\frac{\partial^2 u}{\partial x^2} + \frac{\partial^2 u}{\partial y^2} + 2ik\frac{\partial u}{\partial z} = 0. \tag{2.4}$$

It can be proved [Tjøtta and Tjøtta, 1980] that the neglected term $\partial^2 u/\partial z^2$ is of the order of $1/(ka)^2$, where k is the wave number $2\pi/\lambda$ with λ the wave length, and a is half of the effective transverse field width. Thus, the use of the parabolic equation places the restriction

$$(ka)^2 \gg 1. \tag{2.5}$$

Eq. (2.5) is also used as the criterion of <u>beam field</u> throughout this article. To solve Eq. (2.4) one can write a particular solution as

$$u(x, y, z) = g(z)\exp[f(z)x^2 + h(z)y^2], \tag{2.6}$$

where g(z), f(z) and h(z) are unknown functions to be determined. Substituting Eq. (2.6) into Eq. (2.4) produces

$$x^2(2f^2 + ik\frac{\partial f}{\partial z}) + y^2(2h^2 + ik\frac{\partial h}{\partial z}) + (f + h + \frac{ik}{g}\frac{\partial g}{\partial z}) = 0. \tag{2.7}$$

Eq. (2.7) must be valid for any x and y, therefore each term must vanish separately. Thus,

$$2f^2 + ik\frac{\partial f}{\partial z} = 0; \tag{2.8}$$

$$2h^2 + ik\frac{\partial h}{\partial z} = 0; \tag{2.9}$$

$$f + h + \frac{ik}{g}\frac{\partial g}{\partial z} = 0. \tag{2.10}$$

Solving Eqs. (2.8), (2.9), (2.10) simultaneously gives

$$f(z) = -(B_1 + \frac{2i}{k}z)^{-1}; \tag{2.11}$$

$$h(z) = -(B_2 + \frac{2i}{k}z)^{-1}; \tag{2.12}$$

$$g(z) = \left[(B_1 + \frac{2i}{k}z)(B_2 + \frac{2i}{k}z)\right]^{-1/2}. \tag{2.13}$$

where B_1 and B_2 are arbitrary constants of integration which can be written as complex quantities

$$B_1 = w_x^2 - \frac{2i}{k}z_{x0}; \tag{2.14}$$

$$B_2 = w_y^2 - \frac{2i}{k}z_{y0}. \tag{2.15}$$

Combining Eqs. (2.1), (2.6), (2.11)-(2.15), the general form of Gaussian beam function is obtained as

$$\phi(x,y,z) = \frac{w_x w_y \exp\left[-\frac{x^2}{w_x^2+\frac{2i}{k}(z-z_{x_0})} - \frac{y^2}{w_y^2+\frac{2i}{k}(z-z_{y_0})} + ikz\right]}{\sqrt{[w_x^2 + \frac{2i}{k}(z-z_{x_0})][w_y^2 + \frac{2i}{k}(z-z_{y_0})]}}. \qquad (2.16)$$

In Eq. (2.16) the field solution has been normalized to unity at the field point (x = 0, y = 0, z = 0) by a constant quantity $w_x w_y$. It can be seen that at a position $z = z_{x_0}$, the beam width in the x-dimension takes the minimum value w_x, thus, w_x is referred to as the x-dimension beam waist located at z_{x_0}. Similarly, the y-dimension beam waist w_y is located at z_{y_0}. Now one sees a Gaussian beam is characterized by a complex beam waist parameter in each transverse dimension. A beam axis parameter for cases where the beam axis does not coincide with the z-axis will be introduced in Chapter VI.

In the axisymmetric cases, denoting $w = w_x = w_y$ and $z_0 = z_{x_0} = z_{y_0}$ and using the relation $\rho^2 = x^2 + y^2$, Eq. (2.16) is reduced to a simpler form:

$$\phi(\rho,z) = \frac{w^2}{w^2 + \frac{2i}{k}(z-z_0)} \exp\left[-\frac{\rho^2}{w^2 + \frac{2i}{k}(z-z_0)} + ikz\right]. \qquad (2.17)$$

Using Eq. (2.16) or Eq. (2.17), one can easily find that the neglected term $\partial^2 u/\partial z^2$ is of the order of $1/(kw)^2$ and is negligible in typical ultrasonic applications.

2.2. The Fresnel Paraxial Approximation

In order to show the physical effect of neglecting the term $\partial^2 u/\partial z^2$, an independent approach for deriving the Gaussian beam

function can be used as a reference. Suppose there exists a beam field in free space with an amplitude distribution in the plane z = 0 described by a Gaussian function

$$\phi_0(x,y,0) = \exp\left[-\frac{x^2+y^2}{w^2}\right]. \tag{2.18}$$

To find the wave field in any z-plane, one can substitute Eq. (2.18) into Eq. (1.1) and use the integral relation

$$\int_{-\infty}^{\infty} e^{-\alpha t^2}\, dt = \frac{\sqrt{\pi}}{\sqrt{\alpha}} \qquad Re(\alpha) > 0. \tag{2.19}$$

The angular spectrum function is then found as

$$G(k_x,k_y) = \frac{w^2}{4\pi}\exp\left[-\frac{w^2}{4}(k_x^2+k_y^2)\right]. \tag{2.20}$$

For a beam field of effective beam width much larger than the wave length, the transverse components of the wave vector is much smaller than the axial component. Thus the Fresnel paraxial approximation applies; i.e.,

$$k_z = \sqrt{k^2-k_x^2-k_y^2} \approx k - \frac{k_x^2}{2k} - \frac{k_y^2}{2k}. \tag{2.21}$$

Again, the use of the Fresnel paraxial approximation requires Eq. (2.5) to be satisfied. For the propagation in a linear homogeneous medium, one has:

$$F(k_x,k_y) = 1. \tag{2.22}$$

Substituting Eqs. (2.20)-(2.22) into Eq. (1.2), and making use of Eq. (2.19) produces

$$\phi(x,y,z) = \frac{w^2}{w^2 + \frac{2i}{k}z} \exp\left[-\frac{x^2+y^2}{w^2+\frac{2i}{k}z} + ikz\right]. \tag{2.23}$$

Equation (2.23) is exactly the Gaussian beam function in Eq. (2.17) derived by solving the parabolic equation. Thus, the equivalence between the parabolic approximation and the Fresnel paraxial approximation is proved. The procedure can be used in a non-axisymmetric situation to derive the more general form of Eq. (2.16) as well.

2.3. Physical Significance

A conclusion, then, is drawn as follows: A Gaussian beam of any beam waist(s) located at any position along its axis is a fundamental mode of wave motion in a linear homogeneous free space, as long as the beam field condition Eq. (2.5) is satisfied. This is exactly the reason why the plane wave of any wave vector $\vec{k} = (k_x, k_y, k_z)$ plays an essential role in the general wave field study. In this sense, the Gaussian beam function is eligible to be used as the basic unit in a <u>beam field</u> description.

CHAPTER III

THE GAUSSIAN BEAM FUNCTION AS A BASE FUNCTION SET

The potential of using a Gaussian beam function as the base function in the beam field description makes it mathematically reasonable to write an arbitrary beam field as a superposition of Gaussian beams with different beam waist parameters. However, the applicability and the attractiveness of the Gaussian beam representation depend on how readily the coefficient and beam parameter sets can be determined so that the boundary conditions are satisfied. In this chapter the determination of the coefficient set, as well as the waist parameter set, for the Gaussian beam representation of a given ultrasonic field are discussed. Upon introducing the acoustic boundary condition, the discussion is divided into two parts. The approach based on the use of the orthogonality property of the base function set, as a conventional and well-developed procedure, is outlined first. The lack of the orthogonality of the Gaussian beam function is overcome by making a new function set in which each function is a different linear combination of Gaussian beam functions. Secondly, an alternative to the conventional procedure is described. The alternative is based on the use of optimization theory [Wen and Breazeale, 1987; ibid., 1988]. A discussion of the uniqueness and completeness arguments ends the chapter. For simplicity, the discussion is concentrated on axisymmetric fields. The non-axisymmetric case will be treated in Chapter VI.

3.1. General Considerations

In the Gaussian beam solution of an axisymmetric beam field, all Gaussian beams have the same beam axis, although their beam waists may differ from each other and are located at different positions along the common axis. The velocity potential then is written as

$$\phi(\rho,z)=\sum_{n=1}^{N}\frac{A_n}{B_n+\frac{2i}{k}z}\exp\left[-\frac{\rho^2}{B_n+\frac{2i}{k}z}+ikz\right], \tag{3.1}$$

where N is the number of Gaussian beams in the solution, A_n's are complex coefficients and B_n's are complex beam waist parameters defined by Eq. (2.15). Any particular beam field solution in the Gaussian beam representation differs from others only by a specific set of coefficients and beam parameters determined by the specific boundary conditions. Just as in the plane wave representation, they would be characterized by different spectrum functions. Thus, the calculation of a pair of Fourier integrals now becomes the evaluation of a set of constants.

For mathematical convenience, two dimensionless variables are employed in the formulations. One is the radial coordinate

$$\xi=\rho/a, \tag{3.2}$$

with a the reference dimension (say the radius of the active area of the transducer), and the other is the axial coordinate

$$\sigma=z/z_R, \tag{3.3}$$

where z_R is the Rayleigh distance given by

$$z_R = \frac{1}{2}ka^2. \tag{3.4}$$

Equation (3.1) now can be written as

$$\phi(\xi,\sigma) = \frac{i}{k}\sum_{n=1}^{N}\frac{A_n}{1+iB_n\sigma}\exp\left[-\frac{B_n\xi^2}{1+iB_n\sigma}+ikz_R\sigma\right]. \tag{3.5}$$

Suppose the beam field is bounded by the plane z = 0 with a velocity distribution $V_0(\xi)$. Substituting Eq. (3.5) into the acoustical boundary condition

$$V_0(\xi) = -\frac{\partial\phi}{\partial z}\bigg|_{z=0} = -\frac{1}{z_R}\frac{\partial\phi}{\partial\sigma}\bigg|_{\sigma=0} \tag{3.6}$$

yields

$$V_0(\xi) = \sum_{n=1}^{N}A_n\exp\left[-B_n\xi^2\right]\left[1-\frac{2B_n}{(ka)^2}(1-B_n\xi^2)\right]. \tag{3.7}$$

When the beam field condition $(ka)^2 >> 1$ is applied, Eq. (3.7) reduces to

$$V_0(\xi) = \sum_{n=1}^{N}A_n\exp\left[-B_n\xi^2\right]. \tag{3.8}$$

Equation (3.8) is the relation to be used in coefficient and beam waist parameter set determination.

Generally speaking, most base function sets used in field descriptions are orthogonal. Each function in the set is characterized by a specific sequence parameter and can be described by a general

form in terms of the sequence parameter such that the entire set is completely and exclusively defined. Recursion relations and formulas for calculating coefficients are well developed for immediate use, as is the case for the Legendre function family, Bessel functions, Laguerre polynomials, etc.

In contrast, the Gaussian beam function is not an orthogonal set. It is reported [Niver et al., 1987] that the accuracy of using Gaussian beam functions as base function sets strongly depend on the choice of arbitrarily assignable beam parameters. The lack of a criterion for beam parameter determination has been the focus of the investigations of Lu et al [1987] and Maciel et al [1987].

Since a series of Gaussian beam functions is not an ideal base function set for the use of the traditional procedure based on infinite series theory, there are two choices: either finding a new procedure which best fits the Gaussian beam function or modifying the Gaussian beam function to meet the requirements of the old procedure. Both approaches are described in this chapter and tested and compared in the next chapter.

3.2. Method I: The Conventional Procedure

The conventional procedure of expanding a function in terms of an infinite series is based on the use of the orthogonality relation. Since Gaussian beam functions are not intrinsically orthogonal, the common process is to establish a new orthogonal set in which each function is a different linear combination of Gaussian beam functions.

Let g_m stand for the mth term in the new set, then

$$g_m(\xi) = \sum_{i=1}^{m} C_{m,i} \exp[-B_i \xi^2], \tag{3.9}$$

where $C_{m,i}$ is a constant coefficient set to be determined by the orthogonality relation

$$\int_0^\infty g_l(\xi)\, g_m(\xi) \xi \, d\xi = \delta_{lm} = \begin{cases} 1 & l = m \\ 0 & l \neq m. \end{cases} \tag{3.10}$$

Substituting Eq. (3.9) into Eq. (3.10) yields

$$\sum_{i=1}^{l} \sum_{j=1}^{m} \frac{C_{l,i} C_{m,j}}{B_i + B_j} = 2\delta_{lm}. \tag{3.11}$$

In order to determine $g_m(\xi)$, one can get m equations from Eq. (3.11) as

$$\begin{aligned}
&\frac{C_{m,1}}{B_1 + B_1} + \frac{C_{m,2}}{B_1 + B_2} + \cdots + \frac{C_{m,m}}{B_1 + B_m} = 0; \\
&\frac{C_{m,1}}{B_2 + B_1} + \frac{C_{m,2}}{B_2 + B_2} + \cdots + \frac{C_{m,m}}{B_2 + B_m} = 0; \\
&\frac{C_{m,1}}{B_{m-1} + B_1} + \frac{C_{m,2}}{B_{m-1} + B_2} + \cdots + \frac{C_{m,m}}{B_{m-1} + B_m} = 0; \\
&\frac{C_{m,m}}{2}\left(\frac{C_{m,1}}{B_m + B_1} + \frac{C_{m,2}}{B_m + B_2} + \cdots + \frac{C_{m,m}}{B_m + B_m}\right) = 1.
\end{aligned} \tag{3.12}$$

Solving equation group (3.12) simultaneously, m complex constants (since B_n's are complex numbers) $C_{m,i}$ i = 1,2,...,m can be obtained.

Repeating the procedure for m = 1,m = 2,...,m = N, one gets a complete set of $C_{m,i}$ i = 1,...,m;m = 1,...,N and therefore an orthogonal set of N functions defined by Eq. (3.9). The same g_m set can be used for different boundary conditions. But every time the beam parameter set B_n is reassigned, the $C_{m,i}$ have to be recalculated to define a new set of g_m, as can be seen in Eqs. (3.11) and (3.12).

The boundary condition now can be expanded as

$$V_0(\xi) = \sum_m D_m g_m(\xi), \tag{3.13}$$

where

$$D_m = \int_0^\infty V_0(\xi) g_m(\xi) \xi \, d\xi \quad m = 1, 2, \cdots, N. \tag{3.14}$$

Substituting Eq. (3.9) into Eq. (3.14) gives

$$D_m = \sum_{i=1}^{m} C_{m,i} \int_0^\infty V_0(\xi) \exp[-B_i \xi^2] \xi \, d\xi \quad m = 1, 2, \cdots, N. \tag{3.15}$$

As can be seen, D_m depends both on the boundary condition under investigation (through $V_0(\xi)$) and the pre-assigned beam parameter set B_i (through $C_{m,i}$). Since Eq. (3.15) is a summation of m integrals, one needs to carry out N(N + 1)/2 integrals to find all N D_m's.

It is desired to express the boundary condition in terms of Gaussian beam functions directly. Substituting Eq. (3.9) into Eq. (3.13), collecting the terms with the same beam parameter B_i together, reorganizing the double summation and comparing with the boundary equation Eq. (3.8), Eq. (3.13) finally becomes

$$V_0(\xi) = \sum_{n=1}^{N} A'_n \exp[-B_n \xi^2], \tag{3.16}$$

where

$$A'_n = \sum_{m=n}^{N} D_m C_{m,n}. \tag{3.17}$$

Thus, after going through Eq. (3.11), (3.12), (3.14) and (3.17), the coefficient set A'_n is exclusively determined. The entire procedure is rigorously based on the well-developed infinite series theory and therefore requires the number N to be very large. Unfortunately, as N increases, the calculation of A'_n becomes more difficult even with the high speed computer. To emphasize the fact that Eqs. (3.16) and (3.17) hold only for large N, the notation A'_n is used in these equations to distinguish it from A_n in Eqs. (3.8).

In order to make use of the conventional procedure, the beam parameter set B_n must be pre-determined. An effort [Maciel et al., 1987] has been made to establish a uniquely defined Gaussian beam function set by discretizing the beam waist parameters. Such an approach, however, while achieving mathematical rigor, loses a degree of freedom. A great advantage of Gaussian beam functions over other base function sets is that the Gaussian beam functions provide a degree of freedom in optimizing the beam parameter set B_n which allows the boundary conditions to be matched with approximately half as many terms as would be the case otherwise, as will be shown in the next chapter.

3.3. Method II: The Optimization Procedure

The new approach for determining the coefficient and beam parameter set, developed by the author, is based on optimization theory. In the optimization, the boundary condition $V_0(\xi)$ is used as the objective function, and the left hand side of Eqs. (3.7) and (3.8) containing parameters under determination is assigned as the testing function. Let $T(\xi,A_n,B_n)$ stand for the objective function, one has

$$T(\xi, A_n, B_n) = \sum_{n=1}^{N} A_n \exp[-B_n\xi^2][1 - \frac{2B_n}{(ka)^2}(1 - B_n\xi^2)] \tag{3.18}$$

for small ka, or

$$T(\xi, A_n, B_n) = \sum_{n=1}^{N} A_n \exp[-B_n\xi^2] \tag{3.19}$$

for large ka. A quantity Q is then defined as a measure of the deviation of the testing function from the objective function:

$$Q(A_n, B_n) = \int_0^\infty [V_0(\xi) - T(\xi, A_n, B_n)]^2 \, d\xi. \tag{3.20}$$

The matching between the testing function and boundary condition can be optimized by minimizing Q. This is achieved by choosing A_n and B_n with the conditions

$$\left.\frac{\partial Q}{\partial A_n}\right|_{A_i,B_i} = 0 \qquad i,n = 1,2,\cdots,N \tag{3.21}$$

and

$$\left.\frac{\partial Q}{\partial B_n}\right|_{A_i,B_i} = 0 \qquad i,n = 1,2,\cdots,N. \tag{3.22}$$

By increasing N, the number of Gaussian beams in the testing function, one can find a set of constants A_n and B_n making Q small enough to achieve the desired accuracy. As one might expect, the number N strongly depends on the objective function (boundary conditions or other constraint), as well as the accuracy required.

3.4. Discussion of Uniqueness and Completeness

At this point, it is desirable to consider uniqueness and completeness. Generally speaking, to express an arbitrary function exactly as a superposition of an infinite number of functions in any base function set (e.g., the Gaussian beam functions with specific beam parameters), the completeness of the base function set should be proved. The coefficient set of the series corresponding to a given boundary condition should be unique. For a completely defined physical system, there is only one exact solution. But the exact solution in the Gaussian beam representation is not convenient, even though it is exact and unique. The optimization procedure presented above provides approximate solutions having satisfactory accuracies with the smallest number of Gaussian beam functions with the most desirable beam parameters. The applicable range, the accuracy, and the mathematical convenience are major considerations. The imposition of uniqueness and completeness are important mathematical exercises which would establish ultimately the validity of the specific

Gaussian beam function set. However, this is not the problem addressed in this dissertation. The problem addressed in this dissertation is the determination of a solution, not the determination of the solution.

CHAPTER IV

GAUSSIAN BEAM REPRESENTATION IN DIFFRACTION PROBLEMS

In this chapter, two procedures outlined in Chapter III: (1) the conventional procedure based on the use of the orthogonality property and (2) an optimization procedure developed by the author, are used to determine the coefficient and beam parameter sets in Gaussian beam representation. The diffraction field of a piston ultrasonic transducer is chosen as the first example of Gaussian beam representation. There are several reasons for doing so: first, a piston transducer has been widely used in mathematical representation of applications; secondly, intensive studies on the subject provide material as references; thirdly, the ultrasonic field of a rigid piston transducer exhibits a most pronounced diffraction effect because of the discontinuity of the surface velocity distribution at the transducer edge.

As a reference for comparison of solutions, the solution derived from the Rayleigh integral is outlined and briefly discussed at the beginning. The conventional procedure cannot be used immediately because it requires the base function set to be completely defined, while the beam parameter set B_n of the Gaussian beam functions are arbitrarily assignable. This problem has been an impediment to the use of Gaussian beam functions in the past, but it can now be solved by use of the optimization procedure, as will be shown.

The actual solution is begun by matching the boundary conditions. Since the ka dependence needed for describing the near field cannot be provided by the boundary matching, it is introduced by using the on-axis behavior as an additional constraint. The effect of changing the number of Gaussian beams in the optimized solutions is illustrated by three solutions having different numbers of Gaussian beams. The three B_n sets are then used in the conventional procedure to calculate the coefficient sets A_n, and the comparison between two procedures therefore becomes possible.

At this point, an alternative to the Rayleigh integral is used in on-axis matching. By using the radiating dipole for the on-axis matching, an improvement is obtained in the agreement between the field calculations at a smaller distance from the boundary. This agreement is used as an argument in favor of the radiating dipole model.

Finally, the beam field of a piston transducer supported at the edge is used to demonstrate how the use of Gaussian beam representation becomes much easier when the boundary conditions are less discontinuous. The advantages of experimentally producing a single Gaussian beam are defined as a logical consequence.

4.1. The Reference Solution from the Rayleigh Integral

The diffraction field emitted by a rigid piston transducer is one of the most fundamental problems in acoustics. The Rayleigh surface integral [Rayleigh, 1945] is considered the first exact

expression of the problem. In the axisymmetric situation, the Rayleigh integral takes the form

$$\phi(\rho,z) = A\int_0^{\infty}\int_0^{2\pi} V(r_0)\frac{\exp[-ikR]}{R} r_0\, dr_0\, d\alpha, \tag{4.1}$$

where r_0 is radial coordinate on the transducer surface, $V(r_0)$ is the boundary condition in terms of the vibration velocity distribution on the transducer surface, and R is the distance between the source element and the observation point:

$$R = \sqrt{\rho^2 + r_0^2 + z^2 - 2\rho r_0 \cos\alpha}, \tag{4.2}$$

with α the angle between $\vec{\rho}$ and $\vec{r}_0$.

In the case of a rigid piston transducer, the velocity distribution is given by the step function

$$V(r_0) = \begin{cases} 1 & r_0 \le a \\ 0 & r_0 > a. \end{cases} \tag{4.3}$$

However, even for a boundary condition as simple as Eq. (4.3), the Rayleigh integral cannot be solved analytically. Although an approximation to the farfield can be expressed in a closed form, to evaluate the nearfield and the transition zone, a numerical method—either a direct point-by-point integration or an infinite series—has to be employed. An exceptional case is the on-axis behavior. Substituting Eq. (4.3) into Eq. (4.1) and setting $\rho = 0$ in Eq. (4.2), an analytical on-axis behavior is obtained as

$$|\phi_R(z)| = \sin[(1/2)k(\sqrt{a^2 + z^2} - z)]. \tag{4.4}$$

It is found that Eq. (4.4) oscillates vigorously with z when z is small. This behavior describes, at least qualitatively, the alternation of the interference maxima and minima on the axis. As a convention, the on-axis behavior is usually plotted in terms of the Fresnel distance, defined as $z_0 = a^2/\lambda$, instead of z or the Rayleigh distance z_R given by Eq. (3.3). The difference between z_R and z_0 is only a constant factor π. Since the period and the number of oscillations varies with different values of ka, the near field, especially the extreme near field, strongly depends on ka. This is true when the solution is expressed in terms of the dimensionless variables ξ and σ defined in Eqs. (3.2) and (3.3). However, when z is large enough that the approximation

$$\sqrt{z^2 + a^2} \approx z + a^2/2z \tag{4.5}$$

holds, the ka dependence of Eq. (4.4) is removed as

$$|\phi_R(\sigma)| \approx \sin[1/(2\sigma)]. \tag{4.6}$$

Thus one sees that the diffraction field of a piston transducer predicted by the Rayleigh integral (expressed in terms of ξ and σ) is independent of ka in the farfield and that part of the nearfield where Eq. (4.5) holds. The nearfield, especially the extreme nearfield, depends strongly on ka. This ka dependence is a necessary characteristic for any good nearfield solution.

In calculating the Rayleigh integral to serve as a reference in this chapter, the on-axis behavior was calculated by Eq. (4.4). The off-axis values were evaluated by numerical integration of Eq. (4.1) with the UTCC VAX computer. The curves were plotted by use of the Techplot program of UTCC and printed by a laser printer.

4.2. Boundary Condition Matching and Its Effect on the Solution

The first solution in Gaussian beam representation was obtained by a computer optimization program based on Eqs. (3.18)-(3.22) using Eq. (4.3) as the objective function. The physical model was a typical transducer of 2-MHz in frequency and 1-inch in diameter. The characteristic value ka was 107.8 when used in water. For such a large ka, Eq. (3.18) can be replaced by Eq. (3.19). Thus A_n and B_n are actually ka independent.

Table 4.1 lists the coefficient-beam parameter set for a 15-term Gaussian beam solution to the diffraction field emitted by the piston transducer described above. The surface velocity distribution calculated by Eq. (3.8) and Table 4.1 is plotted in Fig. 4.1. Figure 4.2 shows the corresponding on-axis behavior compared with the exact on-axis solution of the Rayleigh integral in terms of the Fresnel distance z_0. One may notice that while the solution matches the boundary condition very well, the on-axis behavior does not agree with the Rayleigh integral as well as one might hope. There are two reasons for the lack of agreement. First, deviation on the boundary by the same amount (in the sense of least square fitting) but at

Table 4.1. The coefficient and beam parameter sets of a 15-term Gaussian beam solution of the field of a rigid piston transducer (without on-axis matching).

A_n			B_n		
-1.9893	−	0.8955 i	3.2546	−	10.1160 i
-0.3641	−	0.8794 i	2.8537	−	15.7653 i
0.1308	−	0.4722 i	2.5326	−	21.4236 i
0.2207	−	0.1523 i	2.2265	−	27.0111 i
0.0711	+	0.2468 i	2.2144	+	27.6977 i
0.1358	+	0.0313 i	1.8582	−	32.4326 i
-4.5373	+	4.3708 i	3.7920	−	4.6566 i
0.0389	−	0.0315 i	1.2409	+	38.1217 i
0.0101	+	0.0502 i	1.2380	−	37.4291 i
0.1206	+	0.0602 i	1.8534	+	33.1213 i
-0.1851	+	0.4245 i	2.5118	+	22.1077 i
-0.7704	+	0.4284 i	2.8204	+	16.4442 i
-1.9127	−	0.4255 i	3.2028	+	10.7807 i
-1.3775	−	5.3676 i	3.7237	+	5.2752 i
11.4211	+	2.6162 i	4.1371	+	0.2781 i

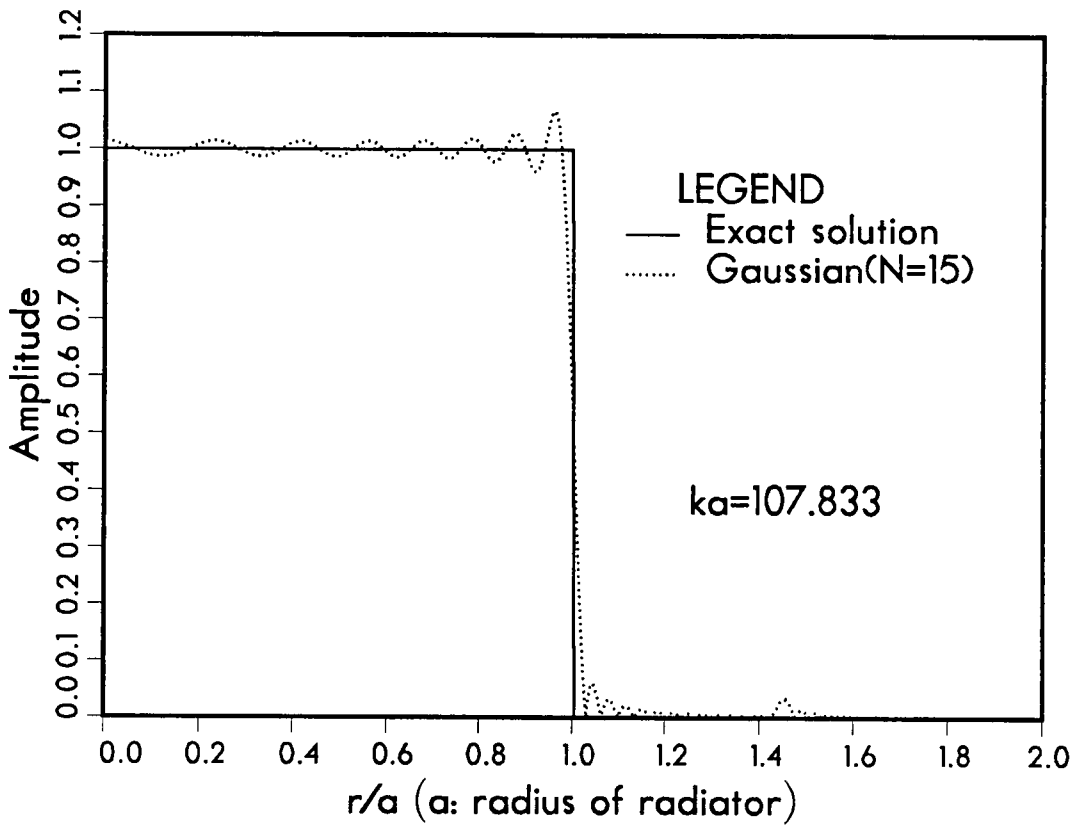


Figure 4.1. The surface velocity distribution of a 15-term Gaussian beam solution (Table 4.1) (without on-axis matching) of a rigid piston radiator.

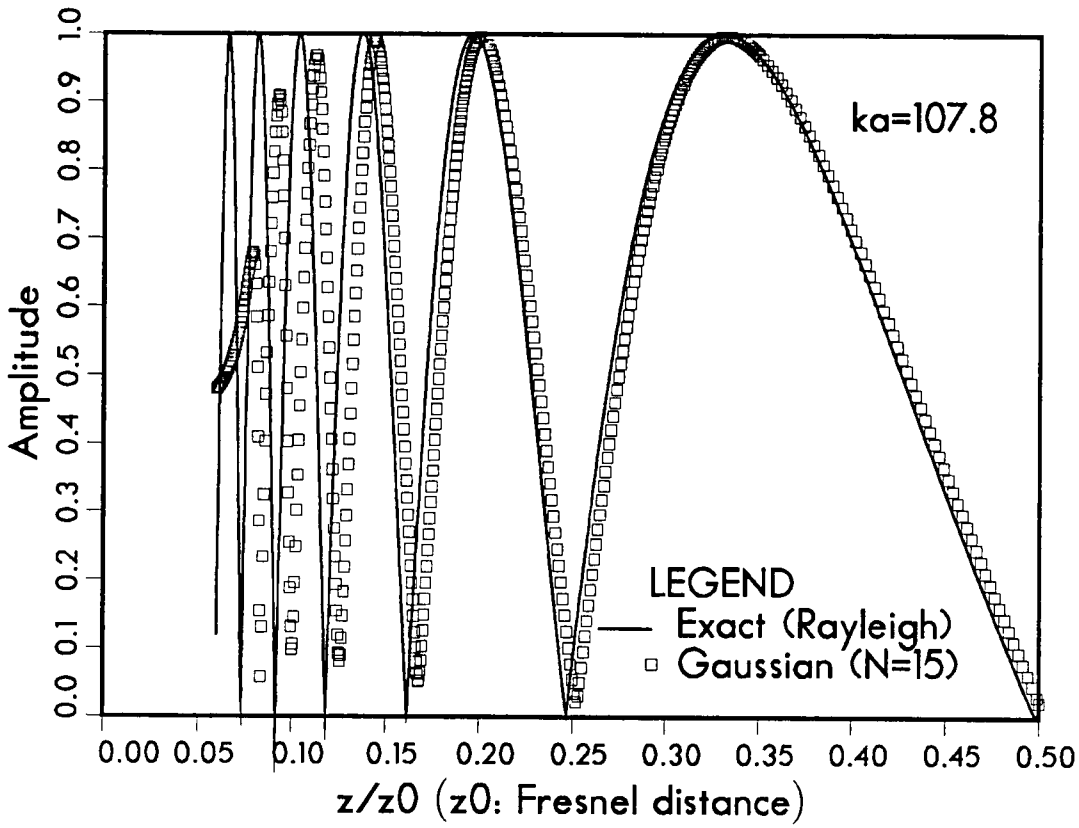


Figure 4.2. The on-axis behavior of a 15-term Gaussian beam solution (Table 4.1) (without on-axis matching) of the field of a rigid piston radiator compared with the on-axis expression of the Rayleigh integral (Eq. 4.4).

different positions (say different distances from the edge), may affect the field distribution quite differently. For this reason, the best matching on the boundary in the sense of least square fitting does not necessarily lead to the best field description as long as the matching is not perfect. Secondly, the coefficient-beam parameter set of the Gaussian beam solution obtained through Eqs. (3.18)-(3.22) is ka independent for large ka (this also is true for the general solution in terms of ξ and σ given by Eq. (3.5) over the entire range of ka). For this reason, even when the boundary matching is perfect, the Gaussian beam solution is not exceptionally good in the extreme nearfield unless the necessary ka dependence is introduced through adjustment of the coefficients A_n and beam parameters B_n. This limitation is not restricted to the Gaussian beam representation. Many other approaches such as Gaussian-Laguerre series solution suffer from the same problem [Cavanagh and Cook, 1980].

4.3. On-Axis Behavior Matching as a Constraint

An improvement in the nearfield agreement with the Rayleigh integral can be achieved by the use of an optimization procedure to match the on-axis behavior. Recalling the derivation of the Gaussian beam function from the parabolic equation, the on-axis factor g(z) is intrinsically related to the profile factors f(z) and h(z) by Eq. (2.10). For this reason, the on-axis behavior can serve as a constraint in addition to the boundary condition $V_0(\xi)$. In other words, the on-axis solution, say Eq. (4.4), can be used as the second

objective function. The corresponding testing function is obtained by substituting $\xi = 0$ into the general solution Eq. (3.5); i.e.,

$$T_2(\sigma, A_n, B_n) = |\phi(0,\sigma)| = \left| \frac{i}{k} \sum_{n=1}^{N} \frac{A_n}{1 + iB_n\sigma} \right|. \tag{4.7}$$

Writing Eq. (4.4) in terms of σ by using the relation $z = z_R\sigma$, one obtains

$$|\phi_R(\sigma)| = \sin[(1/2)k(\sqrt{a^2 + (z_R\sigma)^2} - z_R\sigma)]. \tag{4.8}$$

The quantity Q is then redefined as

$$Q(A_n, B_n) = \int_0^\infty [V_0(\xi) - T(\xi, A_n, B_n)]^2 \, d\xi + G \int_{z_1}^{z_2} [|\phi_R(\sigma)| - T_2(\sigma, A_n, B_n)]^2 \, d\sigma, \tag{4.9}$$

where G is an arbitrarily assignable weighting factor which determines the relative weight of the on-axis matching compared with the boundary condition matching. The limits z_1 and z_2 specify the range where good agreement is most important. Usually z_2 is no larger than unity because the solution usually is good beyond the Fresnel zone even without on-axis matching.

The ka dependence necessary for describing the extreme nearfield now is introduced through use of the constraint Eq. (4.8) in Eq. (4.9). A new set of coefficients A_n and beam parameters B_n determined by matching the boundary condition and the on-axis behavior simultaneously is listed in Table 4.2. The surface velocity

Table 4.2. The coefficient and beam parameter sets of a 15-term Gaussian beam solution (calculated with on-axis matching) of the field of a rigid piston transducer.

A_n			B_n		
-2.9716	+	8.6187 i	4.1869	−	5.1560 i
-3.4811	+	0.9687 i	3.8398	−	10.8004 i
-1.3982	−	0.8128 i	3.4355	−	16.3582 i
0.0773	−	0.3303 i	2.4618	−	27.7134 i
2.8798	+	1.6109 i	5.4699	+	28.6319 i
0.1259	−	0.0957 i	1.9833	−	33.2885 i
-0.2641	−	0.6723 i	2.9335	−	22.0150 i
18.0190	+	7.8291 i	6.3036	+	36.7772 i
0.0518	+	0.0182 i	1.3046	−	38.4650 i
-16.9438	−	9.9384 i	6.5889	+	37.0680 i
0.3708	+	5.4522 i	5.5518	+	22.4255 i
-6.6929	+	4.0722 i	5.4013	+	16.7326 i
-9.3638	−	4.9998 i	5.1498	+	11.1249 i
1.5872	−	15.4212 i	4.9665	+	5.6855 i
19.0024	+	3.6850 i	4.6296	+	0.3055 i

distribution calculated by Eq. (3.8) and Table 4.2 is compared with that of the rigid piston transducer in Fig. 4.3. Figure 4.4 shows the corresponding on-axis behavior compared with Eq. (4.4) which is derived from the Rayleigh integral without any approximation. The graph is plotted only up to half the Fresnel distance because there is no discernible difference between the two curves beyond this point. Excellent on-axis matching is obtained from the farfield all the way down to within 0.08 z_0 from the transducer surface. The price paid, however, is that the boundary matching in Fig. 4.3 now seems less good in the sense of least square fitting. By modifying the boundary matching to that shown in Fig. 4.3, a marked improvement in the on-axis agreement has been achieved, as shown by Fig. 4.4.

To evaluate the off-axis behavior, profiles at distances $z = 10\ z_0$ and $z = 0.13\ z_0$ were calculated using the constant set listed in Table 4.2 in Eq. (3.5). The results are given in Fig. 4.5 and Fig. 4.6. Numerical evaluation of the Rayleigh integral is used for comparison, as no analytical expression is available for the off-axis field points. Variations in the amplitude are well represented even at distances this close to the transducer surface, showing that good agreement in the on-axis behavior is accompanied by good agreement off-axis as well.

4.4. Effect of Changing Number of Gaussian Beams

To show the effect of changing the number of Gaussian beams, solutions using N = 10 and N = 6 were calculated and listed in

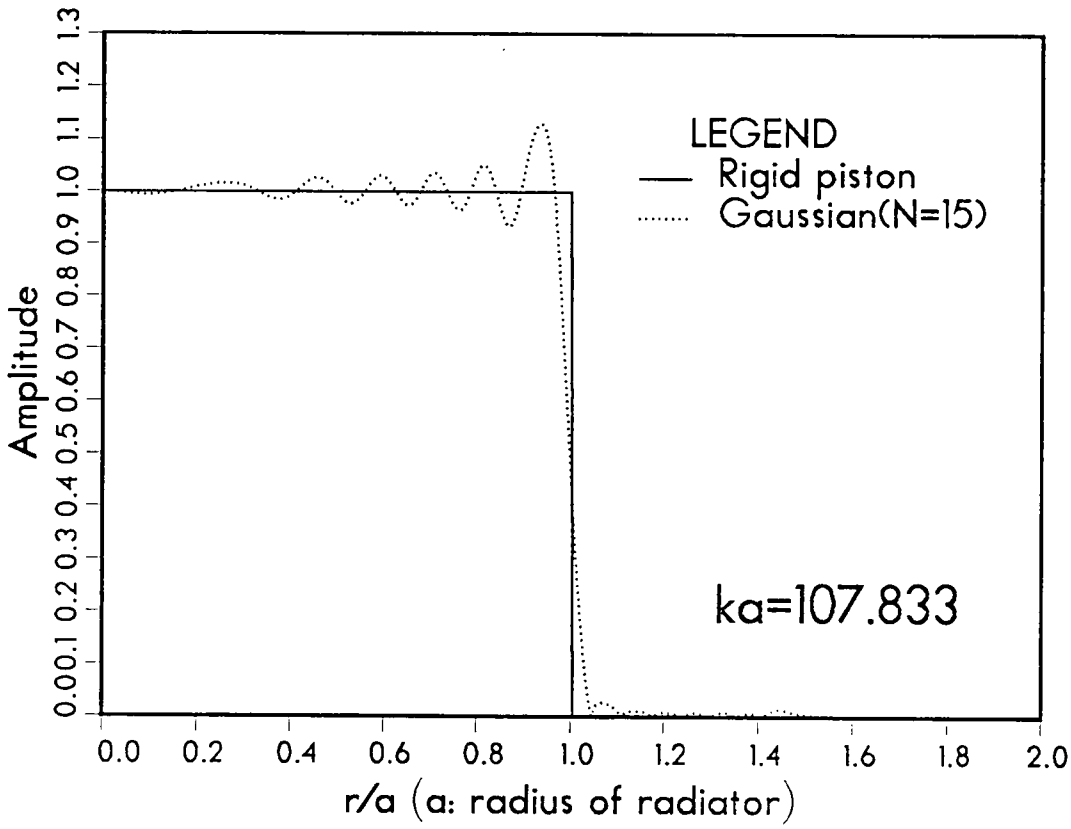


Figure 4.3. The surface velocity distribution of a 15-term Gaussian beam solution (Table 4.2) (calculated with on-axis matching) of a rigid piston radiator.

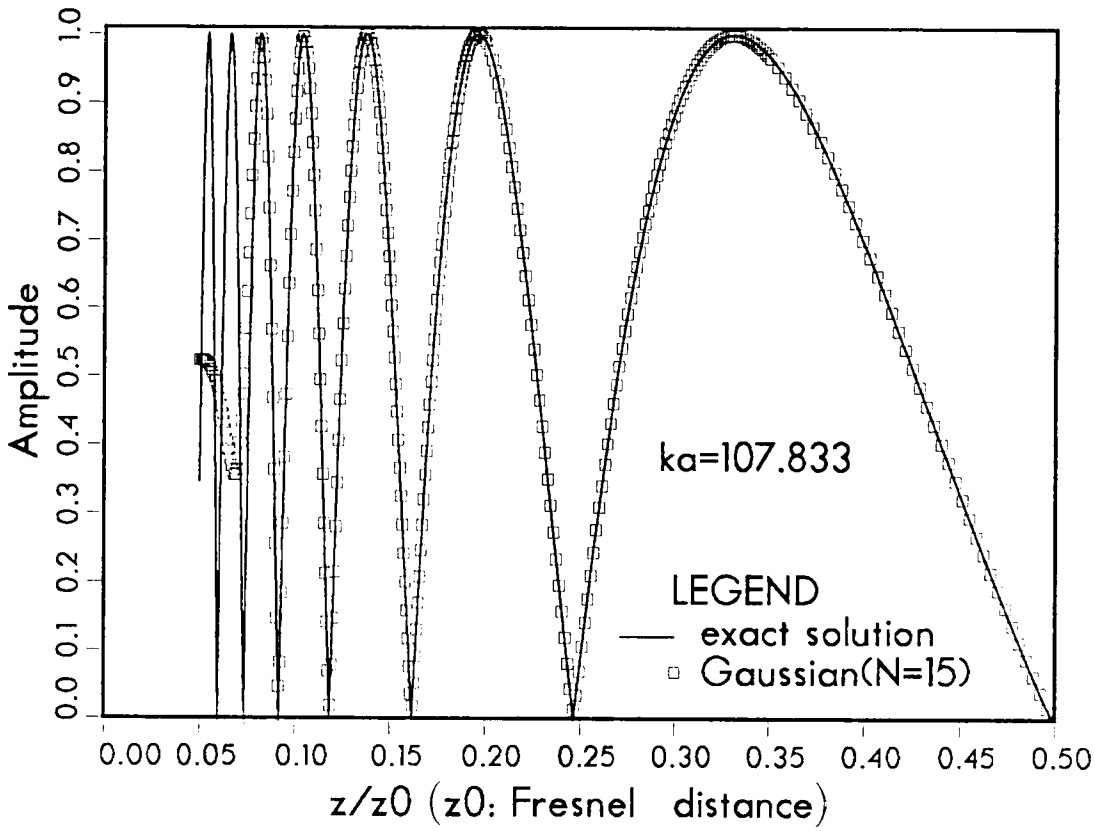


Figure 4.4. The on-axis behavior of a 15-term Gaussian beam solution (Table 4.2) (calculated with on-axis matching) of the field of a rigid piston radiator compared with the on-axis expression of the Rayleigh integral (Eq. 4.4).

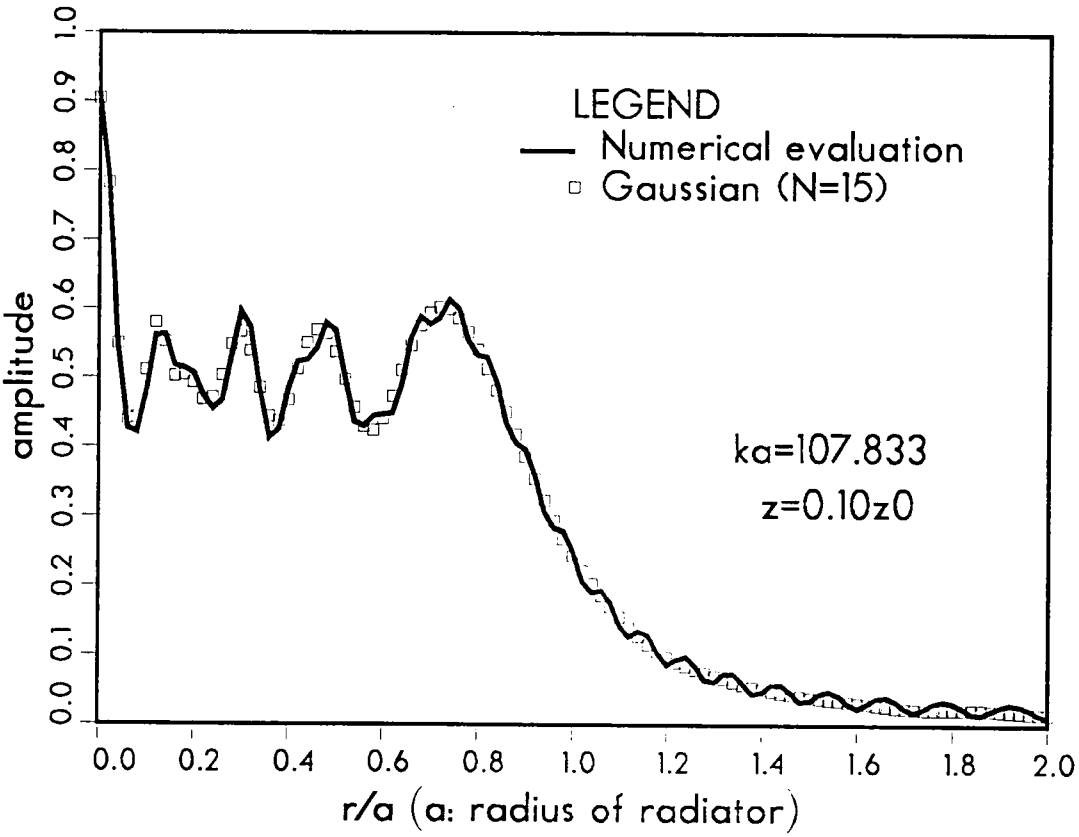


Figure 4.5. The profile at $z = 0.10\ z_0$ of a 15-term Gaussian beam solution (Table 4.2) (calculated with on-axis matching) of the field of a rigid piston radiator compared with the numerical evaluation of the Rayleigh integral.

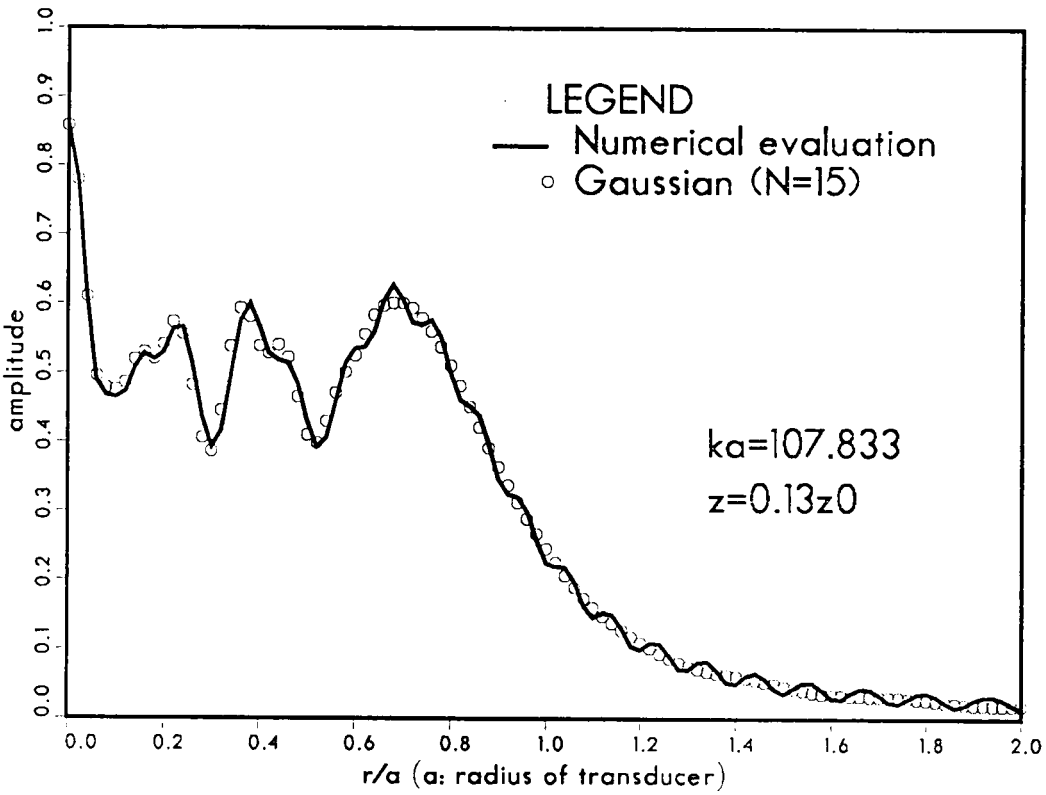


Figure 4.6. The profile at $z = 0.13\ z_0$ of a 15-term Gaussian beam solution (Table 4.2) (calculated with on-axis matching) of the field of a rigid piston radiator compared with the numerical evaluation of the Rayleigh integral.

Table 4.3 and Table 4.4, respectively. The same procedure as used in obtaining Fig. 4.4 was used in the calculation. Thus the results can be compared with Fig. 4.4 directly. As fewer Gaussian beams are used, the region where good agreement can be expected reduces unavoidably. A larger z_1, the lower limit of the on-axis matching, has to be used to ensure good agreement beyond z_1. The corresponding on-axis behaviors are given in Fig. 4.7 and Fig. 4.8. The solution of only six Gaussian beams still covers as much as 84 percent of the Fresnel zone and the entire farfield. The ten-term solution agrees with the Rayleigh integral from the farfield down to 0.12 z_0. As a comparison, a Gaussian-Laguerre series solution [Cavanagh and Cook, 1980] required as many as 65 terms to obtain a less precise agreement than that shown in Fig. 4.7 with 10 Gaussian beams.

Figures 4.9 through 4.12 illustrate the calculated profiles with the 10-term solution in Table 4.3 at 0.13 z_0, 0.25 z_0, 0.45 z_0 and z_0, respectively. As the distance from the transducer increases, the Gaussian beam solution represents the off-axis field more and more accurately. By properly specifying the range of on-axis matching so that a small range is used with a small number N, good agreement in the region of interest can be obtained even with very few Gaussian beams. A degree of freedom thus is provided by the optimization procedure. For mathematical simplicity in analytical calculation, one can use a small number of Gaussian beams. On the other hand, for accuracy in the extreme nearfield one can increase the number of Gaussian beams.

Table 4.3. The coefficient and beam parameter sets of a 10-term Gaussian beam solution (calculated with on-axis matching) of the field of a rigid piston transducer.

A_n			B_n		
11.5180	+	1.2589 i	4.0815	+	0.2655 i
0.0620	−	0.0787 i	1.1531	−	20.9080 i
-4.1687	−	8.8339 i	4.4962	+	5.1466 i
1.6644	+	2.7340 i	4.3610	+	15.0020 i
-5.1473	+	3.2632 i	4.5613	+	10.0050 i
1.1316	−	0.6847 i	3.8529	+	20.0840 i
-1.0062	−	0.2972 i	2.5279	−	10.2830 i
-2.7083	+	3.1715 i	3.3221	−	4.7685 i
-0.1409	−	0.3161 i	1.9003	−	15.7950 i
-0.2073	−	0.2396 i	2.6348	+	25.0140 i

Table 4.4. The coefficient and beam parameter sets of a 6-term Gaussian beam solution (calculated with on-axis matching) of the field of a rigid piston transducer.

A_n			B_n		
1.1218	+	1.8761 i	3.3193	+	8.5227 i
0.8993	−	0.6039 i	3.0764	+	13.3840 i
-0.0706	+	0.5206 i	1.3648	−	5.5288 i
-3.4799	+	1.0460 i	3.1949	+	3.8118 i
2.7188	−	2.5442 i	2.6552	−	0.8769 i
-0.2353	−	0.2601 i	2.2793	+	18.0730 i

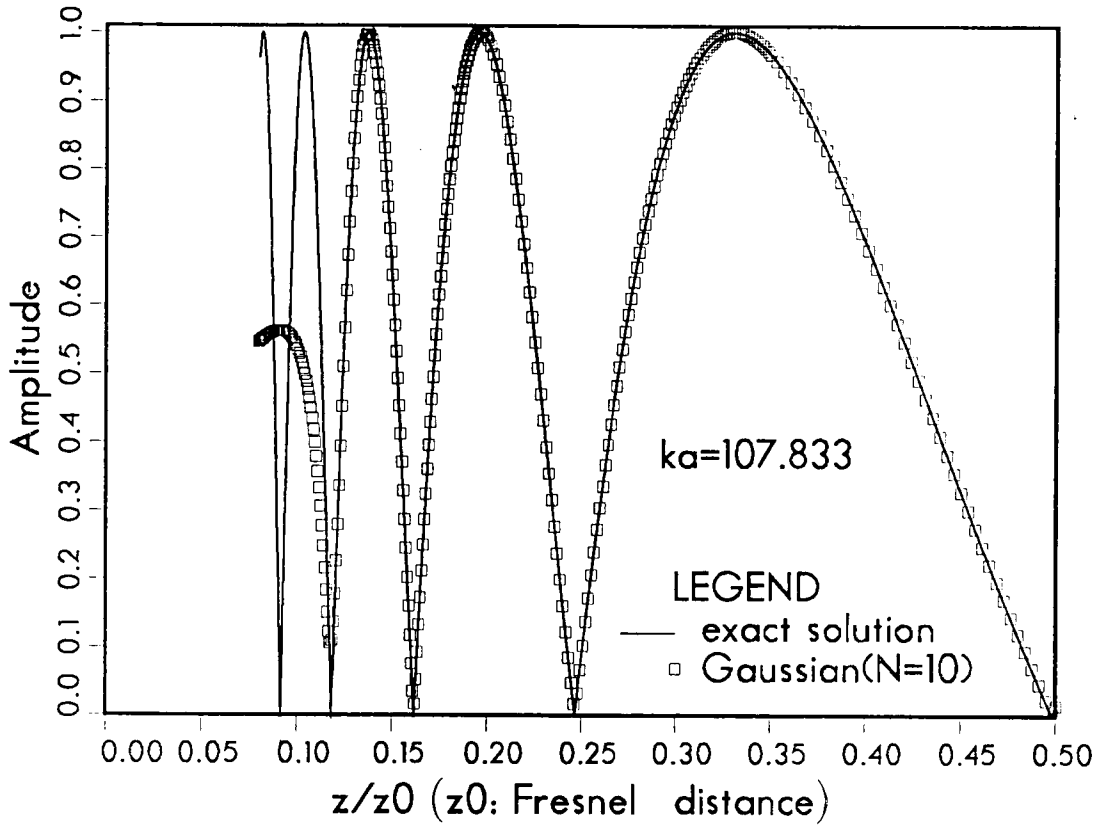


Figure 4.7. The on-axis behavior of a 10-term Gaussian beam solution (Table 4.3) (calculated with on-axis matching) of the field of a rigid piston radiator compared with the on-axis expression of the Rayleigh integral (Eq. 4.4).

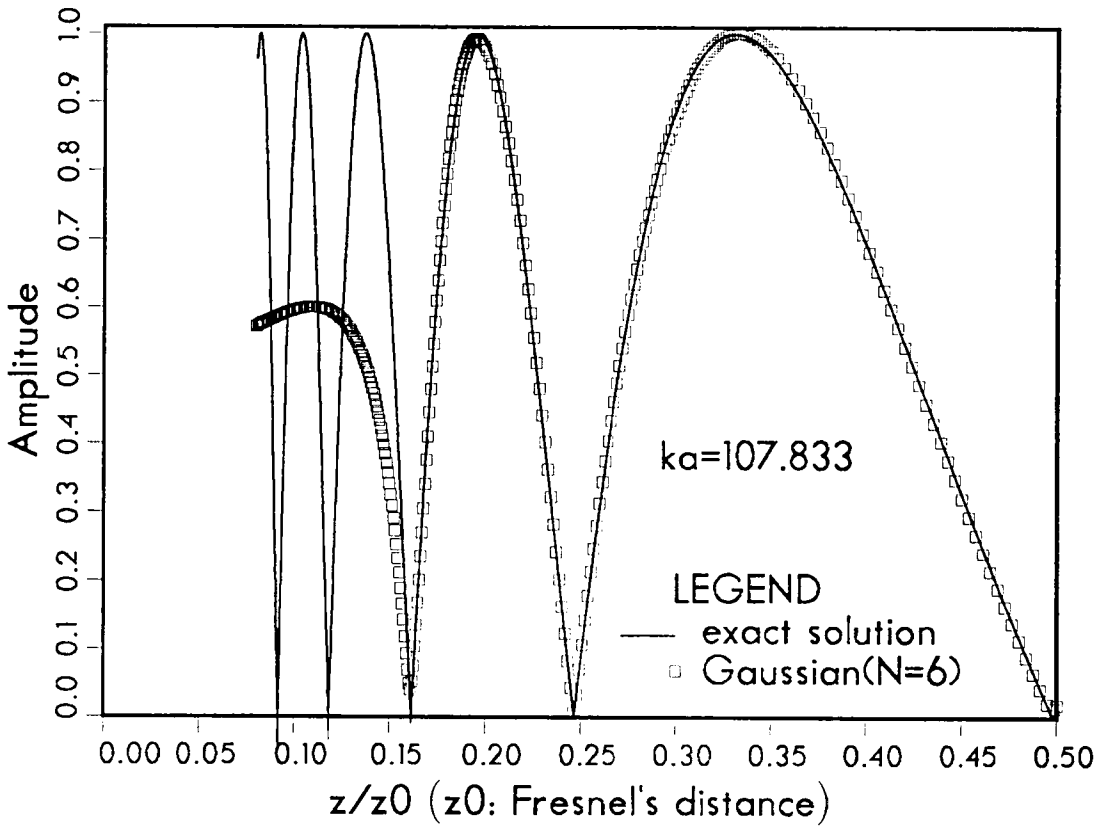


Figure 4.8. The on-axis behavior of a 6-term Gaussian beam solution (Table 4.4) (calculated with on-axis matching) of the field of a rigid piston radiator compared with the on-axis expression of the Rayleigh integral (Eq. 4.4).

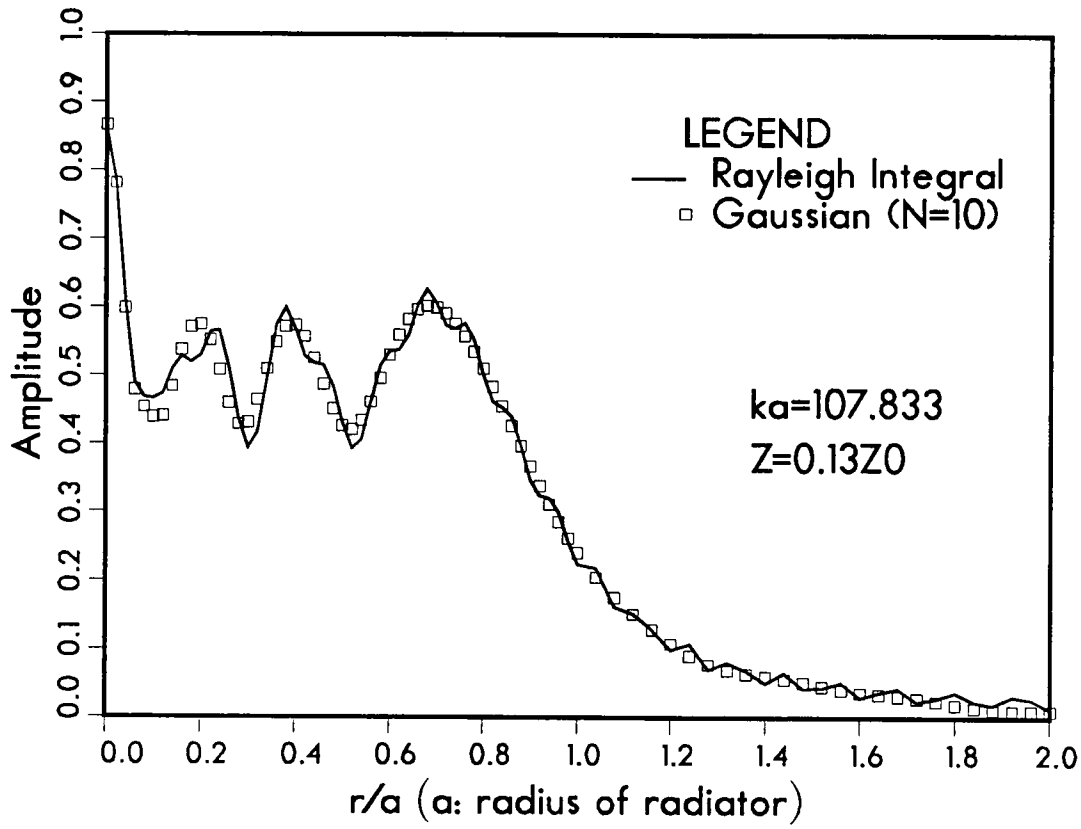


Figure 4.9. The profile at $z = 0.13\ z_0$ of a 10-term Gaussian beam solution (Table 4.3) (calculated with on-axis matching) of the field of a rigid piston radiator.

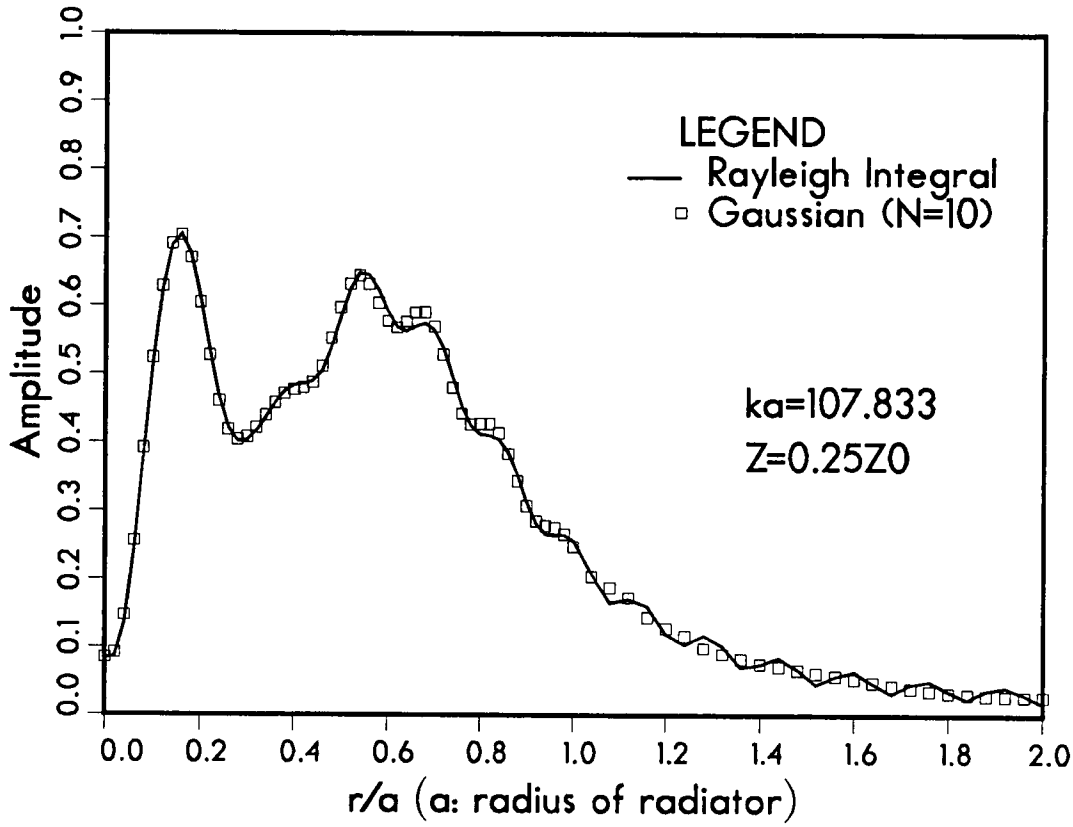


Figure 4.10. The profile at z = 0.25 z_0 of a 10-term Gaussian beam solution (Table 4.3) (calculated with on-axis matching) of the field of a rigid piston radiator.

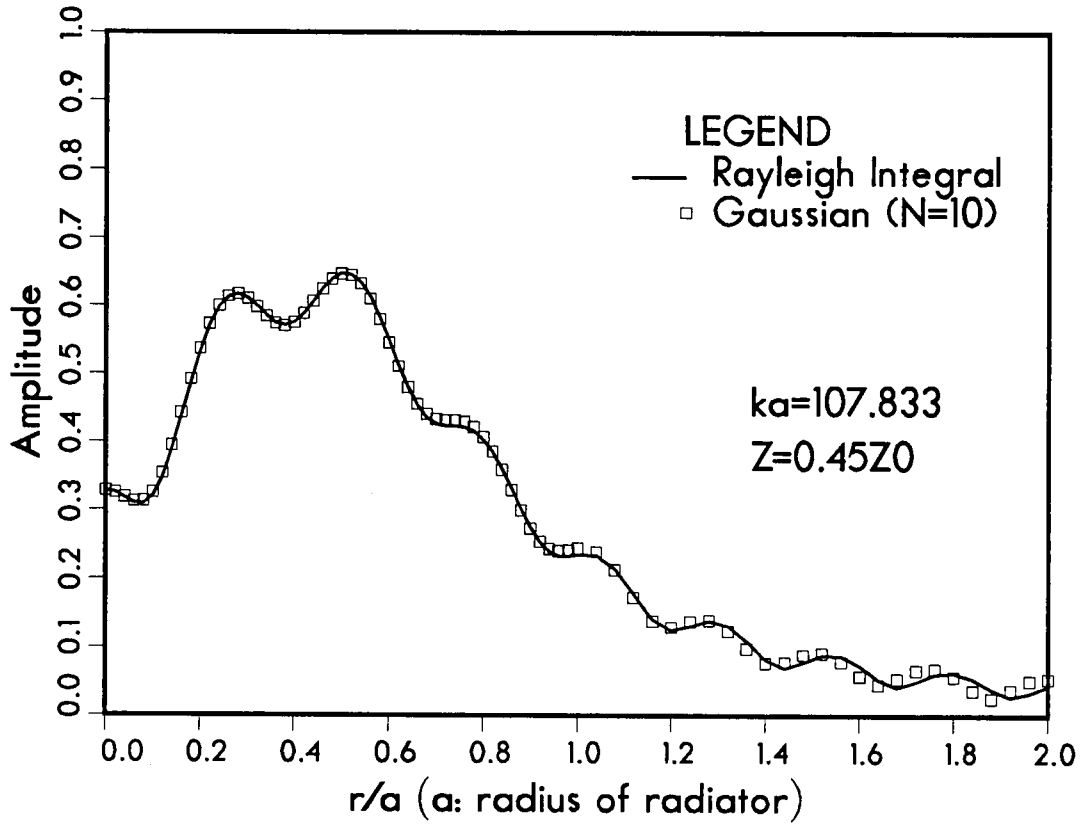


Figure 4.11. The profile at z = 0.45 z_0 of a 10-term Gaussian beam solution (Table 4.3) (calculated with on-axis matching) of the field of a rigid piston radiator.

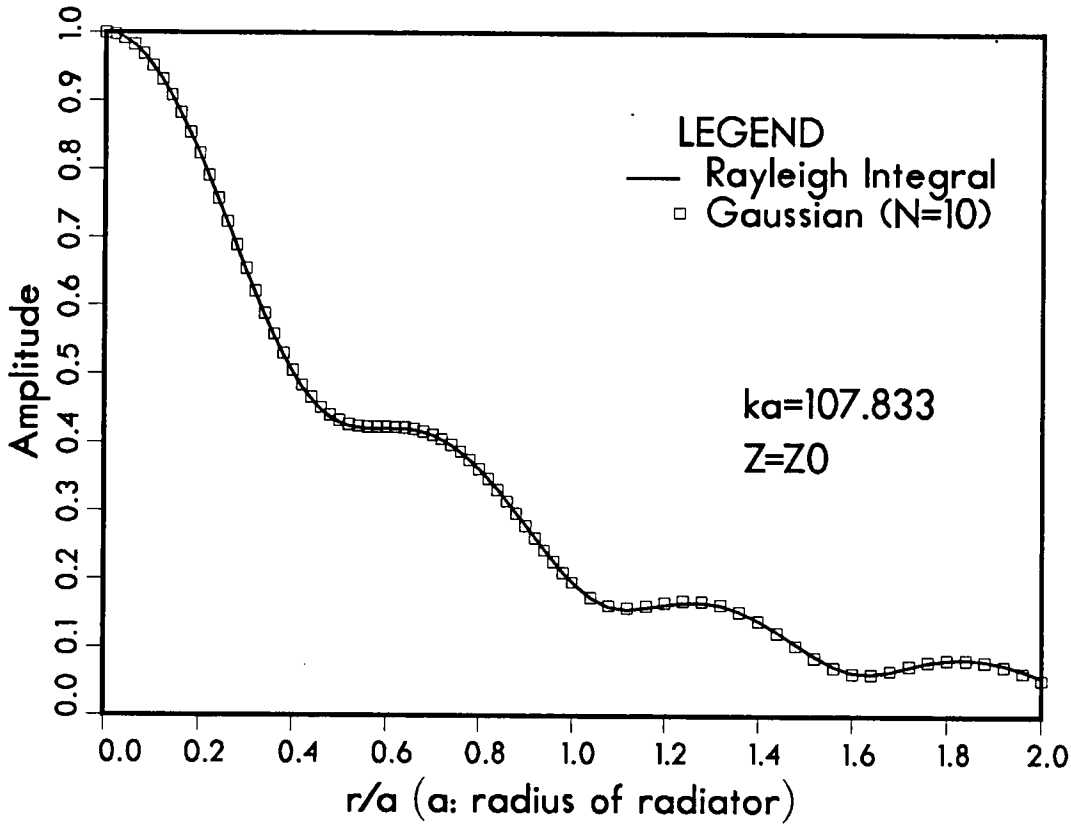


Figure 4.12. The profile at $z = z_0$ of a 10-term Gaussian beam solution (Table 4.3) (calculated with on-axis matching) of the field of a rigid piston radiator.

4.5. Use of Conventional Procedure

As discussed in the previous chapter, the use of the conventional procedure requires the beam parameter set B_n to be given before the calculation of the coefficient set A_n. Thus, the applicability of the conventional procedure depends not only on the boundary conditions but also on how properly the beam parameter set B_n is chosen. No proper way has been defined to judge a B_n set except to carry the entire procedure out, then compare the obtained solution with the given boundary conditions. Of course, one can specify a universal B_n set which covers every possible value that beam parameters may take; however, the number of terms needed could be so large that the computation may become impossibly difficult.

With beam parameter sets obtained by the optimization procedure, it now is possible to test the validity of the conventional procedure. Using the B_n sets listed in Tables 4.2 through Table 4.4 (pp. 34, 41), respectively, the coefficient sets A_n are recalculated by the conventional procedure. The newly obtained A_n' sets are used with the old B_n sets to compose a new solution, as listed in Tables 4.5 through 4.7. The calculated surface velocity distributions using 15 terms (Table 4.5) and 10 terms (Table 4.6) are plotted in Figs. 4.13 and 4.14, respectively. The results using A_n' look reasonable, although they are not as good as the one using the A_n set. However, the on-axis behavior using A_n' are rather poor, as shown in Figs. 4.15 and 4.16. The surface velocity distribution and

Table 4.5. The coefficient and beam parameter sets of a 15-term Gaussian beam solution of the field of a rigid piston transducer calculated by the conventional procedure using the B_n set in Table 4.2 (p. 34).

A'_n			B_n		
-1.8267	+	9.9575 i	4.1869	−	5.1560 i
-3.0898	+	2.2624 i	3.8398	−	10.8004 i
-1.6258	+	0.1990 i	3.4355	−	16.3582 i
-0.4190	−	0.1951 i	2.4618	−	27.7134 i
-1.5414	+	2.9500 i	5.4699	+	28.6319 i
-0.1581	−	0.2336 i	1.9833	−	33.2885 i
-0.7633	−	0.1255 i	2.9335	−	22.0150 i
-29.1930	+	14.2128 i	6.3036	+	36.7772 i
0.0303	−	0.1067 i	1.3046	−	38.4650 i
32.2813	−	11.1395 i	6.5889	+	37.0680 i
-4.3378	+	3.0054 i	5.5518	+	22.4255 i
-7.7465	−	0.9659 i	5.4013	+	16.7326 i
-7.0622	−	8.6683 i	5.1498	+	11.1249 i
4.9733	−	16.4390 i	4.9665	+	5.6855 i
21.3320	+	4.5740 i	4.6296	+	0.3055 i

Table 4.6. The coefficient and beam parameter sets of a 10-term Gaussian beam solution of the field of a rigid piston transducer calculated by the conventional procedure using the B_n set in Table 4.3 (p. 41).

A_n			B_n		
11.8797	+	1.8004 i	4.0815	+	0.2655 i
0.0161	−	0.0917 i	1.1531	−	20.9080 i
-3.1614	−	9.0210 i	4.4962	+	5.1466 i
0.9504	+	2.4513 i	4.3610	+	15.0020 i
-5.0378	+	2.1927 i	4.5613	+	10.0050 i
0.9239	−	0.4757 i	3.8529	+	20.0840 i
-1.1046	−	0.1840 i	2.5279	−	10.2830 i
-2.7922	+	3.4711 i	3.3221	−	4.7685 i
-0.2217	−	0.2776 i	1.9003	−	15.7950 i
-0.2953	−	0.1026 i	2.6348	+	25.0140 i

Table 4.7. The coefficient and beam parameter sets of a 6-term Gaussian beam solution of the field of a rigid piston transducer calculated by the conventional procedure using the B_n set in Table 4.4 (p. 41).

A_n			B_n		
51.9076	+	51.4980 i	3.3193	+	8.5227 i
-2.4445	−	153.6900 i	3.0764	+	13.3840 i
0.1725	−	0.0932 i	1.3648	−	5.5288 i
-17.7715	+	14.3348 i	3.1949	+	3.8118 i
-1.2566	−	5.2639 i	2.6552	−	0.8769 i
-34.9966	+	92.3935 i	2.2793	+	18.0730 i

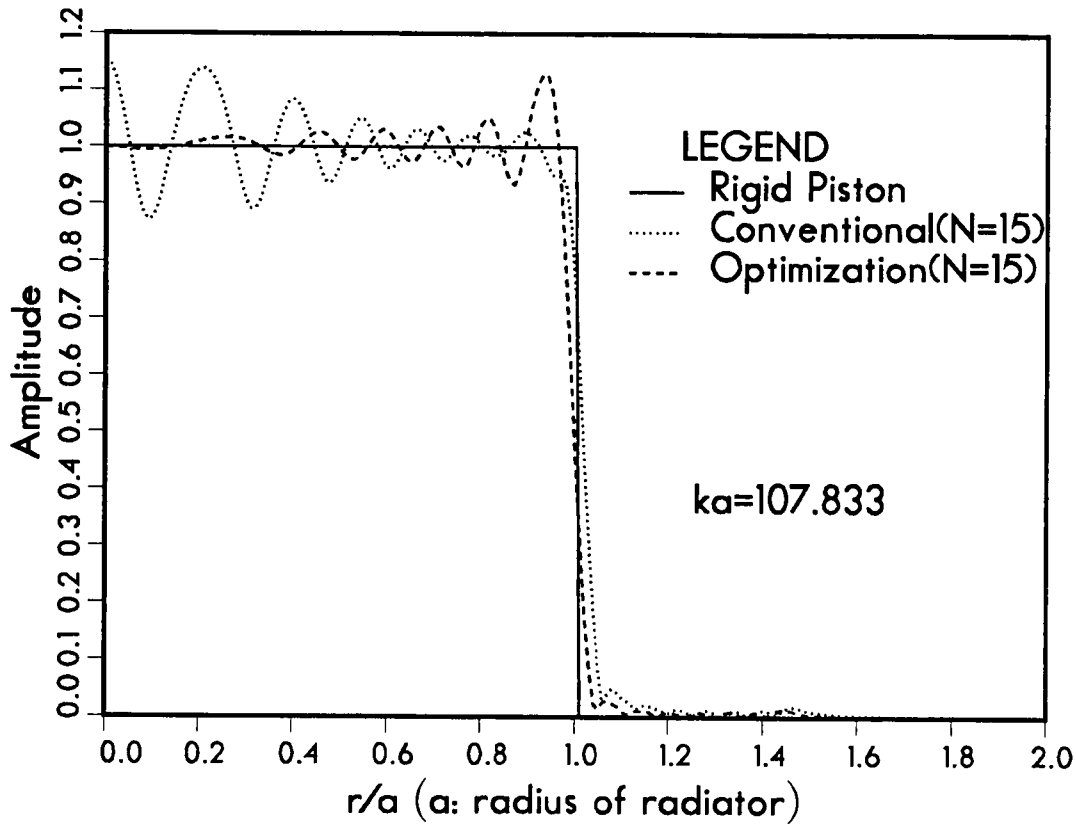


Figure 4.13. The surface velocity distributions of 15-term Gaussian beam solutions with same beam waist parameter set but different coefficient sets obtained by (a) the conventional procedure (Table 4.5); (b) the optimization procedure (Table 4.2) compared with that of a rigid piston radiator.

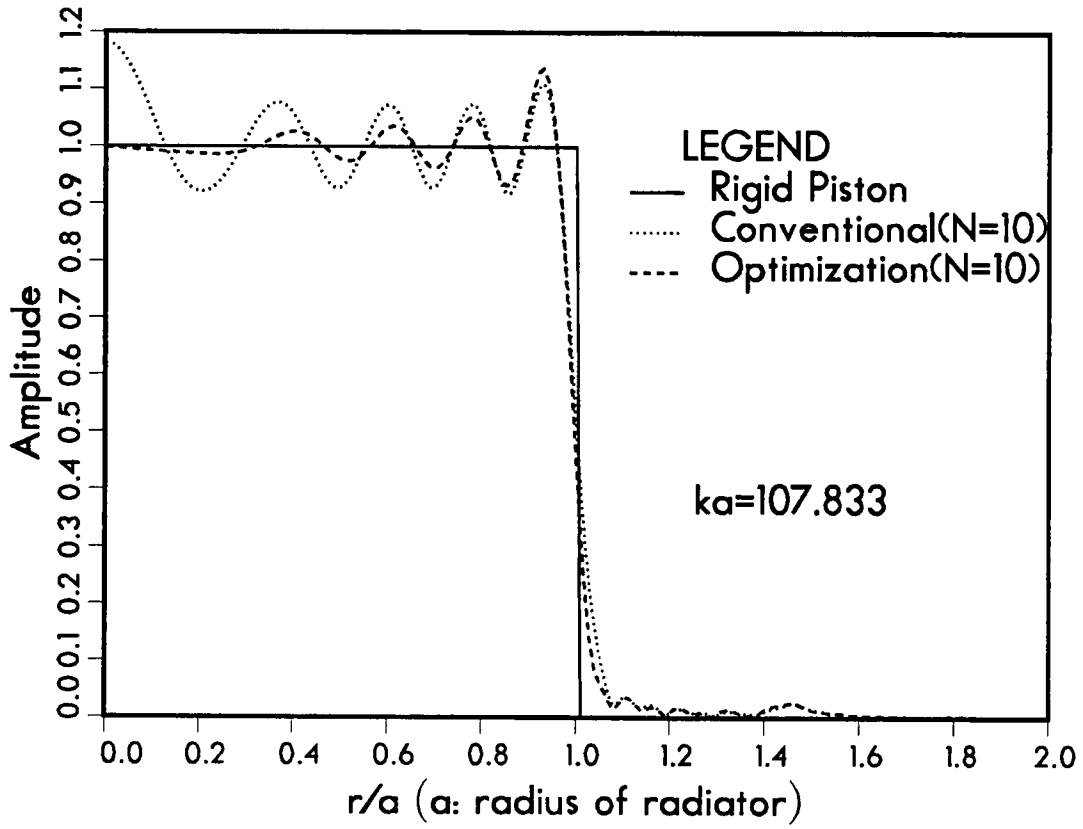


Figure 4.14. The surface velocity distributions of 10-term Gaussian beam solutions with same beam waist parameter set but different coefficient sets obtained by (a) the conventional procedure (Table 4.6); (b) the optimization procedure (Table 4.3) compared with that of a rigid piston radiator.

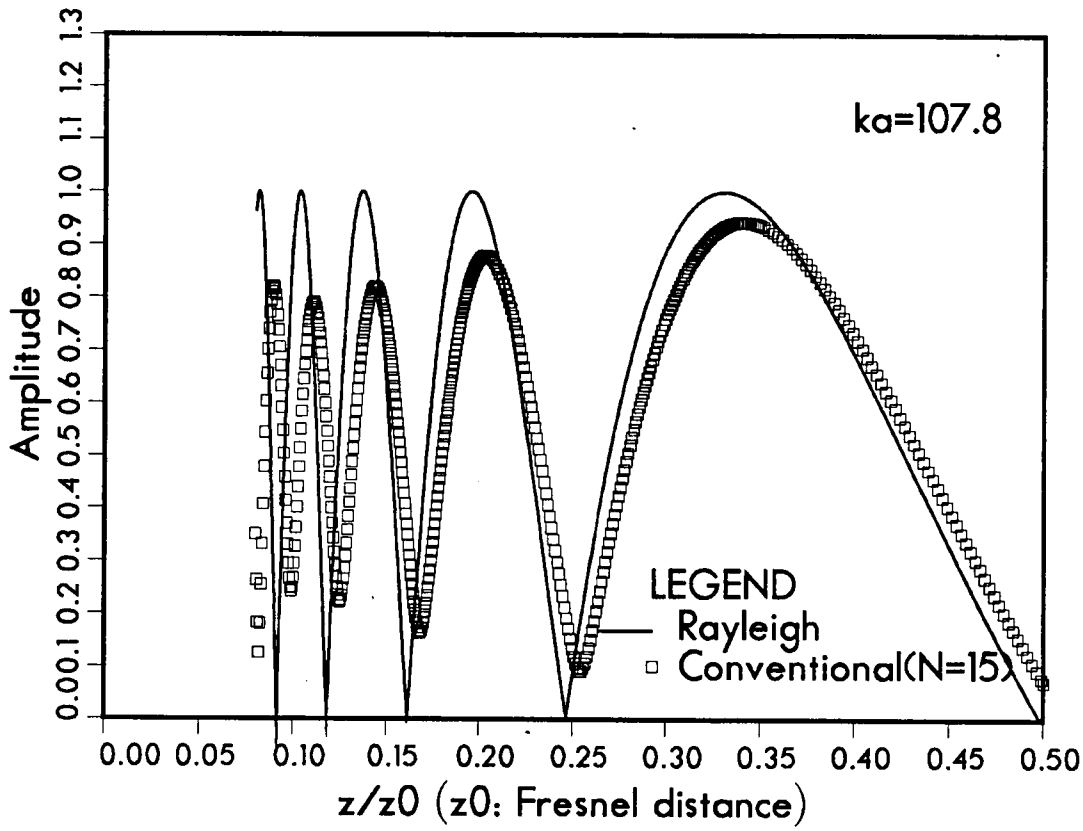


Figure 4.15. The on-axis behavior of a 15-term Gaussian beam solution (Table 4.5) obtained by the conventional procedure using a beam waist parameter set provided by the optimization procedure compared with the on-axis expression of the Rayleigh integral (Eq. 4.4).

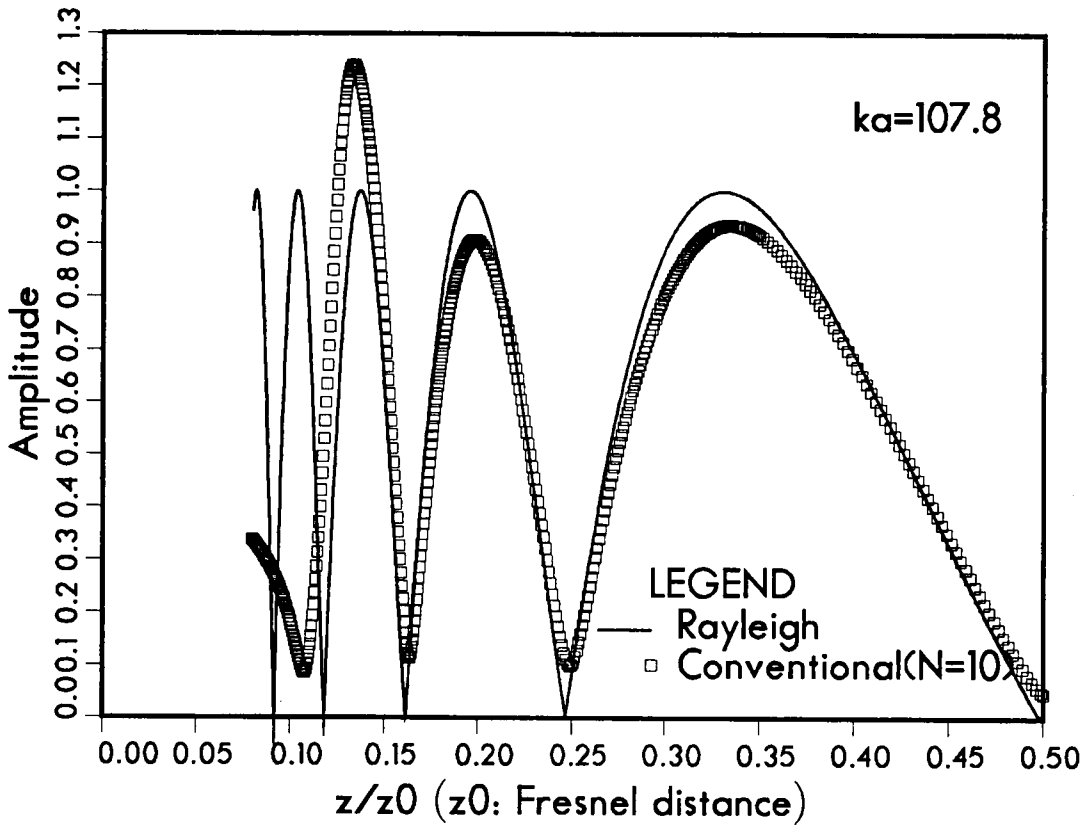


Figure 4.16. The on-axis behavior of a 10-term Gaussian beam solution (Table 4.6) obtained by the conventional procedure using a beam waist parameter set provided by the optimization procedure compared with the on-axis expression of the Rayleigh integral (Eq. 4.4).

on-axis behavior calculated with the 6-term A_n' (Table 4.7) behave so badly that the plots are meaningless, even though the same B_n set is used as was used to calculate Fig. 4.8.

A general comparison between the conventional procedure and the optimization procedure can be drawn as follows:

- The conventional procedure requires a pre-determined beam parameter set B_n, and its validity strongly depends on the B_n chosen. The optimization procedure determines the parameter set according to the imposed physical conditions in an optimized way.
- The conventional procedure requires a larger number of terms to achieve a specific accuracy. The optimization procedure can always be used to improve the result once the number of terms is specified, and can always be adjusted to accurately represent the chosen range of interest.
- Because the Gaussian beam function does not contain ka, the conventional procedure is good only in the range where the ka dependence of the field configuration is negligible— independent of the number of terms used and the accuracy of the boundary matching. This limitation can be successfully overcome in the optimization procedure through introducing the on-axis behavior as an additional constraint.

4.6. The Radiating Dipole Model as a Reference

So far the reference used in on-axis behavior matching is derived from the Rayleigh integral which is known to be based on the

Huygens' point source assumption. In the region close to the transducer surface, however, the point source assumption is not valid either from the point of view of the rigorous theory or from the experimental observation. Another integral expression based on the radiating dipole model used by a number of authors [Archer-Hall and Gee, 1980; Novikov et al., 1981] is given as

$$\phi_D(\rho,z) = A\int_0^a \int_0^{2\pi} \frac{\exp[-ikR]}{R}\left(1+\frac{1}{ikR}\right)\cos\theta\, r_0\, dr_0\, d\alpha, \qquad (4.10)$$

where the subscript D stands for dipole model, θ is the angle between $\vec{R}$ and z axis, a is the transducer radius and R is the distance between the source element and the observation point given by Eq. (4.2). When z is large relative to ρ and a, Eq. (4.10) reduces to the Rayleigh integral. Thus, the point source model is actually a farfield paraxial approximation to the radiating dipole model. A qualitative observation can be made that since a liquidous medium does not support a shear wave, a vertical vibration of a surface element cannot affect the field points in the region near the surface except those around the normal to the element. Even at large distances only the axial component, not the absolute amplitude, actually contributes to the field. This is the reason the factor $\cos\theta$ appears in the radiating dipole model but is neglected in the Rayleigh integral. Thus one sees why the radiating dipole is a better physical model of a source element for nearfield description. In the farfield, the difference between the two models becomes so

small that the two solutions merge into each other, as can be expected. The on-axis behavior of Eq. (4.10) can also be exactly expressed in a closed form as

$$\phi_D(0,z) = \frac{1}{2}\left(\exp\left[-ikz\right] - \frac{z}{\sqrt{a^2+z^2}}\exp\left[-ik\sqrt{a^2+z^2}\right]\right). \qquad (4.11)$$

Using Eq. (4.11); i.e., the radiating dipole model as the objective function in on-axis matching, a new solution is calculated and the coefficient and beam parameter sets are given in Table 4.8.

Table 4.8. The coefficient and beam parameter sets of a 15-term Gaussian beam solution of the field of a rigid piston transducer using radiating dipole model as the on-axis constraint.

A_n			B_n		
-3.3752	−	1.2752 i	3.7945	−	10.1365 i
-0.4823	−	1.3242 i	3.2479	−	15.6435 i
0.1864	−	0.1182 i	2.0325	−	26.9242 i
0.1792	−	0.5171 i	2.6225	−	21.3033 i
-1.1471	+	3.7038 i	5.8735	+	30.2284 i
19.1640	+	3.6494 i	8.5257	+	39.0641 i
-7.2914	+	6.3246 i	4.1858	−	4.5739 i
-14.4237	−	2.6640 i	7.4153	+	39.6390 i
0.0652	+	0.0255 i	1.2867	−	32.1611 i
-0.3694	+	0.0324 i	4.4570	+	49.0526 i
-4.6660	+	2.9117 i	5.7013	+	23.6269 i
-6.8490	−	2.2841 i	5.3979	+	17.6507 i
-3.4697	−	8.8526 i	5.0992	+	11.8571 i
8.6279	−	10.7060 i	4.8915	+	6.3090 i
14.8434	+	11.0720 i	4.5816	+	0.8554 i

Figure 4.17 shows the surface velocity distribution calculated using Table 4.8. With the same number of terms and similar boundary condition matching, good on-axis agreement now is obtained in an even larger range, down to 0.06 z_0, as shown in Fig. 4.18. This indicates that the radiating dipole model is a better reference for evaluating the field calculation than the Rayleigh integral (point source model) even though the Rayleigh integral is most often used. The radiating dipole model also appears to represent the physical situation more accurately.

4.7. Piston Transducer Supported at the Edge

All the above solutions have one feature in common: the most serious disagreement of boundary matching is located near the edge where abrupt variation in velocity amplitude occurs. A physical discontinuity almost always results in such mathematical difficulties. Greenspan [1979] and Novikov et al. [1981] describe discontinuous distribution functions of different degree by a general form

$$V_0(\xi) = \begin{cases} (n+1)(1-\xi^2)^n & \xi \leq 1 \\ 0 & \xi > 1 \end{cases} \tag{4.12}$$

where n is an integer discontinuity parameter. The smaller the n, the larger the sharpness at the edge. The piston transducer described by the step function Eq. (4.3) is the special case of Eq. (4.12) with n = 0. As the second example of Gaussian beam representation, the field of the next most difficult case n = 1 which Greenspan [1979]

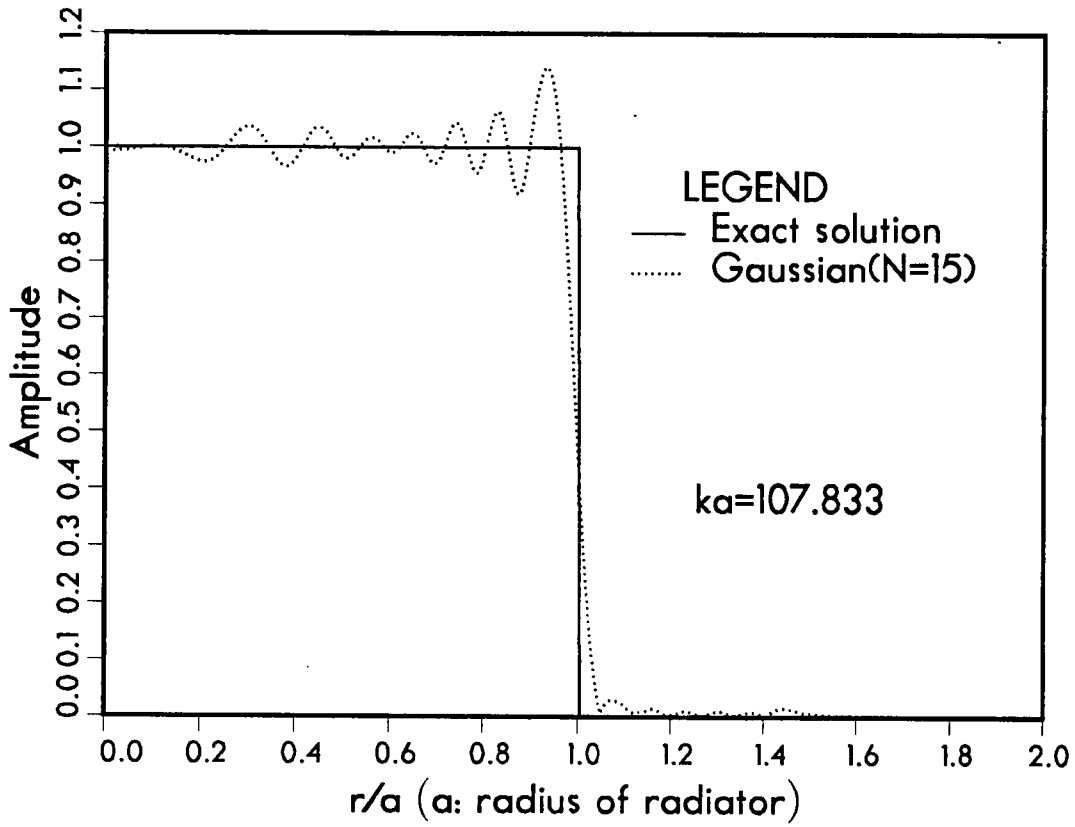


Figure 4.17. The surface velocity distribution of a 15-term Gaussian beam solution calculated using radiating dipole as on-axis constraint (Table 4.8) compared with the one of a rigid piston radiator.

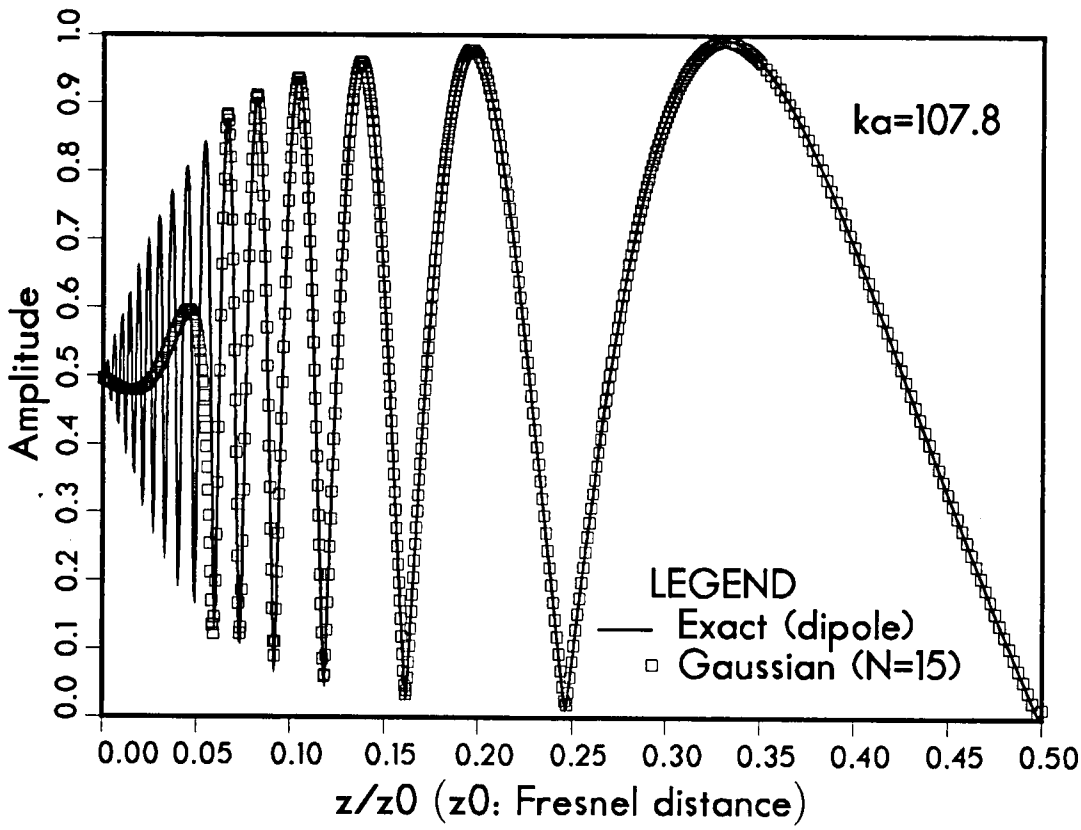


Figure 4.18. The on-axis behavior of a 15-term Gaussian beam solution calculated using radiating dipole model as on-axis constraint (Table 4.8) compared with the exact on-axis expression given by Eq. 4.11.

referred to as a piston simply supported at r = a (i.e., $\xi = 1$) was calculated with 6 Gaussian beam functions. The set of coefficients A_n and the beam parameters B_n used in the solution are listed in Table 4.9. The calculated surface velocity distribution and the on-axis behavior compared with the Rayleigh integral are given in Figs. 4.19 and 4.20, respectively. It can be seen that as the edge effect now is less significant, a 6-term solution has achieved a considerably better agreement with the Rayleigh integral than that given in Figs. 4.3 and 4.4 (pp. 37, 37), for the rigid piston with 15 terms.

Table 4.9. The coefficient and beam parameter sets of a 6-term Gaussian beam solution (calculated with on-axis matching) of the field of a piston transducer supported at r = a.

A_n			B_n		
0.5491	−	1.6184 i	3.8738	−	2.0743 i
-0.0236	+	0.0054 i	1.4663	+	11.8560 i
0.5618	+	1.6190 i	3.8964	+	2.0488 i
-0.0313	+	0.2580 i	2.7802	−	6.6559 i
-0.0345	−	0.2590 i	2.8336	+	6.6903 i
-0.0236	−	0.0051 i	1.4211	−	11.6910 i

4.8. Gaussian Beam and Gaussian Transducer

As the distontinuity parameter n in Eq. (4.12) increases, and the edge effect becomes smaller and smaller, the number of Gaussian beams needed to represent the diffraction field decreases. With $V_0(\xi)$ a Gaussian function, as long as the beam field condition of

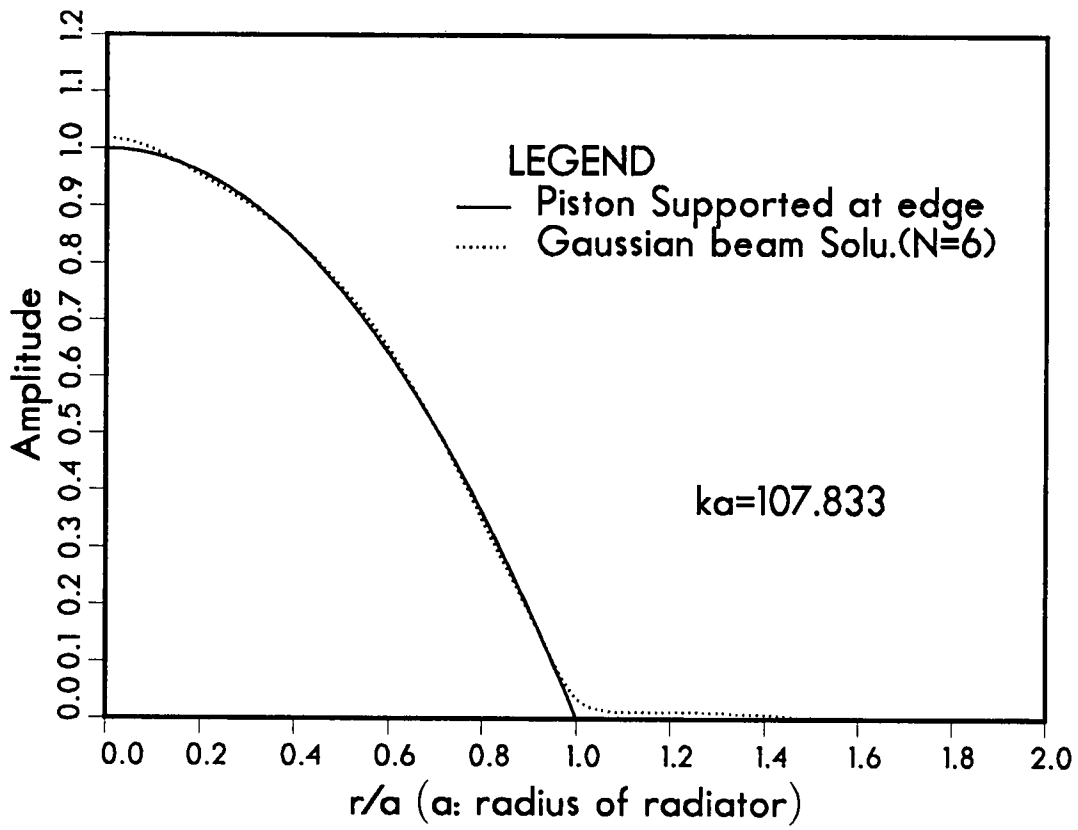


Figure 4.19. The surface velocity distribution of a 6-term Gaussian beam solution (Table 4.9) (calculated with on-axis matching) of a piston radiator supported at r = a.

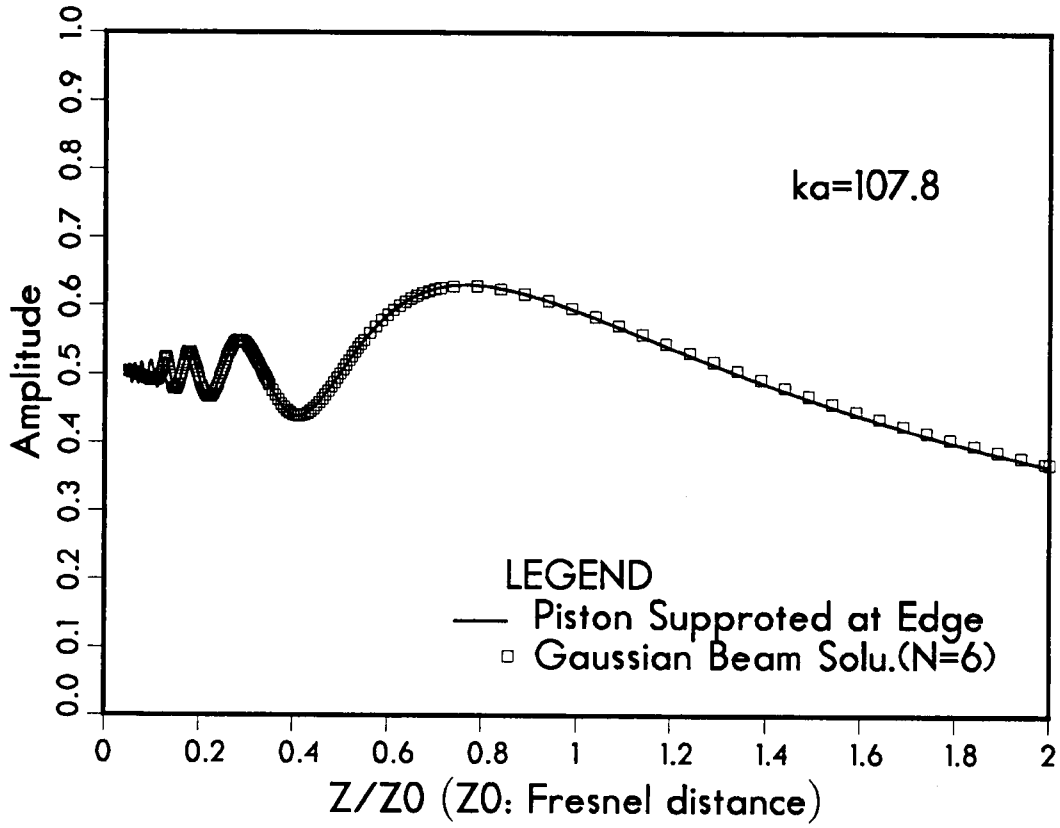


Figure 4.20. The on-axis behavior of a 6-term Gaussian beam solution (Table 4.9) (calculated with on-axis matching) of the field of a piston radiator supported at r = a compared with the exact on-axis expression.

Eq. (2.5) holds so that the boundary condition Eq. (3.8) applies, only one Gaussian beam matches the boundary condition perfectly. Thus a conclusion drawn by previous workers [Novikov et al., 1981; Du and Breazeale, 1985] using an integration approach is reached here: the radiated field of a Gaussian transducer is a single Gaussian beam. Unlike the plane wave, the Gaussian beam is not simply an idealized model. The Gaussian beam can be realized as a physical result. The required Gaussian amplitude distribution has been achieved by shading of the electric field in a transducer [Martin and Breazeale, 1971; Du and Breazeale, 1985]. An improved Gaussian transducer is used to obtain experimental results reported in the next chapter.

CHAPTER V

EXPERIMENTAL VERIFICATION—GAUSSIAN ULTRASONIC BEAM

The Gaussian beam not only is an ideal mathematic model, but it also is physically realizable. However, the previously available Gaussian transducer designs [Martin and Breazeale, 1971; Du and Breazeale, 1985] have been limited by the condition $2 < D/t < 4$, where D is the waist width (for 2-dimensional case) or the waist diameter, and t is the thickness of the piezoelectric material. Since t is proportional to the inverse of the frequency used, this limit means that for a 2 MHz transducer, the diameter (or width for 2-dimensional case) of the Gaussian beam is restricted to values between 2.87-5.74 mm. This limitation has been removed with a new transducer. Experimental results with the new transducer are reported in this chapter.

5.1. The Gaussian Transducer

The sufficient condition for producing a Gaussian beam requires a Gaussian velocity distribution on the radiator (transducer) surface. The Gaussian coefficient could be either a real or a complex number (the latter produces a focused Gaussian beam). A transducer satisfying this condition is a Gaussian transducer. When an x-cut quartz is used as the piezoelectric material (other materials require a detailed mathematical analysis), the velocity distribution

is simply proportional to the normal component of the driving electric field intensity on the transducer surface. The problem becomes to satisfy the condition

$$\left.\frac{\partial E}{\partial z}\right|_{z=0} = E_0 \exp[-\rho^2/w^2], \tag{5.1}$$

where w is the radius at the beam waist (minimum cross section) and E_0 stands for the amplitude of the electric field at the point ($z = 0$, $\rho = 0$).

Several reports have been made on Gaussian transducer development. Von Haselberg and Krautkrämer [1959] proposed a back electrode configuration as an eight-pointed star with the arms shaped so that the area of electrode is roughly Gaussian as a function of radius. An obvious shortcoming of this design is the lack of axial symmetry in the electric field distribution. The piezoelectric material spacing the two electrodes apparently needs to be thick enough to round out the uneven distribution between lobes. In another Gaussian transducer reported by Martin and Breazeale [1971], a narrow strip is employed as the back electrode. When the ratio of the strip width w and the thickness of the piezoelectric material t is between 2 and 4, and the length of the strip l is much greater than t, the electric field on the front electrode is an approximate 2-dimensional Gaussian function due to the electric fringing between the strip and the grounded front electrode [Breazeale et al., 1981]. This Gaussian transducer was used in studying the reflection at the

Rayleigh angle by a schlieren system, and achieved the reflected field predicted for a Gaussian beam incidence [Breazeale et al., 1974; Breazeale et al., 1977]. Du and Breazeale [1985] extended the idea to the 3-dimensional case by using a small disk as the back electrode. Both these transducers are limited by the condition $2 < D/T < 4$ stated at the beginning of this chapter. In many ultrasonic applications, high frequency (thus small t) for good resolution and large beam width for good collimation are desired simultaneously. This also is required to get a large value of ka as assumed in the theory [Chapter II, Section 2.1]. The limitations on frequency and beam size restrict the application of this type of Gaussian transducers.

A Gaussian transducer operating at 4-MHz frequency with a 0.36 inch beam diameter has been made by a new approach developed recently. The new design involves an electrode modification which permits a Gaussian transducer to be made in any size and to work at any frequency. The new transducer has a D/t ratio of 12.74 which is much beyond the limitation imposed on previous Gaussian transducers. An experimental study of the field distribution produced by this transducer is presented as an experimental verification of the physical existence of a Gaussian beam of high frequency and large beam waist.

5.2. Experimental Technique and Field Distribution Study

The experiment was divided into two parts: the schlieren photography and the measurement of the relative field distribution.

The schlieren system used for photographing an ultrasonic field is shown in Fig. 5.1. Light from a 15-milliwatt helium-neon laser is focused onto a circular aperture several microns in diameter fixed in a thin metal plate. Lens 2 is positioned such that the aperture is exactly located at the focal point of the lens. The light passing through Lens 2 becomes parallel and uniformly distributed. A tank filled with water is placed at the position shown. A Gaussian transducer in the tank is driven by a Johnson-Viking CDC generator with a continuous sinusoidal RF voltage at 4 MHz, the resonant frequency of the transducer. An absorber is placed at the other end of the tank to suppress reflection. Lens 3 is positioned so that an object in the tank is imaged on the screen. The ultrasonic field generated by the transducer functions as a diffraction grating so that some of the passing light rays are deviated from the original direction parallel to the axis of the lens. Light rays not diffracted by the sound field are focused by Lens 3 onto its focal point and are blocked by a small black spot positioned there. The diffracted light rays passing by the black spot produce an image of the sound field on the screen. Replacing the screen by a photographic negative, a picture of the ultrasonic field radiated by the transducer can be obtained.

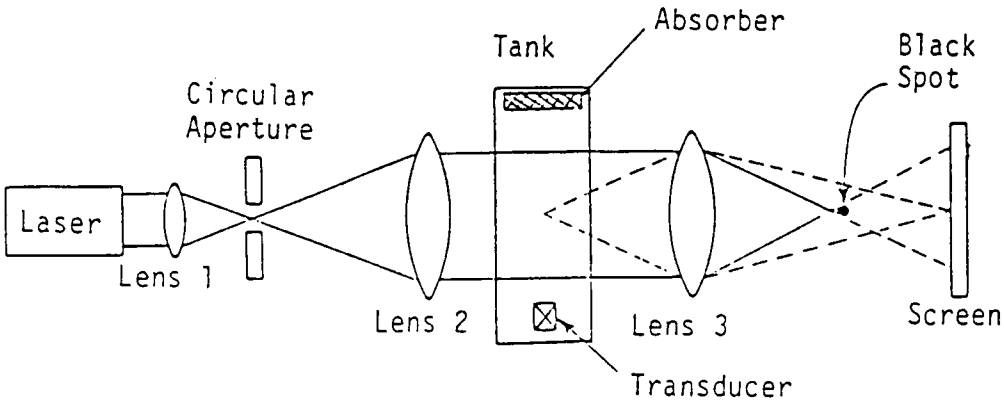


Figure 5.1. Schlieren system.

Figure 5.2 shows three pictures of the same sound beam taken with increasing exposure time. The frequency of the sound beam is 4-MHz and the waist diameter is 0.36 inch. A remarkable feature one can see is that the beam is completely free of sidelobes and of interference maxima and minima in the Fresnel zone, as predicted by the theory. As the exposure time is doubled from one exposure to the next, the beam image is broadened due to Gaussian distribution across the profile. The final image gives considerable detail in the beam skirt, but one still cannot detect the presence of sidelobes. For comparison, a similar photograph of the field of a piston transducer is shown in Fig. 5.3. The simplification in the beam pattern achieved by the Gaussian transducer is apparent.

A more quantitative investigation of the field distribution was made by a hydrophone which has a nominal resolution of 1-millimeter. The Gaussian transducer now is driven by a pulsed sinusoidal RF voltage. A hydrophone is mounted on a 3-dimensional scanning system to measure the relative field amplitude point by point. The measured on-axis data are plotted in Fig. 5.4. The transverse profiles from $z = 20$ mm up to $z = 300$ mm are given in Figs. 5.5 through 5.12. All plots are compared with the theoretical predictions represented by solid curves. An absorption factor $\exp[-\alpha f^2 z]$ is included in the theoretical calculation where $\alpha = 2.5 \times 10^{-14}$ (sec /m) is the absorption coefficient of water at room temperature. Good agreement between theory and experiment throughout the sound field confirms the behavior seen in the schlieren photograph.

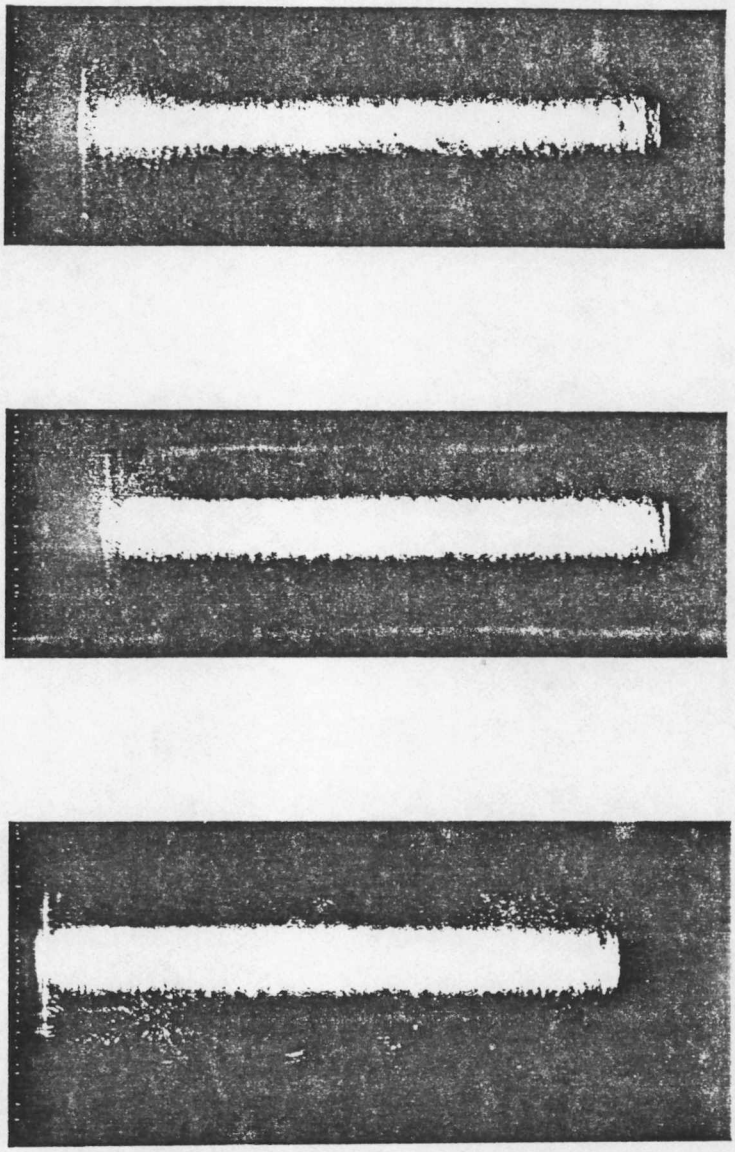


Figure 5.2. Schlieren photographs of the ultrasounic field produced by a 4 MHz, 0.36 inch diameter Gaussian transducer. The exposure time is doubled from one exposure to the next.



Figure 5.3. Schlieren photograph of the field of a piston transducer.

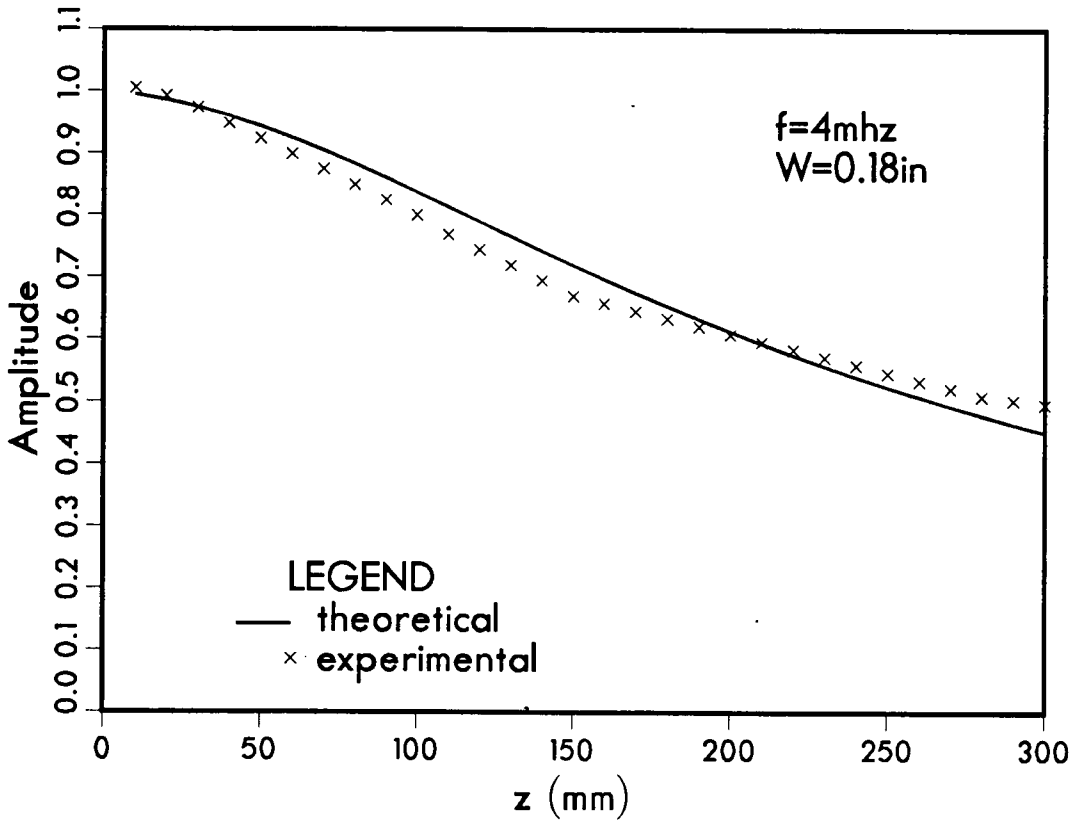


Figure 5.4. The measured on-axis behavior of the beam field produced by a 4 MHz, 0.36 inch diameter Gaussian transducer compared with theory.

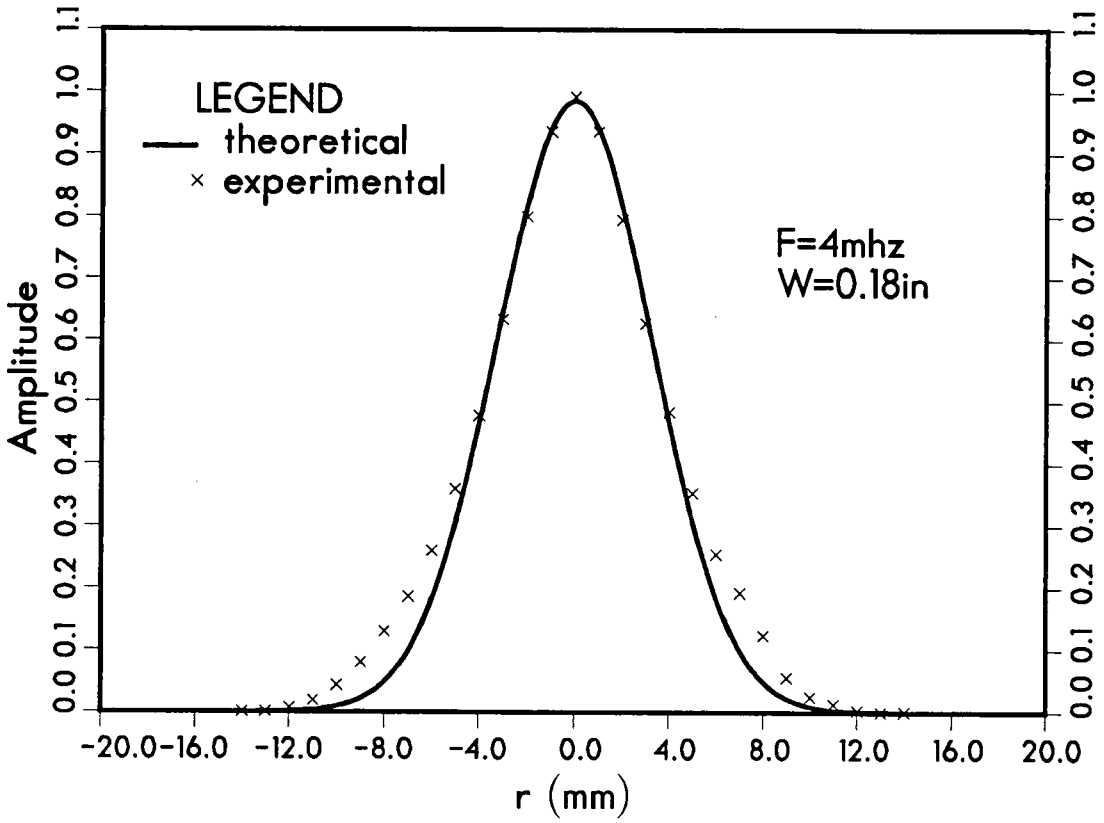


Figure 5.5. The measured transverse profile of the beam field produced by a 4 MHz, 0.36 inch diameter Gaussian transducer at z = 20 mm compared with theory.

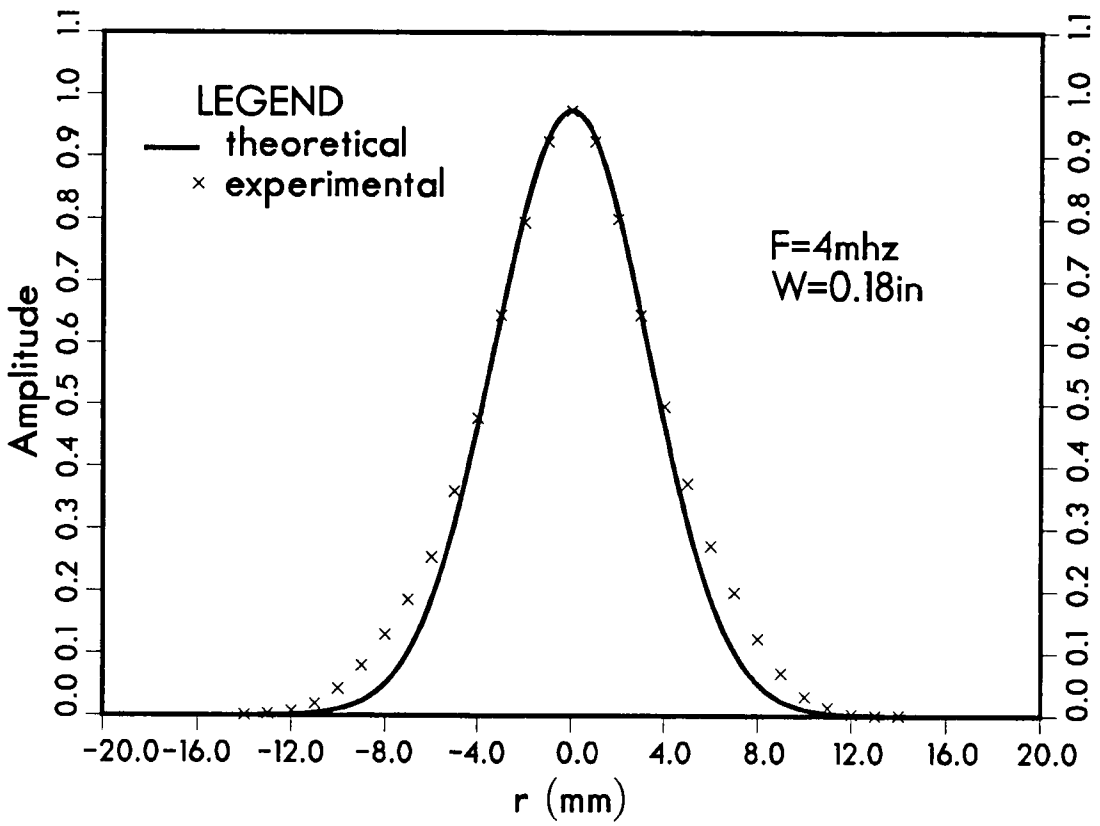


Figure 5.6. The measured transverse profile of the beam field produced by a 4 MHz, 0.36 inch diameter Gaussian transducer at z = 30 mm compared with theory.

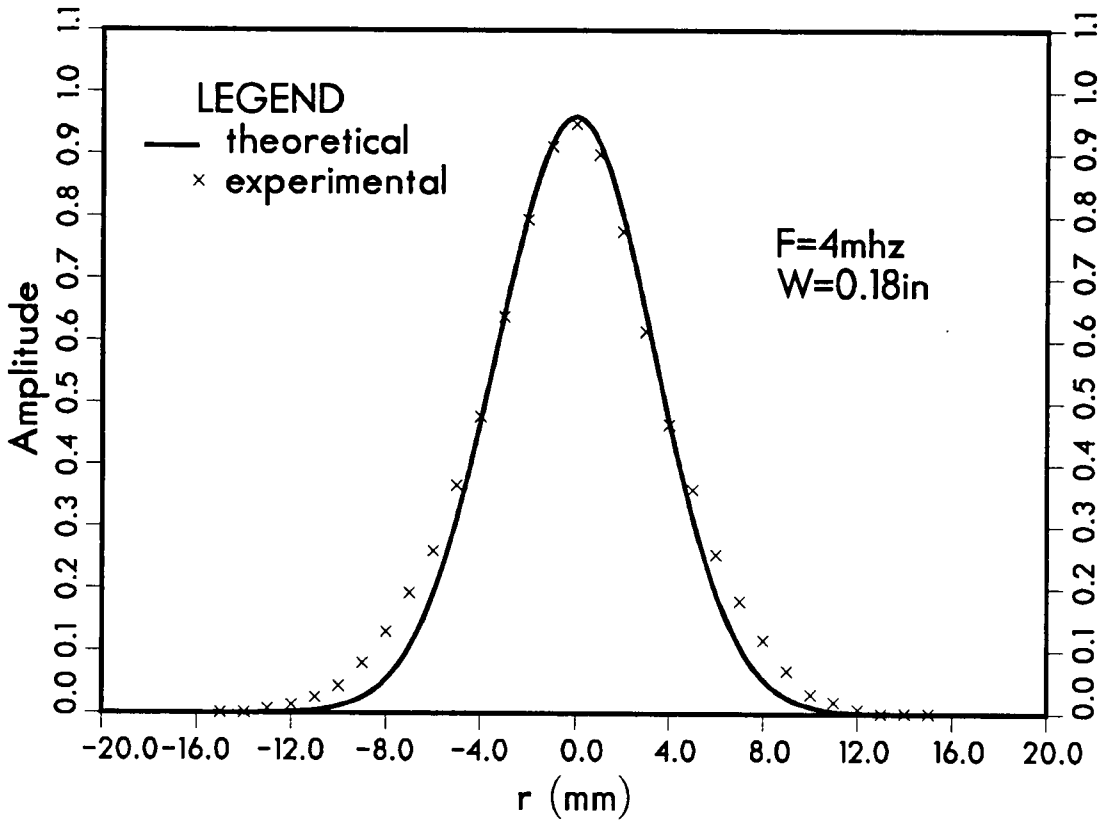


Figure 5.7. The measured transverse profile of the beam field produced by a 4 MHz, 0.36 inch diameter Gaussian transducer at z = 40 mm compared with theory.

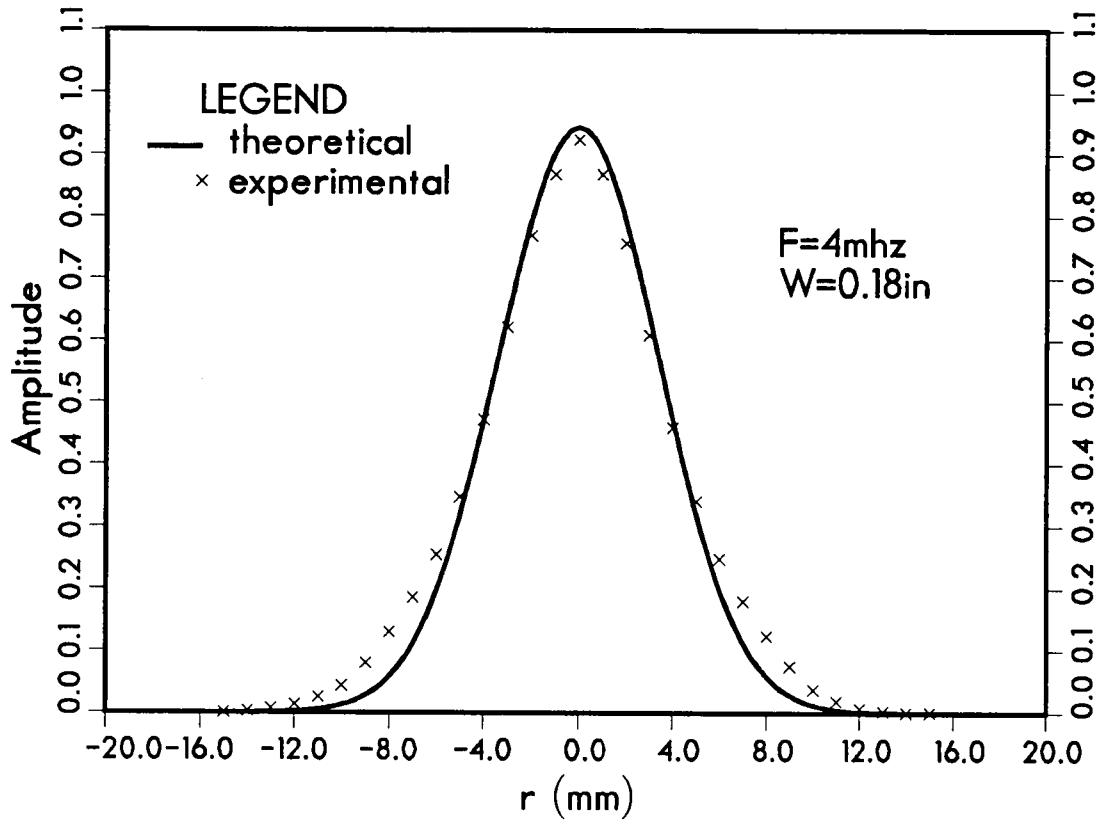


Figure 5.8. The measured transverse profile of the beam field produced by a 4 MHz, 0.36 inch diameter Gaussian transducer at z = 50 mm compared with theory.

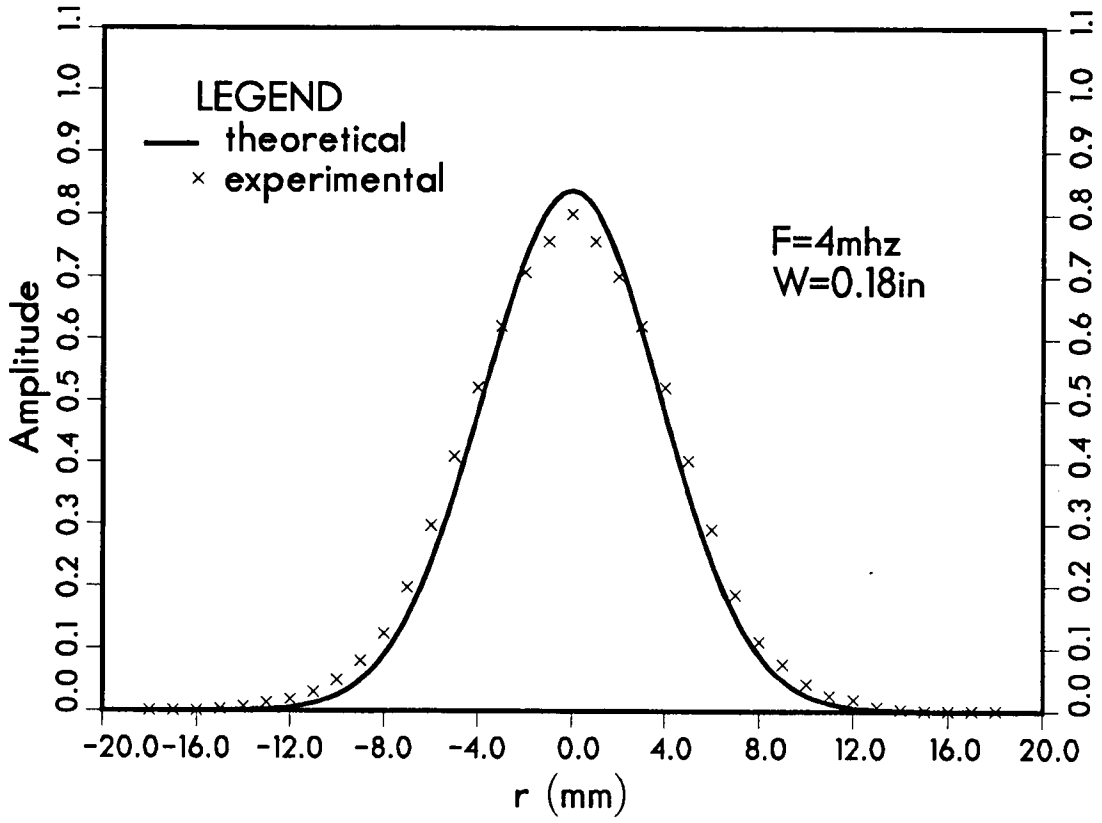


Figure 5.9. The measured transverse profile of the beam field produced by a 4 MHz, 0.36 inch diameter Gaussian transducer at z = 100 mm compared with theory.

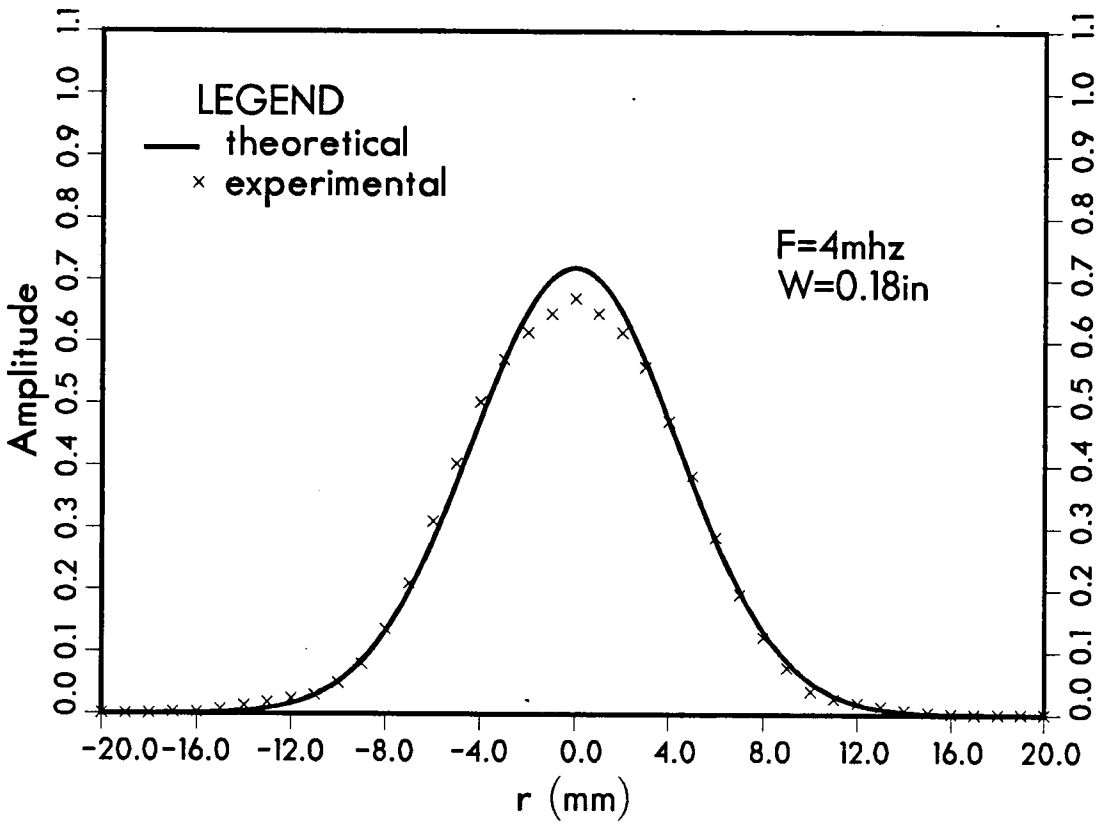


Figure 5.10. The measured transverse profile of the beam field produced by a 4 MHz, 0.36 inch diameter Gaussian transducer at z = 150 mm compared with theory.

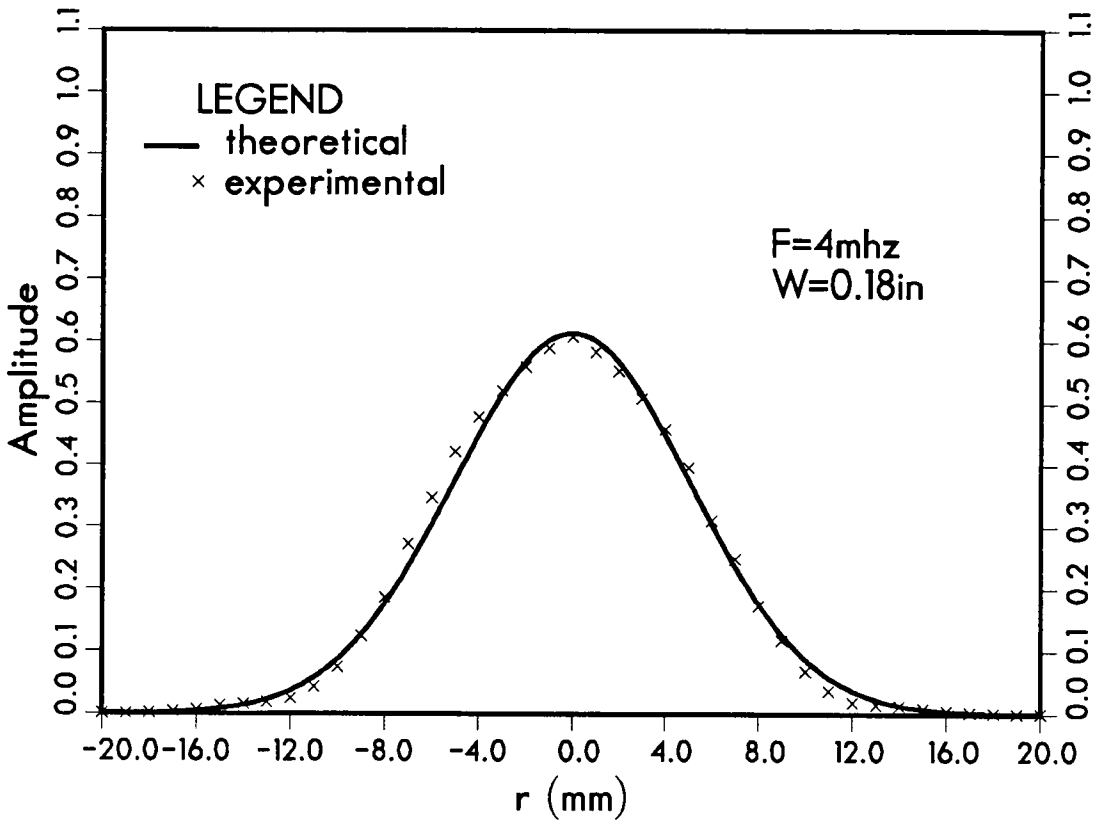


Figure 5.11. The measured transverse profile of the beam field produced by a 4 MHz, 0.36 inch diameter Gaussian transducer at z = 200 mm compared with theory.

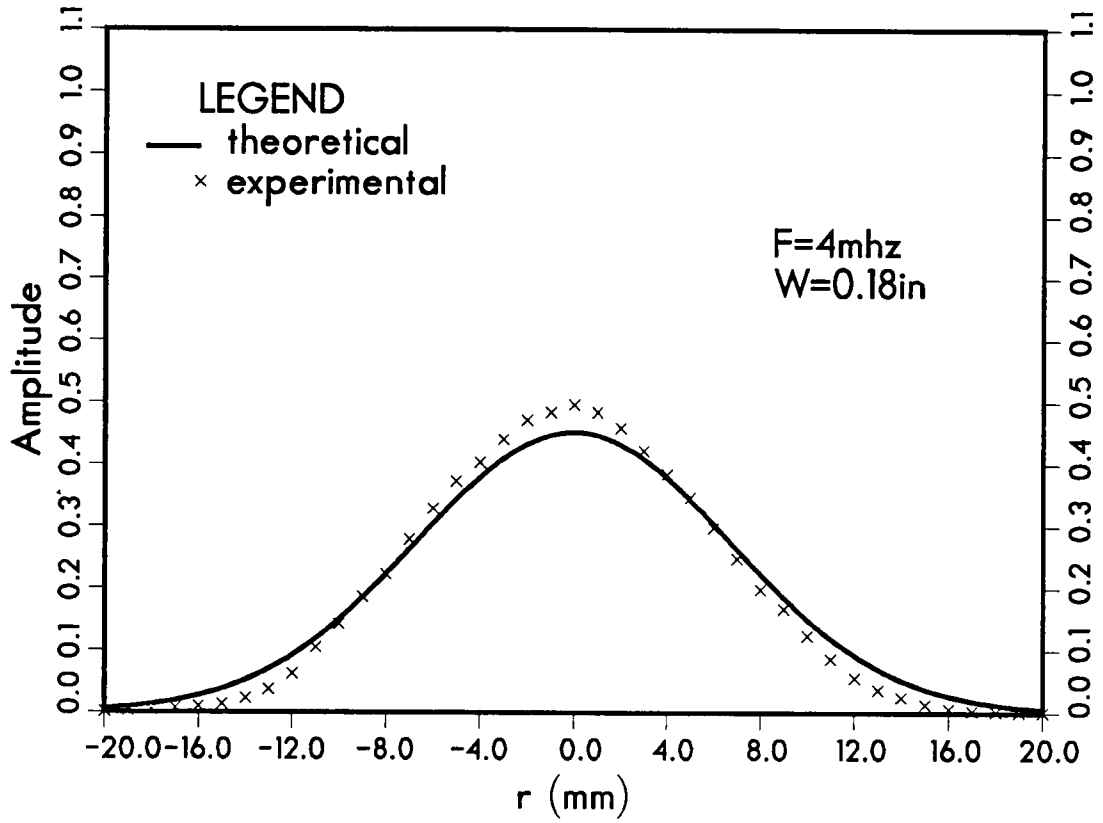


Figure 5.12. The measured transverse profile of the beam field produced by a 4 MHz, 0.36 inch diameter Gaussian transducer at z = 300 mm compared with theory.

CHAPTER VI

NON-AXISYMMETRIC CASES—REFLECTION PROBLEMS

So far the use of the Gaussian beam representation has been limited to axisymmetric situations. In many applications, non-axisymmetric beam fields, such as those formed in reflection and scattering problems, are encountered. In this chapter, one of the most challenging field problems—the reflected field due to a bounded ultrasonic beam incident onto a liquid-solid interface at or near the Rayleigh angle—is used to show how successfully the Gaussian beam representation can be used to describe a non-axisymmetric beam field. A new beam parameter—the beam axis parameter—is introduced to accommodate the non-axisymmetric field distribution. The plane wave representation derived through spatial Fourier analysis is presented as the starting point. The difficulties in solving the Fourier integrals and the previous efforts are examined. By writing the incident beam in the Gaussian beam representation, an analytical spectrum function is obtained as a summation of Gaussian functions. This spectrum function is then used to develop a new approximation to the reflectance so that the Fourier integral is analytically solved as a superposition of Gaussian beams with different beam waists about different beam axes [Wen and Breazeale, 1987].

6.1. The Axis Parameter of a Gaussian Beam

When a sound beam is incident at or near the Rayleigh angle, the reflected field exhibits many remarkable beam effects: the splitting of one beam into two or more; the lateral displacement of the beam axis; the angular deviation from the direction predicted by Snell's reflection law; etc., as can be seen in the schlieren photograph of an ultrasonic beam incident at the Rayleigh angle onto a water-aluminum interface shown in Fig. 6.1. These phenomena arise because at the Rayleigh angle the incident beam excites a leaky surface wave on the solid. The leaky surface wave then reradiates a beam which destructively interferes with the beam that has been specularly reflected. These phenomena strongly suggest a beam field configuration composed of a superposition of Gaussian beams about different axes. For representing a non-axisymmetric beam field, it is necessary to introduce a new beam parameter—the axis parameter.

The reflection problem of a beam field is usually treated as a 2-dimensional problem [Schoch, 1950; Brekhovskikh, 1960; Bertoni and Tamir, 1973; McGuirk and Carniglia, 1975]. A 2-dimensional Gaussian beam can be obtained by substituting $w_y = \infty$ (corresponding to a constant field distribution in y-dimension) into Eq. (2.16); i.e.,

$$\phi(x,z) = \frac{w_0 \exp[ikz]}{\sqrt{w_0^2 + \frac{2i}{k}(z - z_0)}} \exp\left[-\frac{x^2}{w_0^2 + \frac{2i}{k}(z - z_0)}\right]. \qquad (6.1)$$

One can see that while the transverse distribution in the x-dimension remains the same, the on-axis amplitude of a 2-dimensional Gaussian

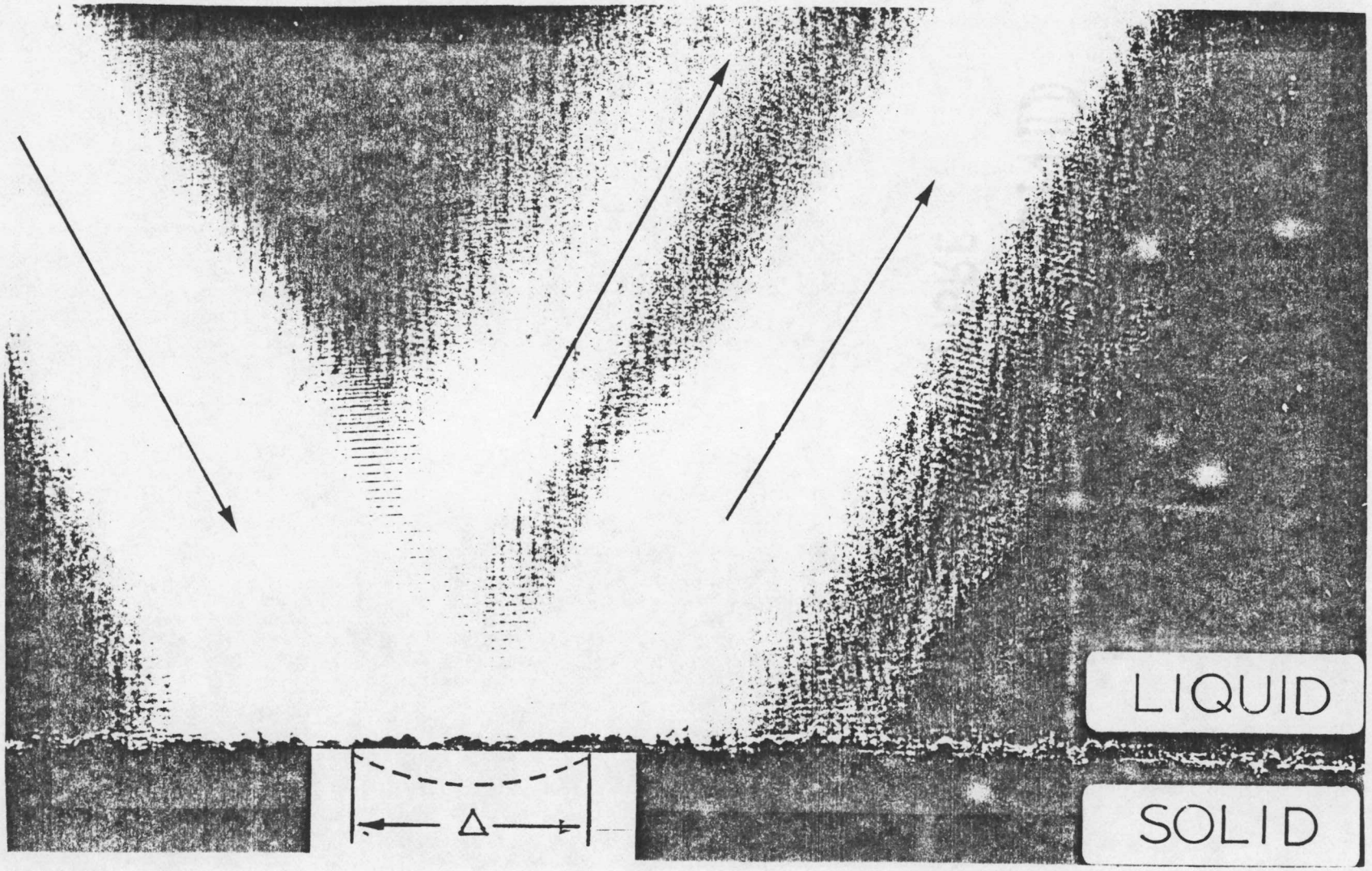


Figure 6.1. A schlieren photograph of an ultrasonic beam incident at the Rayleigh angle onto a water-aluminum interface.

beam decreases much slower with propagation distance than a 3-dimensional Gaussian beam does, as indicated by the square root in the denominator. Equation (6.1) represents a Gaussian beam about an axis (actually the symmetry plane) described by equation x = 0. For a Gaussian beam about an arbitrary axis described by

$$x = x_0 + i\eta, \tag{6.2}$$

where x_0 and η are real constants, one can replace x in Eq. (6.1) by $x - (x_0 + i\eta)$; i.e.,

$$\phi(x,z) = \frac{w_0 \exp[ikz]}{\sqrt{w_0^2 + \frac{2i}{k}(z - z_0)}} \exp\left[-\frac{(x - x_0 - i\eta)^2}{w_0^2 + \frac{2i}{k}(z - z_0)}\right]. \tag{6.3}$$

One can prove that Eq. (6.3) satisfies the cylindrical form of the parabolic equation as well as Eq. (6.1) does. This is a more general form of Gaussian beam function about a complex axis. Its real part x_0 gives the location of the beam axis. The physical significance of the imaginary part η is less obvious. Writing the intensity as $I = \phi\phi^*$, taking the partial derivative of I with respect to x and equating it to zero, one gets an equation for the locus of the intensity maxima

$$x - x_0 = 2\eta k w_x^2 (z - z_0). \tag{6.4}$$

Equation (6.4) implies that the intensity axis (locus of maxima of intensity) does not coincide with the propagation axis (z-axis). The angle between the two axes is given by

$$\tan\alpha = \frac{x - x_0}{z - z_0} = 2\eta k w_x^2. \tag{6.5}$$

Equation (6.5) shows that the imaginary part of a complex axis is a measure of the angular deviation between the intensity axis and propagation axis. For a real beam axis, the imaginary part vanishes; i.e. $\eta = 0$ thus $\alpha = 0$, there is no angular deviation.

At this point, one sees that a 2-dimensional Gaussian beam is characterized by two beam parameters: a waist parameter defining the magnitude and location of the beam waist, and an axis parameter which specifies the position of the beam axis relative to the coordinate axis and the possible angular deviation between the propagation axis and the intensity axis. Such a Gaussian beam serves as the basic unit for the non-axisymmetric beam field description.

6.2. A Plane Wave Representation

Consider the situation illustrated in Fig. 6.2, an ultrasonic beam incident onto a liquid-solid interface at an angle θ_i with respect to the normal to the interface. Since the incident beam is usually described by the incident coordinates, the spectrum function is expressed as:

$$G(k_{x_i}) = \frac{1}{2\pi}\int_{-\infty}^{\infty} \phi_0(x_i, 0)\exp(-ik_{x_i}x_i)\,dx_i, \tag{6.6}$$

where the subscript i stands for the coordinate attached to the

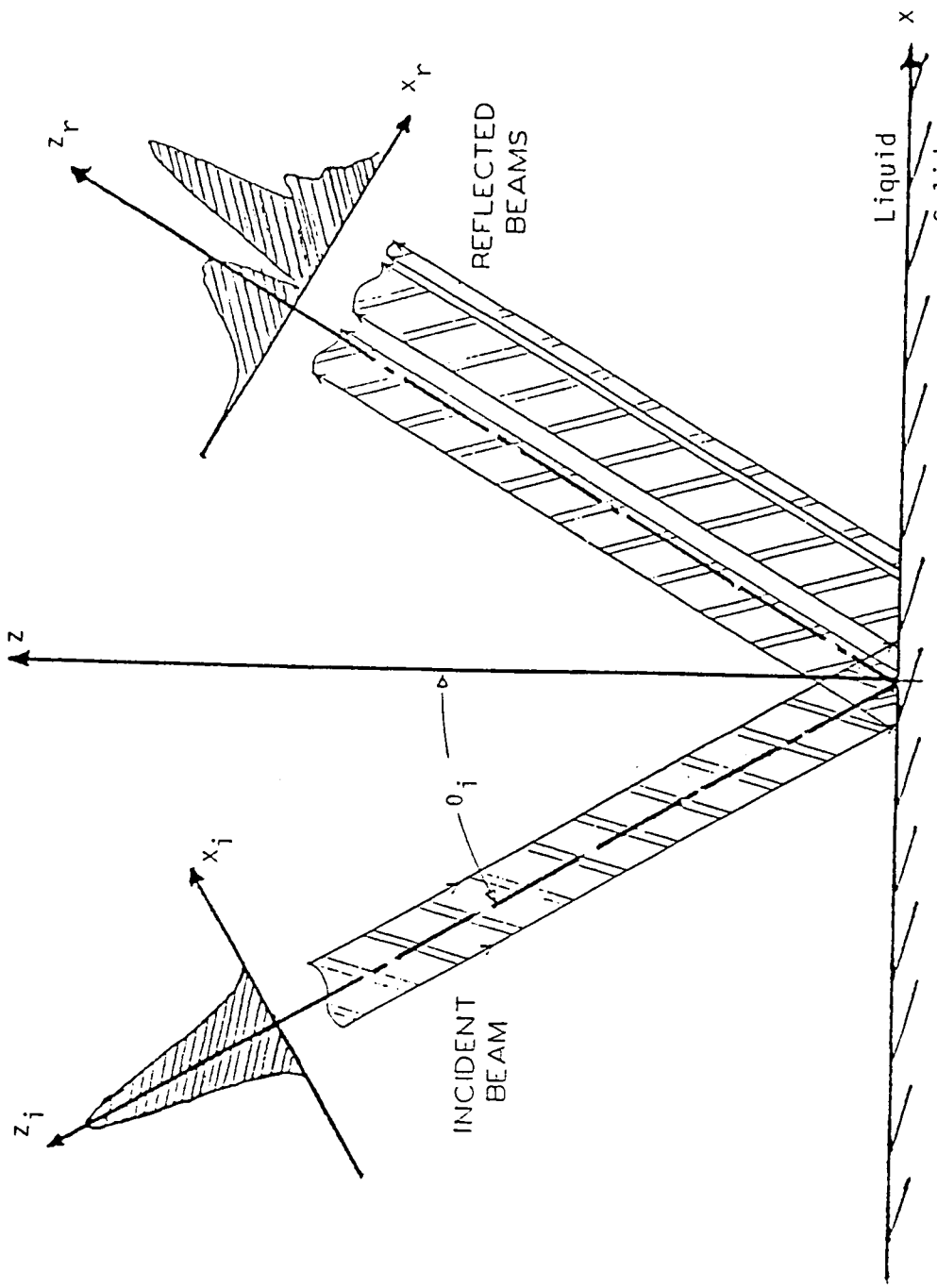


Figure 6.2. The coordinate system used for beam field reflection problem. The subscripts i and r stand for incidence and reflection coordinate, respectively.

incident beam. The reflected field in terms of the reflection coordinates x_r - z_r is expressed as an inverse Fourier transform [Brekhovskikh, 1960]

$$\phi(x_r, z_r) = \int_{-\infty}^{\infty} G(k_{x_r}) R(k_x) \exp(ik_{x_r} x_r + ik_{z_r} z_r)\, dk_{x_r}, \tag{6.7}$$

where $R(k_x)$ is the reflectance function. Due to the existence of the shear waves in solids, the reflectance of a liquid-solid interface for sound is more complicated than the corresponding one for light. Usually, it is expressed in terms of the incident angle θ. Using the relation

$$k_x = k \sin\theta, \tag{6.8}$$

it can be written [Bertoni and Tamir, 1973; Ngoc and Mayer, 1980] as

$$R(k_x) = \frac{(2k_x^2 - k_s^2)^2 - 4k_x^2[(k_x^2 - k_l^2)(k_x^2 - k_s^2)]^{1/2} - i\rho_0 k_s^4[(k_x^2 - k_l^2)/(k^2 - k_x^2)]^{1/2}}{(2k_x^2 - k_s^2)^2 - 4k_x^2[(k_x^2 - k_l^2)(k_x^2 - k_s^2)]^{1/2} + i\rho_0 k_s^4[(k_x^2 - k_l^2)/(k^2 - k_x^2)]^{1/2}}, \tag{6.9}$$

where the k_l and k_s are the wave numbers of longitudinal and shear waves in the solid, respectively, and ρ is the density ratio of liquid to solid. The variable k_x is related to k_{x_r} through the relation

$$k_{x_r} = k \sin(\theta - \theta_i). \tag{6.10}$$

A more direct relation can be derived as

$$\begin{aligned} k_x &= k\sin\theta = k\sin(\theta-\theta_i+\theta_i) \\ &= k\sin(\theta-\theta_i)\cos\theta_i + k\cos(\theta-\theta_i)\sin\theta_i \\ &= \cos\theta_i\, k_{x_r} + \sin\theta_i\,\sqrt{k^2-k_{x_r}^2}. \end{aligned} \tag{6.11}$$

To evaluate Eq. (6.7), one has to rewrite the reflectance in terms of k_{x_r} through Eq. (6.11). (An alternative is to replace all k_{x_r} by k_x through variable substitution. In that case, the final solution is obtained in space coordinate; i.e., the x - z coordinate.)

Equation (6.7) can be further simplified by using the Fresnel paraxial approximation

$$k_{z_r} \approx k - \frac{k_{x_r}^2}{2k}, \tag{6.12}$$

thus Eq. (6.7) becomes

$$\phi(x_r, z_r) = \int_{-\infty}^{\infty} G(k_{x_r}) R_r(k_{x_r}) \exp\left[ix_r k_{x_r} - i(z_r/2k)k_{x_r}^2\right] dk_{x_r}. \tag{6.13}$$

where $R_r(k_{x_r})$ stands for a new function obtained by substituting Eq. (6.11) into $R(k_x)$. Equation (6.13) has been used as a starting point by many authors [Schoch, 1950; Brekhovskikh, 1960; Bertoni and Tamir, 1973; McGuirk and Carniglia, 1975].

6.3. A Short Review on Previous Works

With a sophisticated reflectance function $R_r(k_{x_r})$ and a nested integrand, no analytical solution to Eq. (6.13) has been obtained without using an approximation to $R_r(k_{x_r})$.

A truncated Taylor expansion of the reflectance is the approximation used by most workers [Schoch, 1950; Brekhovskikh, 1960; McGuirk and Carniglia, 1975]. Since the Rayleigh angle is beyond the total reflection angle, only the phase change in the reflectance needs to be considered. By retaining up to the second derivative in the Taylor expansion of the phase factor, an analysis of the integral can be carried out without actually solving it. Qualitative explanations of some observed phenomena, such as the lateral displacement of the axis [Schoch, 1950; Brekhovskikh, 1960], the angular deviation of the reflected beam [Ra et al., 1973; Antar and Boerner, 1974; White et al., 1977; Chan and Tamir, 1985] and the longitudinal shift of the focus [McGuirk and Carniglia, 1977] are achieved. At the Rayleigh angle, however, a singularity of the reflectance function occurs. This makes a truncated Taylor expansion about the Rayleigh angle valid only in a very small range. For this reason, only when the width of incident beam is very large so that the spectrum function behaves like a δ-function, is the use of the Taylor expansion valid, as graphically illustrated by Berton and Tamir [1973].

Noting the limitation of the Taylor approximation and the singular behavior of the reflectance at the Rayleigh angle, Bertoni and Tamir [1973] introduced another important approximation to the reflectance—the Laurent expansion. By using the Laurent expansion about the Rayleigh angle to replace the reflectance, Bertoni and Tamir obtained an analytical solution for the Gaussian beam

incidence. This solution has proved to be the most accurate description to the reflection at the Rayleigh angle [Ngoc and Mayer, 1980] so far. However, the validity of the Laurent expansion also is limited within a small range about the singularity. Bertoni and Tamir's solution requires a large beam waist w_n on the incident beam and describes the reflection well only at or near the Rayleigh angle, as will be shown.

6.4. The Spectrum Function and Its Effect to the Reflectance

Making use of the technique described in Chapter IV, any 2-dimensional incident beam symmetric about its axis can be expressed as a superposition of Gaussian beams of different complex beam waist; i.e.,

$$\phi_0(x_i, z_i) = \sum_{n=1}^{N} \frac{A_n \exp(ikz)}{\sqrt{w_{0_n}^2 + (2i/k)(z - z_{0_n})}} \exp\left[-\frac{x_i^2}{w_{0_n}^2 + (2i/k)(z - z_{0_n})}\right], \quad (6.14)$$

where the subscript i stands for the incident beam coordinate shown in Fig. 6.2, w_{0_n} is the half waist width of the nth Gaussian beam and z_{0_n} is the z_i-coordinate of w_{0_n}. Through Eq. (6.14), the study of any incident beam is reduced to the much easier study of Gaussian beams of different waist parameters.

Substituting Eq. (6.14) into the Fourier transform Eq. (1.1) and using the integral formula Eq. (2.19), the spectrum function is solved analytically as

$$G(k_{x_i}) = \sum_{n=1}^{N} \frac{A_n w_n}{2\sqrt{\pi}} \exp\left[-(1/4) w_n^2 k_{x_i}^2\right], \tag{6.15}$$

where w_n is the complex beam waist defined by

$$w_n^2 = w_{0_n}^2 - \frac{2i}{k} z_{0_n}. \tag{6.16}$$

Through the use of the Gaussian beam representation, the first Fourier integral in the spatial Fourier analysis now may be solved analytically. Equation (6.13) now becomes

$$\phi(x_r, z_r) = e^{ikz} \sum_{n=1}^{N} A_n \int_{-\infty}^{\infty} \left(\frac{w_n}{2\sqrt{\pi}} \exp\left[-(1/4) w_n^2 k_{x_r}^2\right] \right) R_r(k_{x_r}) \exp\left[i x_r k_{x_r} - i(z_r/2k) k_{x_r}^2\right] dk_{x_r}. \tag{6.17}$$

Except for the summation, Eq. (6.17) is the same expression Bertoni and Tamir [1973] used in their study of the reflection of a single Gaussian beam. However, their solution is restricted to an incident Gaussian beam, while Eq. (6.17) applies to any incident beam. For convenience, the summation is dropped in the remaining discussion since each term in the solution behaves in the same way.

Equation (6.17) has an important advantage over Eq. (6.13): although the integration is over the entire range (from $-\infty$ to ∞) of k_{x_r}, the dominant contribution comes only from a small extent centered at zero and specified by the spectrum function—a Gaussian function $\exp[-(1/4)w_n^2 k_{x_r}^2]$. Since the magnitudes of the last two

factors in the integrand are limited within unity, the behavior of $R_r(k_{x_r})$ outside the effective range (where the Gaussian function becomes vanishingly small) has no effect on the integration. Thus the range of validity required for a good approximation to the reflectance is determined by the spectrum function. The larger the beam waist w_n, the narrower the spectrum function. Hence the smaller is the required range of validity in the approximation to the reflectance. In the extreme case where w_n goes to infinity, one has

$$\lim_{w_n\to\infty} G(k_{x_r}) = \lim_{w_n\to\infty} \frac{w_n}{2\sqrt{\pi}} \exp\left[-(1/4)w_n^2 k_{x_r}^2\right] = \delta(k_{x_r}). \tag{6.18}$$

Where the δ-function is defined as

$$\delta(x) = \begin{cases} \infty & x = 0 \\ 0 & x \neq 0, \end{cases} \tag{6.19}$$

which has a very useful property of

$$\int_{-\infty}^{\infty} H(x)\delta(x)\,dx = H(0). \tag{6.20}$$

where H(x) stands for any function of x. Since the spectrum function of an infinite plane wave is a δ-function given by Eq. (6.19), one sees that a plane wave is a special case of the Gaussian beam with an infinitely large beam waist. In such a case, the reflectance affects the integration only at a single point of $k_{x_r} = 0$. The integral can be solved by making use of Eq. (6.20). However, for a finite w_n, a

range specified by the spectrum function is still required for a good approximation to the reflectance.

6.5. A New Approximation to the Reflectance Function

Since the required range of validity is determined by w_n, w_n must enter the determination of any approximation to ensure the required range of validity. Of course, another important requirement, mathematical convenience, has to be satisfied too. This is the reason for making an approximation.

A new approximation satisfying both the above requirements is introduced at this point. The approach is based on the optimization procedure described in Chapter III and demonstrated in Chapter IV. With the reflectance function as the objective function, the testing function now is chosen as

$$T(k_{x_r}) = \sum_{m=1}^{M} C_{m_1} \exp\left[C_{m_2} k_{x_r}^2 + C_{m_3} k_{x_r}\right], \tag{6.21}$$

where C_{m_i} (m=1,2,...,M;i=1,2,3) are complex constants to be determined.

In determining C_{m_i} it is important to specify a proper range of optimization. A range too small lowers the accuracy, too big increases the difficulty in calculation but helps little in improving the accuracy. It is found that the spectrum function is an ideal natural range delimiter which optimizes the testing function in such a way that the effect of the disagreement between the testing function

and the reflectance in the integration is minimized. This is achieved by using the spectrum function as a weighting function in the optimization; i.e.,

$$Q(C_{m_i}) = \int_{-\infty}^{\infty} [R_r(k_{x_r}) - T(k_{x_r})]^2 \exp[-(1/4)w_n^2 k_{x_r}^2]\, dk_{x_r}. \qquad (6.22)$$

Thus one sees the beam waist w_n enters the determination of the approximation through the spectrum function. When the incident beam has a small waist w_n so that the required range is comparatively large, one can use a larger number of Gaussian functions to get the required accuracy. As will be shown, the new approximation to the reflectance obtained through the spectrum function weighted optimization achieves both mathematical convenience and a sufficient range of validity simultaneously.

6.6. The Gaussian Beam Representation of a Reflected Field

Upon finding the constant set C_{m_i} in Eq. (6.21), replacing $R_r(k_{x_r})$ by $T(k_{x_r})$, the integrand in Eq. (6.17) becomes an exponential function having a quadratic argument. Writing the argument as a complete square and making use of Eq. (2.19), Eq. (6.17) can be analytically solved as

$$\phi(x,z) = e^{ikz} \sum_{m=1}^{M} \frac{w_m C_{m_i}}{\sqrt{w_m^2 + \frac{2i}{k}(z - z_{0_m})}} \exp\left[-\frac{(x - x_{0_m} - i\eta_m)^2}{w_m^2 + \frac{2i}{k}(z - z_{0_m})}\right], \qquad (6.23)$$

where

$$w_m^2 = Re\,[w_n^2 - 4C_{m_2}];$$

$$z_{0_m} = Im\,[(k/2)w_n^2 - 4C_{m_2}];$$

$$C_{m_3} = x_{0_m} + i\eta_m. \tag{6.24}$$

Compared with Eq. (6.3), Eq. (6.23) exhibits the following physical picture: the ultrasonic field of a Gaussian beam having a beam waist w_n reflected by a liquid-solid interface described by $R(k_x)$ (in the coordinate associated with the interface) or $R_r(k_{x_r})$ (in the reflected beam coordinate) is composed of M Gaussian beams propagating in the same direction but about the different beam axes described by $x_r = x_{0_m}$. Each Gaussian beam has a different beam waist w_m located at a different position z_{0_m} along its own axis.

As an example, the reflected fields of Gaussian incident beams with different beam waists incident at different angles onto a water-aluminum interface are represented in the Gaussian beam representations. Table 6.1 lists C_{m_i} sets for five different combinations of incident angle θ_i and beam waist w. The profiles calculated by using C_{m_i} listed in Table 6.1 in Eq. (6.23) are plotted in Figs. 6.3 through 6.7 and compared with solutions of Bertoni and Tamir's [1973]. The numerical evaluation of the exact integral solution Eq. (6.17) carried out by UTCC VAX computer with an accuracy of 10^{-5} is also given as a reference.

It can be seen that when $\theta_i = 30.5°$, the Rayleigh angle for the water-aluminum interface, Bertoni and Tamir's solution agrees

Table 6.1. The coefficient and beam parameter sets of Gaussian beam representations of reflected fields of Gaussian beams with different beam waists incident onto a water-aluminum interface at angles near the Rayleigh angle $\theta_R = 30.5°$.

$\theta_i = 30.5°$ $w = 15mm$

m	C_{m_1}	$C_{m_2}(10^{-4}m^2)$	$C_{m_3}(10^{-2}m)$
1	$-0.2052 - 0.6131i$	$+0.3500 + 0.1653i$	$-0.7584 - 1.2804i$
2	$-0.7409 + 0.3149i$	$-0.0170 - 0.0781i$	$+0.0475 - 0.7564i$

$\theta_i = 30.5°$ $w = 5mm$

m	C_{m_1}	$C_{m_2}(10^{-4}m^2)$	$C_{m_3}(10^{-2}m)$
1	$-0.2321 + 0.6145i$	$-0.0007 - 0.0132i$	$+0.0395 - 0.2694i$
2	$-0.6067 + 0.3234i$	$+0.0790 - 0.0864i$	$+0.1983 - 1.0117i$
3	$-0.1102 - 0.2497i$	$+0.4880 + 0.1166i$	$-0.6867 - 1.7076i$
4	$-0.0010 - 0.9910i$	$+0.0298 + 0.0220i$	$-0.2061 - 0.4403i$

$\theta_i = 30.5°$ $w = 10mm$

m	C_{m_1}	$C_{m_2}(10^{-4}m^2)$	$C_{m_3}(10^{-2}m)$
1	$-0.5278 + 0.6382i$	$+0.0082 - 0.0441i$	$+0.0804 - 0.5026i$
2	$+0.0276 - 0.0751i$	$+0.1656 + 0.2793i$	$-1.2370 - 2.8449i$
3	$-0.4489 - 0.8660i$	$+0.1887 - 0.0061i$	$-0.6912 - 0.8827i$

$\theta_i = 29.5°$ $w = 10mm$

m	C_{m_1}	$C_{m_2}(10^{-4}m^2)$	$C_{m_3}(10^{-2}m)$
1	$+0.4781 - 0.0691i$	$-0.0197 - 0.0160i$	$+0.0239 + 0.0997i$
2	$-0.1851 + 0.2736i$	$+0.1774 + 0.2249i$	$-0.5891 - 2.0397i$
3	$+0.0851 - 1.1265i$	$+0.1236 - 0.1323i$	$+0.3773 - 1.1945i$

$\theta_i = 28.5°$ $w = 10mm$

m	C_{m_1}	$C_{m_2}(10^{-4}m^2)$	$C_{m_3}(10^{-2}m)$
1	$+0.1376 - 0.3304i$	$+0.1968 + 0.0996i$	$+1.0612 - 0.2274i$
2	$+0.0367 - 0.0170i$	$+0.5809 - 1.0357i$	$+1.3777 - 4.0089i$
3	$+0.7172 - 0.0435i$	$+0.0135 - 0.0280i$	$-0.0715 + 0.1127i$

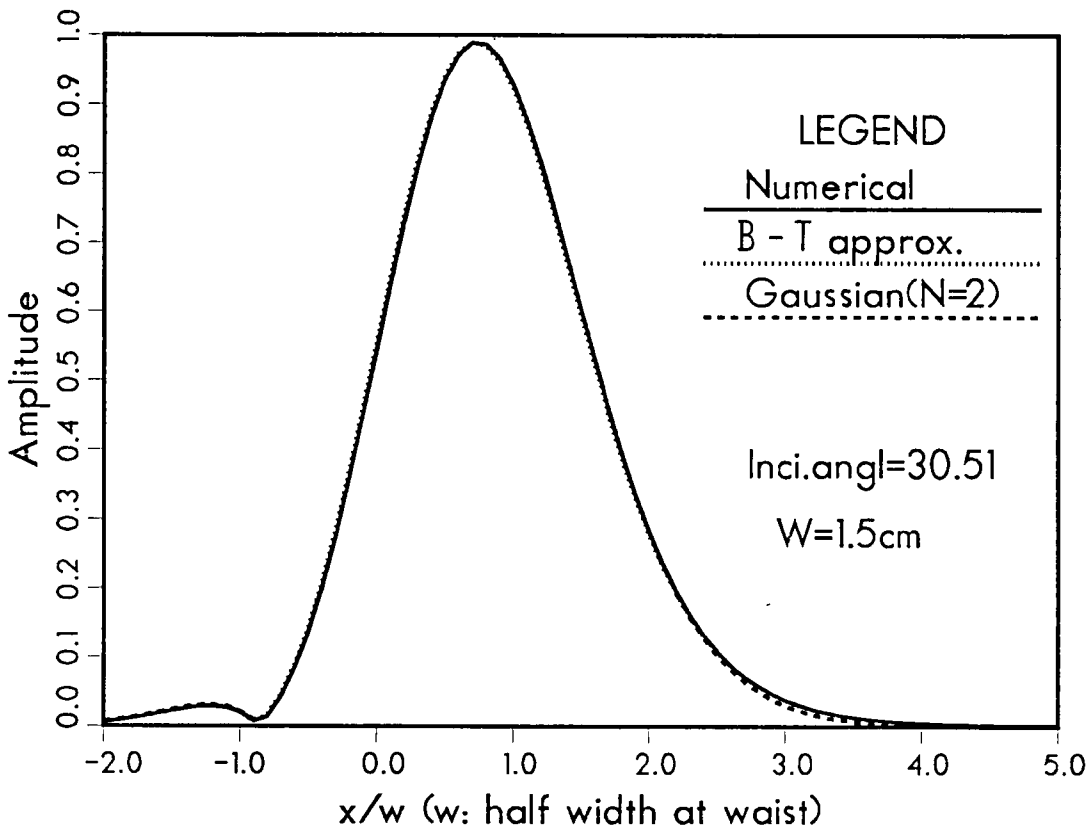


Figure 6.3. Reflected beam profiles on a water-aluminum interface calculated by numerical integration, Bertoni-Tamir's solution, and Gaussian beam representation for a Gaussian beam of half width w = 1.5 cm incident at the Rayleigh angle θ_i = 30.5°.

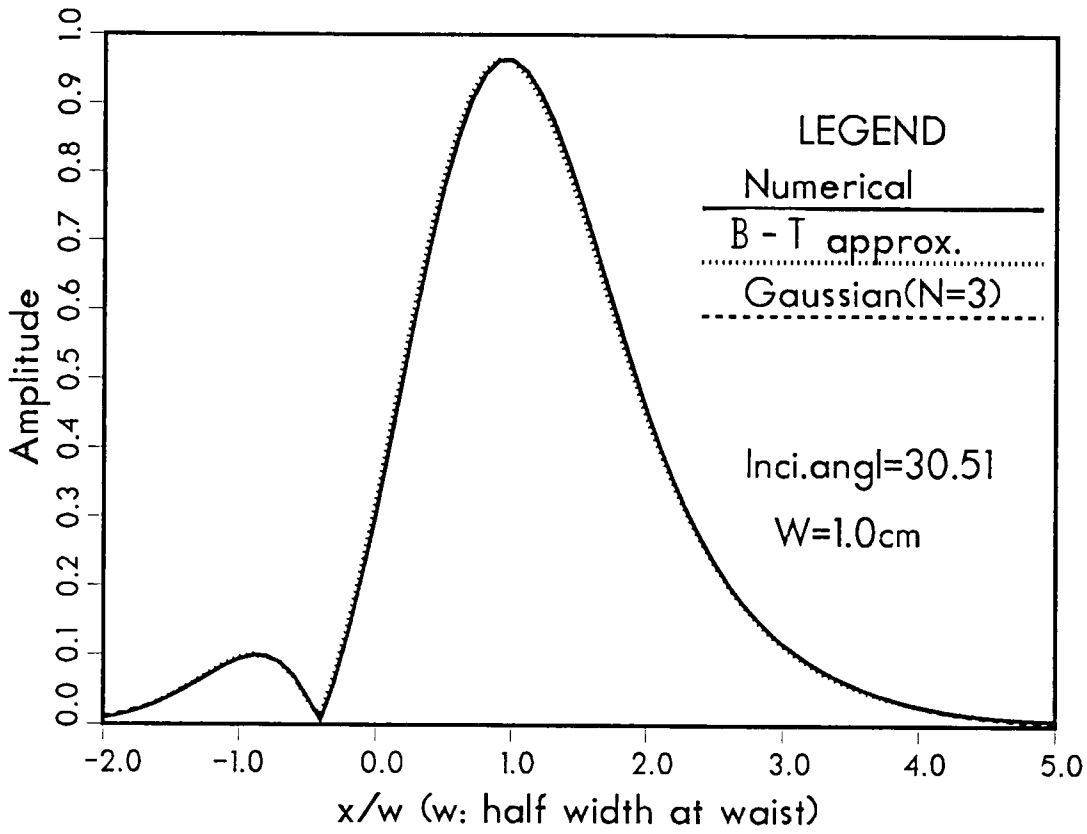


Figure 6.4. Reflected beam profiles on a water-aluminum interface calculated by numerical integration, Bertoni-Tamir's solution, and Gaussian beam representation for a Gaussian beam of half width w = 1.0 cm incident at the Rayleigh angle θ_i = 30.5°.

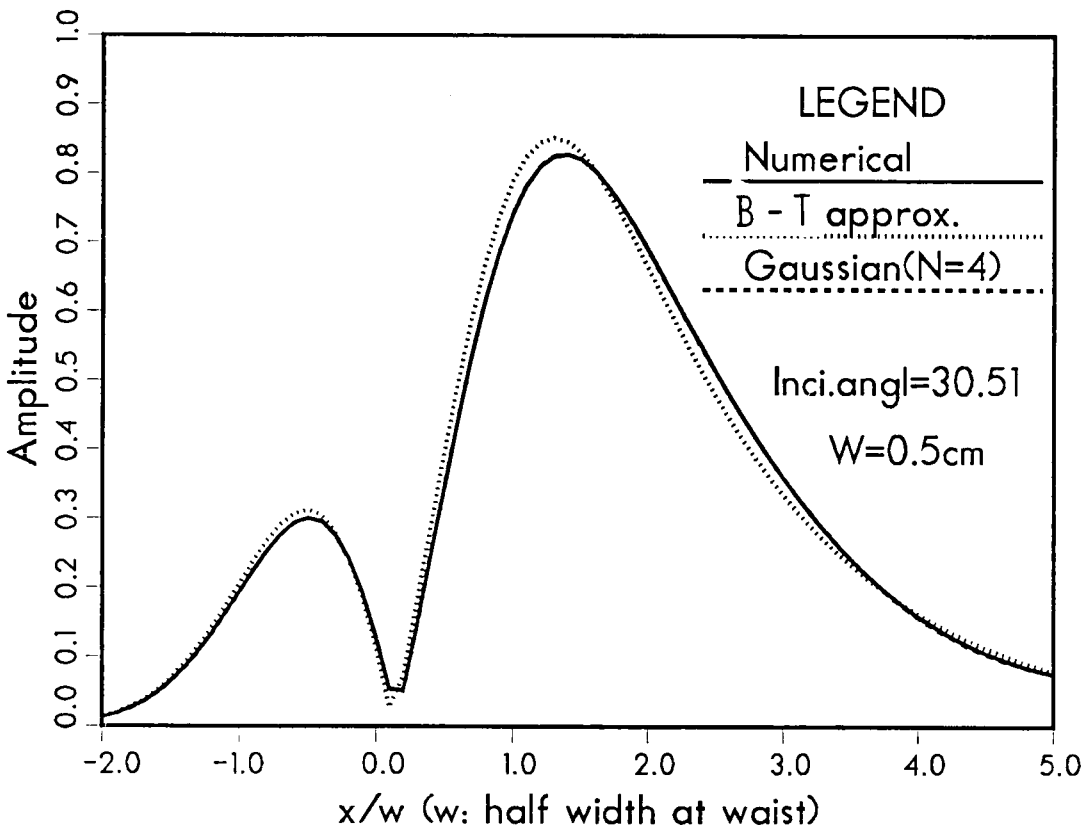


Figure 6.5. Reflected beam profiles on a water-aluminum interface calculated by numerical integration, Bertoni-Tamir's solution, and Gaussian beam representation for a Gaussian beam of half width w = 0.5 cm incident at the Rayleigh angle θ_i = 30.5°.

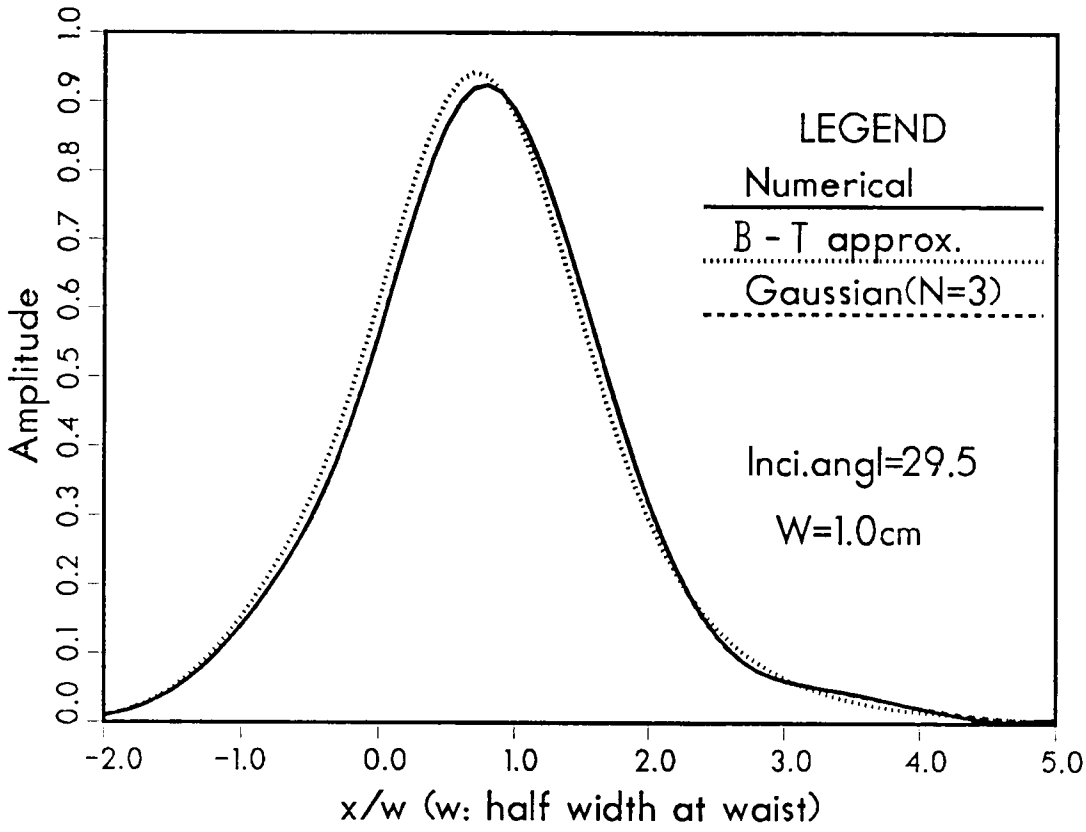


Figure 6.6. Reflected beam profiles on a water-aluminum interface calculated by numerical integration, Bertoni-Tamir's solution, and Gaussian beam representation for a Gaussian beam of half width w = 1.0 cm incident at θ_i = 29.5°.

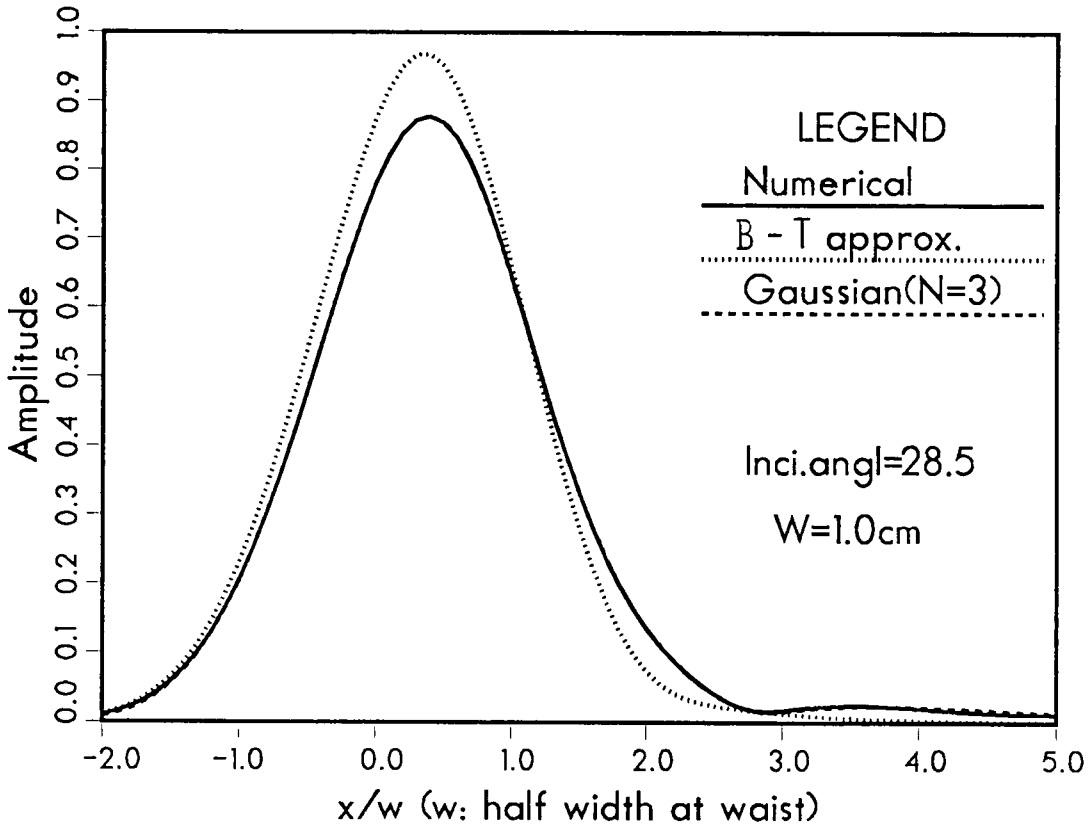


Figure 6.7. Reflected beam profiles on a water-aluminum interface calculated by numerical integration, Bertoni-Tamir's solution, and Gaussian beam representation for a Gaussian beam of half width w = 1.0 cm incident at θ_i = 28.5°.

with the integral evaluation well for w = 1.5 cm, well for w = 1.0 cm, and fair for w = 0.5 cm. On the other hand, by adjusting the number of terms in the solution, the Gaussian beam representation can always give a good accuracy. The dashed lines standing for the Gaussian beam representations agree with the numerical integration so well that they are hardly discernible, except at the edge of the field. In the case of w = 1.5 cm, only two Gaussian beams represent the field as well as Bertoni and Tamir's solution. Figures 6.6 and 6.7 show that as the incident angle θ_i differs from the Rayleigh angle, Bertoni and Tamir's solution becomes less and less valid. In contrast, the Gaussian beam representation retains the same agreement with the numerical solution for any incident angle. The sharpest contrast is in the phase shift as a function of position in the beam shown in Fig. 6.8. The reflection at the Rayleigh angle is characterized by a 180° phase shift. Although Bertoni and Tamir's solution best represents the amplitude distribution at the Rayleigh angle, it fails to reproduce this abrupt phase shift. However, the Gaussian beam representation reproduces the phase shift quite well.

Through the introduction of the beam axis parameter, the Gaussian beam representation is applied to non-axisymmetric beam fields with very satisfactory results. The technique can also be extended to 3-dimensional situations by using separate beam parameters in the y-dimension. The approach described in this chapter is not limited to the reflection problems; any physical process described by any function can be used as the objective function as well and

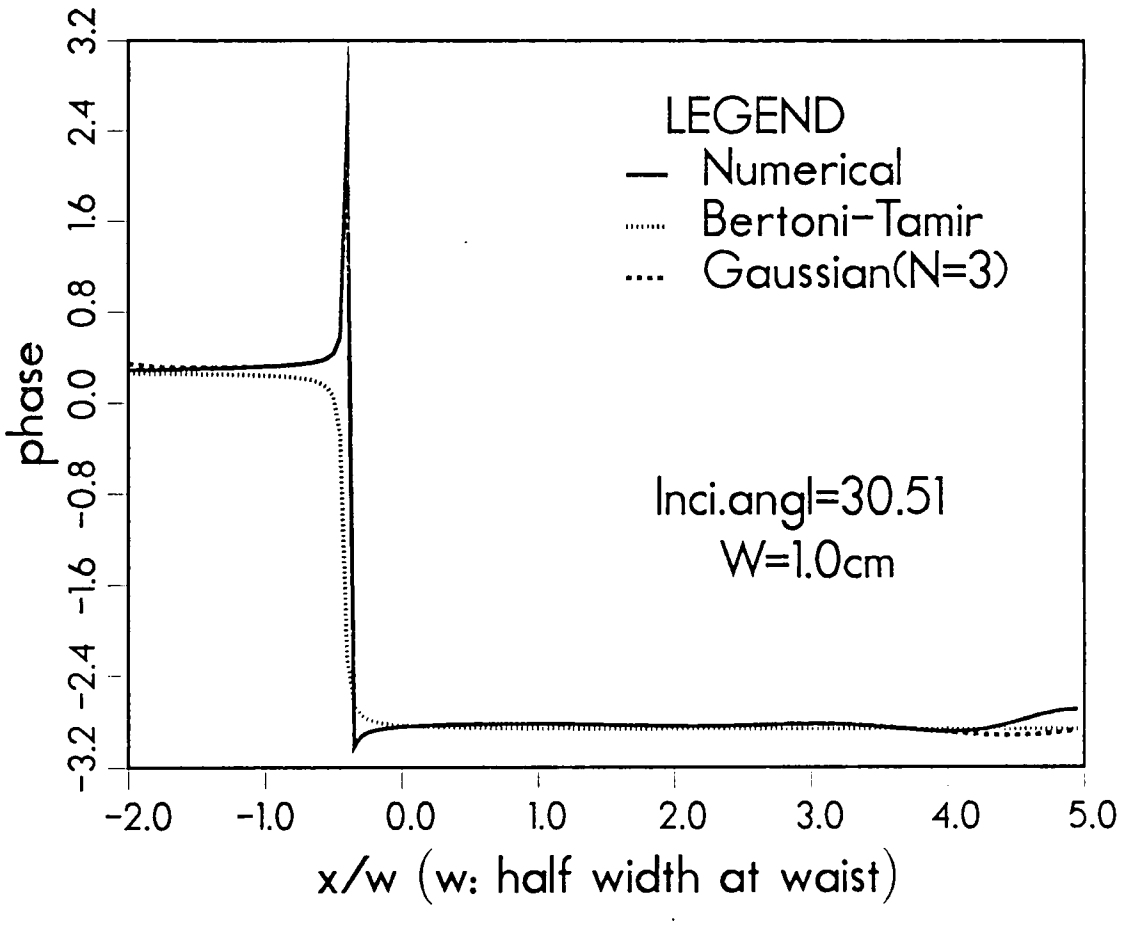


Figure 6.8. Phase distributions in the reflected beam on a water-aluminum interface calculated by numerical integration, Bertoni and Tamir's solution, and Gaussian beam representation for a Gaussian beam of half width w = 1.0 cm incident at the Rayleigh angle θ_i = 30.5°.

produces a Gaussian beam representation of the resultant beam field. The Gaussian beam representation is a general method of analysis to all kinds of beam fields.

CHAPTER VII

SUMMARY

The diffraction field of an axisymmetric planar radiator and the non-axisymmetric field of a bounded ultrasonic beam incident at or near the Rayleigh angle have served as specific examples of a general approach to the beam field problems. A systematic method of analysis of the beam fields has been established. By using as a natural field component the Gaussian beam, rather than representing the field by superposition of infinite plane wave components, an ultrasonic field (or any other wave fields satisfying the condition $ka \gg 1$) now can be expressed in an analytical form. The process given in Chapter IV enables one to express any beam source as a superposition of a number of Gaussian beams of different beam waists. Since the Fourier transform of a Gaussian beam can be obtained in an analytical form—a Gaussian function—the spectrum function of any beam field can be solved analytically as a superposition of Gaussian functions. The technique of approximating the effect of a physical process (like Rayleigh reflection) as the sum of several Gaussian functions ultimately solves the second Fourier integral in the spatial Fourier analysis. Combining the above two techniques, the beam field resulting from any physical process acting on any initial beam field can be described in the Gaussian beam representation—

a superposition of Gaussian beams of different beam waists about different beam axes, but propagating in the same direction.

The Gaussian beam representation has the following advantages over the plane wave representation (integral solutions) or series solutions:

1. The Gaussian beam representation is always in an analytical form—even after the action of a series of physical processes—and all terms in the solution behave the same in analytical manipulations.

2. Instead of evaluating a pair of Fourier integrals, the computation becomes the determination of a set of coefficients and beam parameters. For a large number of field points the computer time is reduced considerably.

3. The use of the optimization procedure is especially useful in solving the inverse problems frequently encountered in ultrasonic applications, such as flaw detection and underwater objects identification. Upon finding the coefficient and beam parameter sets through the measured data, the physical conditions (e.g., shape of scattering object) producing such a field can be deduced by mathematical inversion. Such a process often is very difficult for solutions involving integrations over the boundary.

4. The optimization procedure outlined in Chapter III and demonstrated in Chapter IV can be applied to a considerably larger range of situations. For non-planar boundaries, multi-boundaries, or boundaries for which the Green's functions are not available, an integral solution or the coefficient set of a series solution cannot

be properly defined. Such situations can be handled readily by the Gaussian beam representation through the use of the optimization procedure.

5. The Gaussian beam representation is based on a natural, physically realizable model. Although a single plane wave has very admirable mathematical and physical properties, what one meets is always an infinite series of plane waves which is much harder to handle. In contrast, a Gaussian beam can be actually used to simplify the mathematics. As the new Gaussian transducer demonstrated in Chapter V becomes generally available, the Gaussian beam representation will become even more attractive.

BIBLIOGRAPHY

BIBLIOGRAPHY

Antar, Y. M. and W. M. Boerner, Can. J. Phys. 52, 962-972 (1974).

Archer-Hall, J. A. and D. Gee, NDT Int. 13, 95 (1980).

Bertoni, H. L. and T. Tamir, Appl. Phys. 2, 157-172 (1973).

Breazeale, M. A., L. Adler, and L. Flax, J. Acoust. Soc. Am. 56, 866-872 (1974).

Breazeale, M. A. and M. A. Torbett, Appl. Phys. Lett. 29, 456-458 (1976).

Breazeale, M. A., L. Adler, and G. W. Scott, J. Appl. Phys. 48, 530-537 (1977).

Breazeale, M. A., F. D. Martin, and B. Blackburn, J. Acoust. Soc. Am. 70, 1791-1793 (1981).

Brekhovskikh, L. M., Waves in Layered Media (Academic, New York, 1960).

Cavanagh, E. and B. D. Cook, J. Acoust. Soc. Am. 67, 1136-1140 (1980).

Chan, C. C. and T. Tamir, Opt. Lett. 10, 378-380 (1985).

Du, G. and M. A. Breazeale, J. Acoust. Soc. Am. 78, 2083-2086 (1985).

Goos, F. and H. Hänchen, Ann. Physik (Leipzig) 1 (6), 333-345 (1947).

Greenspan, M., J. Acoust. Soc. Am. 65, 608-621 (1979).

Harris, G. R., J. Acoust. Soc. Am. 70, 186-204 (1981).

Hasegawa, T., N. Inoue, and K. Matsuzawa, J. Acoust. Soc. Am. 74, 1044-1047 (1983).

Haselberg, K. V. and J. Krautkrämer, Acustica 9, 359 (1959).

King, L. V., Can. J. Res. 11, 135-155 (1934).

Lotsch, H. K. V., Optiks 32, 116-137, 189-204 (1970); 32, 299-319, 553-569 (1971).

Lu, I. T., L. B. Felsen, and J. M. Klosner, J. Acoust. Soc. Am. 82, S77 (1987).

Maciel, J. J. and L. B. Felsen, J. Acoust. Soc. Am. 82, S103 (1987).

Martin, F. D. and M. A. Breazeale, J. Acoust. Soc. Am. 49, 1668-1669 (1971).

McGuirk, M. and C. K. Carniglia, J. Opt. Soc. Am. 67, 103-107 (1977).

Neubauer, W. G., J. Appl. Phys. 44, 48-55 (1973).

Ngoc, T. D. K. and W. G. Mayer, J. Acoust. Soc. Am. 67, 1149-1152 (1980).

Niver, E., C. J. Ruiz, M. S. Vogas, and L. B. Felsen, J. Acoust. Soc. Am. 81, S9 (1987).

Novikov, B., O. V. Rudenko, and V. I. Timoshenko, Nonlinear Underwater Acoustics, Chapter 4 (American Institute of Physics, New York, 1987).

Oberhettinger, F., J. Research NBS 65B, 1-6 (1961).

Ra, J. W., H. L. Bertoni, and L. B. Feison, SIAM J. Appl. Math. 24, 396-413 (1973).

Rayleigh, L., Theory of Sound (Dover, New York, 1945), Vol. II, Sec. 278.

Schoch, A., Ergeb. Exakt. Naturwiss. 23, 127 (1950).

Tamir, T., J. Opt. Soc. Am. A3, 588-565 (1986).

Tamir, T. and H. L. Bertoni, J. Opt. Soc. Am. 61, 1397-1413 (1971).

Tjøtta, J. N. and S. Tjøtta, J. Acoust. Soc. Am. 68, 334-339 (1980).

Tjøtta, J. N. and S. Tjøtta, J. Acoust. Soc. Am. 71, 824-833 (1982).

Wen, J. J. and M. A. Breazeale, Proc. IEEE 1987 Ultrasonics Symposium, Denver, Colorado.

Wen, J. J. and M. A. Breazeale, J. Acoust. Soc. Am. 82, S89 (1987).

Wen, J. J. and M. A. Breazeale, J. Acoust. Soc. Am., accepted for publication, May 1988.

White, I. A., A. W. Snyder, and C. Pask, J. Opt. Soc. Am. 67, 703-705 (1977).

VITA

Jing Jiang Wen was born in Wuhan City, Hubei, China, on October 20, 1951. He moved to Beijing with his family in 1953 and grew up there. He was not able to continue his education from 1966 to 1977 because China's education system was at a standstill due to the social upheaval of the "Cultural Revolution." He entered Northern Jiaotong University, Beijing, in March 1978 and received his Bachelor of Science degree in Physics there in January 1982. From February 1982 through July 1983 he was an assistant engineer in The Institute of Household Electric Appliances, Beijing, and an editorial staff member of the Chinese magazine Science and Technology of Household Electric Appliances. He entered the Graduate School of The University of Tennessee, Knoxville, in September 1983.

He was married to Shiqi Liu in January 1981. They have two children, Haifan and Helen.